THE ROLE OF SEDIMENTARY SULFIDE IN SEAGRASS DECLINE IN BARNEGAT BAY-LITTLE EGG HARBOR, NEW JERSEY.

By

NICOLE L. WAITE

A thesis submitted to the

Graduate School-New Brunswick

Rutgers, The State University of New Jersey

In partial fulfillment of the requirements

For the degree of

Master of Science

Graduate Program in Oceanography

Written under the direction of

Silke Severmann

And approved by

_____

_____

_____

New Brunswick, New Jersey

January, 2015

ABSTRACT OF THE THESIS

The Role of Sedimentary Sulfide in Seagrass Decline in Barnegat Bay-Little Egg Harbor, New Jersey.

By NICOLE L. WAITE

Thesis Director:
Silke Severmann

Barnegat Bay-Little Egg Harbor (BBLEH) is a highly eutrophic estuary on the New Jersey coast that has experienced parallel seagrass loss in past decades. Further damage to the ecologically and economically important seagrass communities are likely to occur as eutrophication continues. Previous eutrophication studies in BBLEH have not addressed the sediment chemistry, and therefore could be missing a critical component in understanding the current, and potential future, health of the estuary. Of particular importance is the possible accumulation of toxic dissolved sulfide in sediment pore waters. This study investigated the impacts of eutrophication on sedimentary sulfide as a threat to seagrass populations and the underlying redox state and buffering capacity of the sediments in controlling sulfide accumulation in BBLEH.

Sediments in BBLEH are becoming sulfidic year-round within the top 7cm. Sulfide accumulation is low in summer and fall (below 250µM) but concentrations reach 2000µM in spring throughout the estuary. Concentrations are similar between barren and seagrass sediments. However, dissolved H_2S and Fe^{2+}, and solid phase Mn, U, and Mo indicate that

sediments in the northern, more eutrophic, segment are more reducing, transition to an anoxic state and begin to accumulate H_2S at shallower sediment depths (2-4cm), where it is more likely to intrude into seagrass roots, than in the central and south segments (4-7cm) of the estuary. Furthermore, Fe-S chemistry suggest that reactive Fe is lower in the north with Fe-oxyhydroxides and FeS having been converted to pyrite, while Fe-oxyhydroxides and FeS are still present in the central and south segment. Thus, the buffering capacity has been exhausted and sulfide removal is diminished in the north, but not in the central and south. This study shows that continued eutrophication since the 1990's has made the northern segment of the BBLEH more susceptible to future sulfide toxicity, thereby posing a greater threat to the survival of seagrass in that region. Findings suggest that greater emphasis needs to be placed on sediment conditions that may negatively impact seagrass and coastal ecosystems in future eutrophication assessments.

Acknowledgements

First and foremost, to my family – Mom, Dad, Amanda, and Samantha. I could not have done this without all of your support and help getting through everything that came along with coming to grad school. I love you all so much.

To Silke, thank you cannot begin to express how grateful I am to have you as a mentor. Thank you for stepping in when I was lost and needed someone. I appreciate it more than you know.

To my committee – Mike and Liz, thank you for your support, advice, and guidance.

To all of the GPO students – thank you for being a support system and always being there on difficult grad school days to listen and help and on good grad school days too to hang out, grab a drink, play disc golf, and to be my friend. I couldn't have asked for a better group of grad students to experience this with!

A special shout out to our cohort, the best cohort, – Jack, Alex, Filipa, Nic, Christien, Brittany, Kevin, and Katie, Since before day 1 of grad school, you have all been amazing friends. Kaycee, Chris, Donato, Michelle, Patrick, Amy, and Fedor – I'm so happy you all are at Rutgers. I can't imagine it without you. Words cannot express how happy I am to have you all in my life. Thank you for being there to talk, to laugh, to have fun with, to give hugs when they were needed most, and for being my family here. I'm lucky to know each of you!

To Gregg and Gina – thank you for letting me tag along on your SAV trips and for helping me take many sediment cores. My thesis wouldn't have been possible without you.

To Ali – lab, long hours, many weekends, and donut Saturdays would not have been any fun without you. Thank you for your help, advice, support, and friendship.

To the Vetriani Lab and Patty – thank you for including me and giving me a pseudo-lab group and for including me in lunches and office activities!

Lastly, I would also like to thank IMCS and RUMFS for supporting me, providing funding for my research, and for not only giving me a place to work and complete my graduate degree, but for also giving me a community.

Table of Contents

List of Tables

List of Figures

I. Introduction

A. Seagrass Ecosystems

Seagrass communities are highly productive coastal ecosystems distributed throughout the world. Located in both tropical and temperate environments, they cover 0.1 to 0.2% of the global ocean (Duarte 2002; Orth et al. 2006), can be found in brackish and estuarine waters, and live in sandy to muddy sediments. Despite being subtidal, seagrasses have high light requirements and therefore the upper depth limit of their distribution is dominantly controlled by the underwater irradiance (Duarte 2002).

Seagrass beds are highly valuable ecosystems that provide many important ecosystem functions. Seagrass ecosystems are crucial in the carbon cycle, with a net carbon production of 0.6 Pg per year globally (Duarte 2002). Most of this carbon becomes trapped in the detrital organic matter pool and is either exported to the deep ocean waters or becomes buried in the sediments of seagrass beds, making seagrass communities areas of CO_2 sequestration (Duarte 2002; Orth et al. 2006). Although seagrasses help to sequester CO_2, a recent review by Cai (2011) of coastal ocean carbon fluxes suggests that generally, estuaries degas ~0.25 Pg m^{-2} y^{-1} of CO_2 to the atmosphere. Therefore, continued loss of seagrass habitats will likely increase the flux of CO_2 from estuaries to the atmosphere. Additionally, seagrass beds serve as nursery habitats and food sources for many fish and invertebrate species (e.g., hard clams), act as sediment erosion buffers that provide additional protection of coastlines during extreme weather events, supply oxygen to the water and sediments, and play important roles in the retention of nutrients and toxins (Duarte 2002; Orth et al. 2006; McGlathery et al. 2007).

The destruction of seagrass beds has been suggested to have detrimental effects that reach far beyond the local coastal ecosystem. Because of their proximity to land, seagrass

ecosystems are increasingly threatened by humans through eutrophication, physical disturbances, shoreline development and climate change (Duarte 2002).

B. Eutrophication

Increasing urbanization, development, and agriculture often results in nutrient enrichment, particularly of nitrogen, to coastal ecosystems, causing eutrophication, a known ecosystem degrader. For example, the northern Gulf of Mexico receives large quantities of nutrients, primarily derived from fertilizer used in farmlands, from the Mississippi River, causing large and prolonged hypoxic events (e.g., Rabalais et al. 2002; Rabalais et al. 2009). Coastal lagoonal bays that have restricted circulation, along with limited freshwater inflow and oceanic exchange, tend to have long residence times are particularly prone to eutrophication (Kennish 2009). At least two-thirds of U.S. estuaries have been classified as moderately or highly eutrophic (Bricker et al. 2007). In an assessment of U.S. mid-Atlantic coastal bays, one-third of the estuaries had become more eutrophic between 1990 and 2004 and Barnegat Bay, NJ was found to be the most eutrophic (Bricker et al. 2007).

Common consequences of eutrophication include increased micro- and macroalgal growth, phytoplankton blooms, harmful algal blooms, and benthic habitat alteration. Greater oxygen consumption occurs as the increased organic matter is respired in the water column and the sediments, resulting in low oxygen, or hypoxic, waters (defined as concentrations of about 3.0-0.2ml/l; Rabalais et al. 2002). In turn, these consequences cause permanent changes to the biotic ecosystems, including fish and other faunal population declines and essential habitat loss (Burkholder et al. 2007; Kennish et al. 2007; McGlathery et al. 2007; Diaz and Rosenberg 2008; Kennish 2009).

A well-documented major consequence of eutrophication in many temperate estuarine and marine coastal habitats has been significant seagrass loss and a shift from an ecosystem dominated by benthic primary production and seagrass to an algal dominated ecosystem (Figure 1; Duarte 2002; Orth et al. 2006; Burkholder et al. 2007; Kennish et al. 2007; McGlathery et al. 2007; Howarth et al. 2011). Phytoplankton blooms and algae growth severely shade seagrass, thereby limiting its photosynthetic ability. Increased epiphyte growth on seagrass blades is another consequence of eutrophication, further decreasing light penetration and obstructing the high light levels required by seagrass (Burkholder et al. 2007; McGlathery et al. 2007).

C. Sulfide and Seagrass

Sedimentary conditions can also greatly impact the health and survival of seagrasses, which largely take up nutrients from sediment pore waters through their root and rhizome system (Short and McRoy 1984). Below the sediment surface, dissolved sulfide accumulation can contribute to seagrass loss. Like nutrients, dissolved sulfide in the pore waters can enter the plant through the seagrass roots. Sulfide is a phytotoxin that can directly poison cellular metabolic processes and reduce nutrient uptake and growth (Burkholder et al. 2007; McGlathery et al. 2007). Studies have shown negative seagrass responses in the presence of pore water sulfide, including shortened shoot and blade length, decreased number of leaves per shoot, decreased rate of leaf growth, and declined plant survival (Carlson et al. 1994; Goodman et al. 1995; Terrados et al. 1999; Holmer and Bondgaard 2001; Calleja et al. 2007).

The threshold for sulfide toxicity appears to be species dependent. Most notably, *Thalassia testudinum*, a tropical seagrass species, has suffered large die-off events in Florida Bay where pore water sulfide concentrations reached 1000-3000μM. Sulfide concentrations in healthy beds were less than 1000 μM (Carlson et al. 1994). *Posidonia oceanica*, a Mediterranean

Sea species, experiences seagrass decline at sulfide concentrations as low as 10µM (Calleja et al. 2007). In lab experiments, *Zostera marina* leaf growth is reduced (Figure 2) in conjunction with sucrose additions that resulted in increased sedimentary microbial sulfate reduction rates and dissolved sulfide accumulation to concentrations of 70-100 µM (Terrados et al. 1999). Other lab experiments report a reduction in the photosynthetic response of *Z. marina* at moderate sulfide levels of >400µM , with the seagrass showing higher light intensity requirements and an overall decrease in photosynthetic rates (Goodman et al. 1995). Although sulfide toxicity to seagrass has been widely studied, many eutrophication studies have not addressed sulfide accumulation and sediment redox state beyond determining sulfide levels as factors in seagrass decline.

D. Controls on Sulfide

In eutrophic conditions where large amounts of organic matter are produced in the surface waters and respired in bottom waters and sediments, oxygen is quickly depleted by aerobic decomposition, and organic matter decomposition dominantly occurs through anaerobic respiration by heterotrophic bacteria. Respiration processes occur via a redox cascade of electron acceptors. In marine systems, sulfate rapidly becomes the primary electron acceptor for anaerobic organic carbon oxidation (Jorgensen 1977; Canfield et al. 1993). Sulfate reduction produces sulfide, which can then accumulate in the sediment pore waters (Carlson et al. 1994). The degree of dissolved sulfide accumulation in the sediment pore waters, and therefore the amount of toxin present, is largely controlled by the rate of microbial sulfate reduction and is expected to increase as eutrophication and organic carbon production continue to increase.

Dissolved sulfide in the sediments is readily oxidized by free oxygen to form sulfate and intermediate sulfur species (e.g., elemental S; Jorgensen 1977; Thamdrup et al. 1994). The introduction of oxygen into the sediments to oxidize sulfide is dominated by bioirrigation and

bioturbation by plants and burrowing fauna (e.g. polychaetes, bivalves, and crustaceans), with minor contributions from passive diffusion. When organisms burrow into the sediments, the burrows create channels for oxygenated bottom waters to penetrate into the sediments, cause mixing of the sediments, and aids in sulfide oxidation (Aller 1990; Aller and Aller 1998; Mortimer et al. 1999). Seagrass can also actively transfer oxygen to the below-ground biomass through a gas filled lacunae system in the leaves and roots and oxidize sulfide to prevent sulfide intrusion (Pedersen et al. 2004). The oxygen supplied to the roots is either produced directly by the plant during photosynthesis or from oxygen already available in the water column. Because seagrass uses oxygen produced in its blades to combat sulfide intrusion below ground, that oxygen is not released into the water column, and may thereby contributing to hypoxic conditions in the ambient bottom water (Figure 3; Carlson et al. 1994; Pedersen et al. 2004).

The biodiffusion of oxygen into the sediments has been shown to become restricted as sulfide accumulation occurs and inhibits healthy growth of the plants. Oxygen production declines from decreased seagrass leaf growth (Terrados et al. 1999; Holmer and Bondgaard 2001) and seagrass roots also begin to shorten (Hemminga 1998), thereby limiting the ability of seagrass to transport oxygen belowground. Moreover, once seagrass starts to die, the dead plant material is deposited into the sediments, enhancing the benthic oxygen demand while at the same time further inhibiting the ventilation of the sediments through the plants' root system. After seagrass health is compromised, this series of positive feedback mechanisms reduces the plants' ability to recover from seasonal hypoxic events and accelerates the expansion of barren dead zones (Goodman et al. 1995).

Dissolved sulfide accumulation is significantly affected by the buffering capacity of the sediments, which is controlled by the amount of reactive Fe-oxide present in the sediments (Jorgensen 1977; Thamdrup et al. 1994; Ruiz-Halpern et al. 2008). Reactive Fe-(oxyhydr)oxide

oxidizes sulfide to elemental sulfur, while being reduced to dissolved Fe^{2+} (Equation 1). Subsequently, any excess sulfide reacts with the $Fe^{2+}$and is precipitated as Fe-monosulfide (FeS) and pyrite (FeS_2) (Equations 2 and 3), thereby removing toxic dissolved sulfide (Poulton et al. 2004)

$$2Fe^{3+} + S^{2-} \rightarrow 2Fe^{2+} + S^0 \quad [1]$$
$$2Fe^{2+} + 2S^{2-} \rightarrow 2FeS \quad [2]$$
$$FeS + S^{2-} \rightarrow FeS_2 \quad [3]$$

After all the reactive oxide is used up and all dissolved Fe^{2+} is titrated, dissolved sulfide accumulates in the pore waters. In experimental manipulations, sediments with organic matter additions were seen to have increased sulfide concentrations, whereas sediments with additions of both reactive Fe-(oxyhydr)oxide and organic matter had no change in sulfide concentrations when compared to sediments with no organic matter or iron additions (Figure 4; Ruiz-Halpern et al. 2008), illustrating the importance of Fe to buffer sulfide.

When reactive Fe pools in the sediments are small, the buffering capacity can easily be exceeded allowing dissolved sulfide to accumulate at shallow sediment depths near seagrass roots (4-5cm; Viaroli et al. 2008). The amount of reactive Fe-(oxyhydr)oxide in the sediments varies geographically, depending on the geology of the catchment area, the volume of continental run-off, and the frequency of winter storm events that may deposit large amounts of fresh terrestrial material in the coastal zone (Wheatcroft and Sommerfield 2005; Severmann et al. 2010). Seagrass also helps to capture fine particles that contain much of the reactive Fe-(oxyhydr)oxide. When seagrass disappears, less of this fine fraction, and thus less reactive Fe-(oxyhydr)oxide, is retained, creating a feedback mechanism that can alter the buffering capacity of the sediments. These mechanisms are therefore important in controlling how much dissolved sulfide can accumulate in the sediments and to what extent sulfide becomes a threat to seagrass (Jorgensen 1977; Thamdrup et al. 1994; Poulton et al. 2004; Ruiz-Halpern et al. 2008)

E. Sedimentary Changes from altered Redox State

Fundamentally, sulfide production is dependent on the redox state of the sediments. Sediments become more and more reduced with more intense eutrophication which facilitates more sulfide production and a greater likelihood for sulfide accumulation. Trace elements are useful indicators of sedimentary redox state (e.g., Cochran et al. 1986; Shaw et al. 1990; Barnes and Cochran 1993; Calvert and Pedersen 1993; Morford and Emerson 1999; Brumsack 2006; Lyons and Severmann 2006; McManus et al. 2006; Tribovillard et al. 2006; Banks et al. 2012; Helz and Adelson 2013). When sediments transition from oxic to anoxic conditions, some metals, such as Fe and Mo, become dissolved (e.g. through the reduction of Fe-oxyhydroxide) and as they build up in the pore waters close to the sediment-seawater interface, they flux out of the sediments via diffusive and advective processes (Banks et al. 2012). Mn-oxides are present under oxic conditions, but as sediments become reducing, Mn-oxides are used in anaerobic organic matter degradation or undergo abiotic reactions with other reduced species (e.g., dissolved Fe^{2+} and H_2S) and become reduced to aqueous Mn^{2+} (Shaw et al. 1990).

Other metals such as Mo and U are adsorbed onto particles or form authigenic mineral phases and become sequestered in the sediments (e.g., through formation of metal sulfides and organo-metallic complexes; Banks et al. 2012). The presence of H_2S promotes Mo incorporation into pyrite, and thus under sulfidic conditions, higher concentrations of solid Mo are expected (Shaw et al. 1990; Helz and Adelson 2013). In estuarine sediments, U is stably dissolved under oxic conditions. But, at the start on the anoxic zone U becomes reduced from U(VI) to U(IV) and concentrations increase above the detrital background, with various degrees of authigenic enrichment, is observed (Cochran et al. 1986; Barnes and Cochran 1993). Cadmium, Zn, Re, and V precipitation is also observed under reducing conditions, making these metals possible proxies for anoxia as well (Calvert and Pedersen 1993; Crusius and Thomson 2000; Tribovillard et al.

2006). Furthermore, the combination of these proxies can help to tease apart subtle differences in the redox conditions. For example, an enrichment of U and Mo likely indicates sulfidic conditions, while an enrichment in U without an enrichment in Mo likely indicates anoxic conditions that are not yet sulfidic (McManus et al. 2006; Tribovillard et al. 2006).

Beyond providing a measure of redox state, certain trace metals can provide information about the flux of terrigenous inputs and amount of organic matter to the sediments. Elements such as Al, Ti and Zr are indicative of the terrigenous detrital fraction in the sediments, providing a potential indication of land inputs (Brumsack 2006). Barium is found to correlate with organic carbon, but it's preservation may be lowered under suboxic conditions and it can precipitate under sulfate reducing conditions, thus, Ba is more controversial and less reliable as a measure of productivity in areas of high productivity (McManus et al. 1998; Tribovillard et al. 2006). Uranium accumulation is also well known to positively correlate with organic carbon flux to the sediments (Cochran et al. 1986; Anderson 1987; Anderson et al. 1989; Shaw et al. 1990; Crusius and Thomson 2000; Brumsack 2006; McManus et al. 2006). As such, trace metal chemistry of sediments provide insight into the amount of productivity occurring and the organic carbon supply to the sediments that influence sulfide dynamics in the sediments.

II. Study Site

Barnegat Bay-Little Egg Harbor (BBLEH) is a shallow, coastal lagoon estuary comprised of three contiguous coastal bays running along the central New Jersey coast: Barnegat Bay, Manahawkin Bay, and Little Egg Harbor (Figure 5). The estuary is separated from the Atlantic Ocean by a set of barrier islands that are breached in only two locations: Barnegat Inlet in the central estuary and Little Egg Inlet at the southern tip. The average depth of BBLEH is 1.5m, with

greater depths (up to 6m) predominately in the channel and along the western side (up to 3m) of the bay. Due to the shallow depths and enclosed topography of BBLEH, water circulation and flushing are restricted, with flushing times up to ~70 days in the summer (Kennish 2001).

The watershed encompasses a wide variety of landscape types, from developed areas to wetlands. Excluding water, urban development accounts for ~30%, forests account for ~40%, wetlands account for ~26%, barren areas account for ~3%, and agricultural lands account for ~1% of land in the watershed (Figure 6; Lathrop and Haag 2007). Significant freshwater sources to BBLEH are riverine inputs and groundwater seepage. The largest rivers (Toms River, Metedeconk River, and Cedar Creek) are in the north region of the estuary while smaller coastal streams drain into the south region (Kennish 2001).

Seagrass beds are found along the barrier islands in the eastern estuary in shallow (1-2m) waters with sandy-muddy sediments. The dominant seagrass species in BBLEH is eelgrass (*Zostera marina*), with widgeon grass (*Ruppia maritima*) also found in the north region of the estuary, where salinities are lowest (Lathrop et al. 2001; Kennish et al. 2008; Kennish et al. 2010; Fertig et al. 2013a). Macro-algal blooms (red and green algae, e.g., *Ulva lactuca and Gracilaria tikvahiae*) are prominent in the estuary and have been increasing in size and frequency in recent years. Between 2004 and 2010, 10 0.45 blooms per m^2 in size, 19 0.67 blooms per m^2 in size, and 36 1.57 blooms per m^2 occurred. Of these, 6, 17, and 24 occurred between 2008-2010, respectively (Kennish et al. 2011). Salt marshes fringe the estuary, predominately in the less developed regions of Little Egg Harbor in the south (Lathrop and Haag 2007).

Substantial population and development increases along the central coast of New Jersey since the mid 1970's have resulted in progressive increases in land use, non-point source pollution, and nutrient loading to BBLEH (Kennish et al. 2007). Highest pollution and nutrient inputs occur in the north (Figure 5) in the more developed area encompassing Toms River, Brick,

and Lakewood (Hunchak-Kariouk and Nicholson 2001; Seitzinger et al. 2001; Wieben and Baker 2009), with at least 60% of nitrogen loading coming from the Toms and Metedeconk Rivers (Wieben and Baker 2009). Water column total nitrogen concentrations are highest in the north (598±141 µg/L) region of the estuary where nutrient loading and water residence times are greatest, while lower concentrations in the central (408±93 µg/L) and south (433±141 µg/L) segment are aided by greater flushing at Barnegat and Little Egg Inlets (Fertig et al. 2013b). The long residence times of water, except at the Barnegat and Little Egg Inlets, allow nutrients and therefore organic matter to accumulate, contributing to low oxygen levels (Kennish et al. 2007). As a result, the estuary has become steadily more eutrophic, shifting from a moderately eutrophic estuary in the 1990's (Seitzinger and Pilling 1993) to a highly eutrophic one today (Bricker et al. 2007; Kennish et al. 2007; Kennish et al. 2011; Fertig et al. 2013a).

Between the 1970's and 2000, the effects of eutrophication were most felt in the northern region of BBLEH. However, symptoms of eutrophication (e.g. increased algal growth and seagrass decline) are beginning to spread and are now affecting the southern and central regions of BBLEH as well. Eutrophication index values, which have been used to assess BBLEH, provide a metric score of how eutrophic a system is by integrating data on 15 biotic and abiotic variables related to water quality (e.g. dissolved oxygen and total nitrogen concentrations), light availability (e.g. Chlorophyll-a, total suspended solids, and macroalgal cover), and seagrass demographics (e.g. *Z. marina* biomass and percent cover). On this scale, a lower index value indicates greater eutrophication. Eutrophication index values for the central and south regions have decreased over time from 73 to 45 and from 71 to 45, respectively, from the early 1990's to 2010, indicating that these regions are becoming more affected by eutrophication. In contrast, eutrophication index values in the north region increased from 14 in 1991 to 50 in 2009 as a result of less severe macroalgal blooms, more light penetration, and the already lower

presence of *Z. marina*. However, while the central and south are becoming increasingly eutrophic, the north region still has the lowest eutrophication index value on average and within the same year and continues to be the more degraded region of the estuary (Fertig et al. 2013b).

Population increase and development along the coast are also congruent with seagrass loss over time (Lathrop et al. 2001; Kennish et al. 2008; Kennish et al. 2010; Fertig et al. 2013a). Surveys using aerial photography and GIS mapping conducted between the 1960's and 1990's reported a decline in seagrass coverage in BBLEH of approximately 30-35% throughout the entire estuary (Figure 7). Greater loss occurred in the north (45-60% decline) region of the estuary, while the central and south regions experienced ~30% decline (Lathrop et al. 2001). A comparison of seagrass extent in BBLEH between 2004-2006 and 2008-2010 found that in the last 5-10 years, areal coverage of seagrass has generally declined, mean blade length has decreased, and loss of both above- and below-ground seagrass biomass was particularly prominent throughout the bay. The rate of seagrass decline was greatest from 2004 to 2006, indicating that biomass may have reached a steady state now, albeit with lower abundance than in the past. The declines observed in the seagrass beds of BBLEH are widely attributed to benthic macroalgal blooms, epiphyte growth, and detritus throughout the bay that severely decrease the amount of light reaching the plants, believed to have been caused from the continued nutrient loading of the bay (Kennish et al. 2008; Kennish et al. 2010; Fertig et al. 2013a).

The estuary has significant pressure from commercial and recreational use, and coastal development. The year-round population in the watershed is ~575,000, and in the summer months, the population increases substantially, approaching ~1,500,000. As such, BBLEH hosts a suite of recreational activities, including boating, recreational fishing, swimming, and beach

visits, with an estimated annual economic value of $1.2 billion. Commercial fisheries are also prominent in BBLEH, producing $48.6 million annually, making BBLEH the 16th most valuable commercial fishing port in the United States. Seagrass beds are nursery grounds and habitats for many of these fishery species, including finfish (e.g. summer and winter flounder, Atlantic silverside, blue fish), hard shell clams, and blue crabs (Kaufmann and Cruz-Ortiz 2012).

While commercial and recreational fisheries in Barnegat Bay are still prominent, they have been in decline as eutrophication has increased and ecosystem health has declined, although there is no direct evidence between these declines and seagrass loss, and may have multiple causes. Hard clam landings that comprised 80% of commercial fishing in Ocean County in 1988 have since decreased from ~3524m^3 in the 1970's to only ~21m^3 per year today. The blue crab fishery has also seen a decline in landings, making up 23% of fishing in Barnegat Bay in the 1990's but only 15% today (Kaufmann and Cruz-Ortiz 2012). Therefore, the eutrophication, decline in ecosystem health, and loss of seagrass in BBLEH has many detrimental effects on the economy of the region.

III. Objectives and Hypotheses

The goal of this study was to investigate dissolved sulfide levels in the sediments as a potential threat to seagrass populations of BBLEH. The objectives were to use analyses of the sedimentary redox state, dissolved sulfide, and the ability of the sediments to buffer against sulfide in the system to determine the effects of the extent of eutrophication on the sediment conditions. Sediment characteristics were compared along the north-south eutrophication gradient in the estuary to examine how eutrophication is reflected in the sediments and how it impacts dissolved sulfide. Sediment characteristics were also compared locally between seagrass beds and adjacent barren areas (i.e. those that did not have any seagrass or seagrass

roots present at the time of sampling) to address factors that could impact where seagrass is surviving. However, how long sediments have been barren for is unknown. Using sediment dissolved and solid phase composition I have investigated whether the more eutrophic regions of Barnegat Bay are more reducing and consequently are more prone to sulfide accumulation. I have compared the degree of anoxia in areas covered by seagrass with barren areas and evaluated how the redox conditions in the sediments may affect the ability of seagrass to recover from past declines.

Two main hypotheses drive this study: 1) Sulfide accumulation will be greatest and sediment conditions are more reducing in the northern region of the estuary where nutrient loading, and likely organic matter decomposition, is greatest. Lower sulfide levels and more oxic sediments will be present in the south and central regions where nutrient loading is less and flushing from the open Atlantic Ocean is greater. 2) Seagrass decline and recovery in BBLEH is affected by sulfide and Fe-S dynamics, which will be evidenced by a difference in chemistry between seagrass beds and adjacent barren areas.

IV. Methods

A. Field Sampling

a. Sampling Locations

Sediment and pore water samples were collected from the eastern part of BBLEH along the nutrient loading gradient throughout the seagrass growing season in 2012 and 2013. Sampling occurred in August and October 2012, and in March, June/July, August, and October 2013. The estuary was divided into three segments, North, Central, and South (Figure 5), and samples were collected in two seagrass beds and two adjacent barren areas per segment, for a total of twelve sampling locations (Figure 8). (See Figure's A1-A3 in Appendix for spatial

heterogeneity examples between sites). Exact sampling locations were not marked, rahter sites were revisited using GPS locations and cores were taken in the same area (within ~ 20-25m) at each sampling period but not in the same spot. Barren areas were checked to make sure no seagrass roots were present in the sediment. Seagrass beds contained *Z. marina* or *R. maritima* or both, depending on the site. Seagrass sampling sites also contained variable amounts of algal debris that was not further quantified.

b. Sample Collection

Sediment cores, 3-inches in diameter and 15-20cm deep were collected by manually pushing the corer into the sediment and carefully removing it at each sampling location for pore water analysis. The corer was made of clear PVC to easily identify the sediment-water interface. Pre-drilled holes, taped closed prior to core collection, were used to extract pore waters from the sediment core while still in the core liner by inserting Rhizon samplers at 1, 2, 3, 4, 5, 7, 9, 11, 13, 15 cm below the sediment water interface. Seagrass roots penetrate to only 4-7cm below the sediment-water interface, and therefore 15cm is assumed sufficiently deep to capture the conditions impacting seagrass survival. Rhizons were dry when inserted into cores. Rhizons have been used successfully in marine sediment studies (Seeberg-Elverfeldt et al. 2005; Dickens et al. 2007; Shotbolt 2010) and allow for *in situ* pore water extraction, thereby eliminating the need for glove bags and anaerobic environments typically required in pore water sampling to minimize exposure to oxygen. During sampling, pore waters are extracted through the porous tubing wall of the Rhizon samplers by applying a vacuum, using an acid cleaned disposable syringe. The mean pore size of the porous tubing is ~0.15µm, and therefore no further filtration is required. Eight to 10mL of pore water was extracted at each depth. Generally, sufficient pore water volume was obtained within 2-3 minutes of extraction and

portioned into aliquots. Little core compaction occurred during pore water extraction, except in very sandy cores (dominantly the central barren sites). Pore water aliquots for dissolved sulfide analysis were preserved with 50µL of 20% zinc acetate per 2mL sample to precipitate sulfides as Zn-sulfide, and final concentrations were corrected for the added Zn-acetate. Aliquots for dissolved Fe analysis were acidified to 0.2% HCl and pH <2 using 4µL of 50%HCl per 1mL sample.

At each site, an additional core, 1.5-inches in diameter, was obtained for solid-phase sediment analysis. Cores were sectioned at the same intervals pore waters were collected (0-1, 1-2, 2-3, 3-4, 4-5, 5-7, 7-9, 9-11, 11-13, 13-15cm) and frozen until analysis. Sediment samples were analyzed for October 2012, June/July 2013, and October 2013 sampling periods.

B. Pore Water Analyses

Dissolved sulfide analysis was conducted within one to two weeks of sample collection using the mixed diamine reagent N,N-dimethyl-p-phenylenediamine sulfate and ferric chloride, spectrophotometric method developed by Cline (1969). Precision for H_2S in this study, on average, was within 15% (1sd), as determined by analysis of 3 aliquots each of 50% of pore water samples. Dissolved Fe in pore waters was determined spectrophotometrically on acidified samples using a modified Ferrozine method after Stookey (1970), using HEPES (4-(2-hydroxyethyl)-1-piperazineethanesulfonic acid) as a buffer and hydroxylamine HCl as a reducing reagent.

C. Sediment Analyses

a. Sequential Iron Extractions

A sequential extraction procedure modified after Huerta-Diaz and Morse (1990) and Aller et al. (2004) was used to quantify reactive Fe in the solid sediments. Reactive Fe is defined

as Fe that is susceptible to reaction with sulfide and traditionally includes dithionite-extractable Fe or equivalent and Fe in pyrite (Berner 1970; Canfield et al. 1992; Raiswell and Canfield 1998). In this study I have applied an HCl extraction after Aller and Blair (1996) and Aller et al. (2004), which has been shown to extract highly reactive Fe phases (Fe_{HCl}) including Fe-oxyhydroxides, FeS, and carbonates but not crystalline Fe-oxides or pyrite. Care was taken to use sediments from the inside of each sample that had not been exposed to oxidation during sample storage. First, 6M HCl was added to freshly thawed samples and shaken for 15 minutes to release Fe_{HCl}. The extract was then diluted and the Fe_{HCl} concentrations were measured using the ferrozine method with and without a reducing reagent to distinguish between total Fe_{HCl} and $Fe(II)_{HCl,}$ respectively, in the sample (Viollier et al. 2000). Following the 6M HCl extractions, a 10M HF solution was added to the sediments for 16 hours to release Fe in silicates and any remaining crystalline Fe oxides. The liquid from this extraction was discarded and concentrated HNO_3 was added for 2 hours to release remaining Fe, assumed to only be held in pyrite. The extract was diluted and analyzed with ferrozine with a reducing reagent, to measure total pyrite Fe (Fe_{py}).

b. Total Sediment Digestion

Sediment samples were analyzed for a suite of elements and trace metals, including Al, Fe, Ca, Mn, Mo, Ti, Ni, Co, Cu, and U. Prior to microwave-assisted acid digestions, aliquots of ground, homogenized, freeze-dried sediments were ignited at 480°C for 6 hours in a muffle furnace to combust organic matter. Sample and standard weights were corrected for loss-on-ignition and final concentrations are reported as concentrations in dried, non-ignited sediments.

Concentrated acids (3mL HNO_3, 2mL HCl, 1mL HF) and 3mL MilliQ water were added to sediment samples and microwave-assisted total digestions were conducted in an Anton Paar Multiwave 3000 using a step-wise power increase program. An initial ramp of 10 minutes was

followed by a hold for 10 minutes at 300W. Subsequently, another 10 minute ramp was followed by a 10 minute hold at 500W. The digestion finished with a last 10 minute ramp, and a 30 minute hold at 800W. With this program, temperatures in the digestion vessels reached above 200°C and the maximum pressure was 60bar, allowing for complete digestion of the sediments. Following microwave digestion, samples were dried down and treated three times with 50% nitric acid and repeated dry-downs at ~100°C to drive off any remaining HF and prevent the formation of insoluble fluorides. Dried samples were subsequently re-dissolved with 5mL of 10% HNO_3 and stored in capped centrifuge tubes until analysis. Prior to analysis, samples were diluted to a final HNO_3 concentration of ~2%, and analyzedby Inductively Coupled Plasma-Mass Spectrometry (ICP-MS) using a Thermo Scientific iCAP Q. An internal standard containing Sc, Ge, Rh, In, and Bi was used throughout analysis and the instrument was run in the collision cell mode. Raw counts were corrected for instrument drift using In as the internal standards after determining that this method of drift correction produces the lowest relative standard deviation for repeat analysis of the same sample aliquot (RSD). Calibration curves were produced using linear regression of calibration standards run at the beginning of each run.

The precision and accuracy of the total digestions was evaluated using the percent recoveries of three standard reference materials (SRM) – NRS Estuarine Sediment 1646, USGS MAG-1 Marine Mud, and USGS SCO-1 Cody Shale. SRM's were digested at random, but generally were run once in every 6-8 batches of samples. Accuracies of metal concentrations from total digestions are shown in Table 1 and indicate that ignited samples produce better results than non-ignited samples. 89% or better accuracy was obtained for all metals for EST 1646 and MAG-1, while lower recoveries were obtained for SCO-1. EST 1646, the SRM that best resembles the sediments from BBLEH, has a range of accuracies from 90% to 115%, indicating that this digestion method is appropriate for ignited estuarine samples.

c. Carbon-Nitrogen-Sulfur Analysis

Ground, homogenized, freeze dried sediment samples were analyzed for total C, N, and S on a Carlo Erba NA 1500 elemental analyzer. Previous work on Barnegat Bay sediments from a range of locations and grain size has shown that the measured concentrations of total carbon and organic carbon was within error (personal communication with G. Taghon), implying that the sediments contain no significant amount of total inorganic C. Calcium measurements were done on the total digestions (see above), and be used to verify the absence of significant amounts of inorganic C in the sediments. For CNS analysis, approximately 30-35mg of bulk samples were weighed into tin capsules and vanadium pentoxide was added to catalyze complete S combustion. Check standards and calibration curves were made using sulfanilamide. Precision of sulfanilamide and Standard Reference Materials are shown in Table 2.

D. Statistical Analyses

Data for both pore waters and solid sediment phases were averaged for summer and fall sampling periods. With the exception of pore water results from March 2013, no consistent seasonal trend was discernable (for examples, see Appendix Figure A4-A7), and I will therefore focus on the spatial trends. Pore water results from March 2013 were significantly different than those in the summer and fall. Therefore, March data were excluded from the averaging.

One-way Analysis of Variance (ANOVA) tests were performed and significant differences were determined at the 95% confidence level (when the test statistic, $p, < 0.05$) using the open-source program R. One-way ANOVA's are used to compare means of sample sets by testing the null-hypothesis that each set is drawn from the same population and there is no difference between the means. Two main questions were tested: 1. Did the analyte (e.g. H_2S, Fe, C, N, S, trace elements) vary by segment?; 2. Did the analyte vary by bottom type within a segment?

A change point analysis was done to identify changes in depth profiles of redox sensitive species to indicate at which depth, if any, a transition from oxic to suboxic or anoxic/sulfidic conditions can occur (indicated by the horizontal dashed line on depth profiles Figures 9,10,14,15, and 16). This method determines where there is a significant change in the mean of samples below and above each depth. The analysis was done using the set of functions in the Bayesian Analysis of Change Point Problems (BCP) package in R, which uses Markov Chain Monte Carlo (Barry and Hartigan 1993). For comparison, change points were also determined by calculating the sum of squared residuals (SSR) according to equation [4] and a potential change point was identified at the depth where the SSR was the lowest (Bai 1997). Both methods identified similar change points.

$$SSR(k) = \sum_{i=1}^{k}(X_i - \bar{X}_1)^2 + \sum_{i=k+1}^{N}(X_i - \bar{X}_2)^2 \, , \bar{X}_1 = \frac{\sum_{i=1}^{k} X_i}{k} \, , \bar{X}_2 = \frac{\sum_{i=k+1}^{N} X_i}{N-k} \qquad [4]$$

Principal component analysis (PCA) was conducted using Euclidean distances to identify prominent sources of variance in pore waters and sediments of BBLEH. Prior to analysis, data were normalized by subtracting the variable mean from the sample value and dividing by the standard deviation to give equal weight to each variable in the analysis.

V. Results

A. *Pore Waters*

Pore water profiles of dissolved Fe (Figure 9), averaged for all summer and fall sampling periods (August, October 2012, 2013, and June 2013) showed low levels of Fe in the surficial sediments, with higher concentrations measured in the south segment (15-35µM) than in the central and north segments (8-15µM; $p=1.41 \times 10^{-10}$). Concentrations in all sites initially increased with depth at all sites to a subsurface maximum. There was a peak at 2cm in the north

seagrass, central seagrass and barren, and south barren sites and at 3cm at the south seagrass site, followed by a decrease with depth. At 15cm in all cores, Fe concentrations were ~5-10µM. The north barren site did not show a peak, and instead had its highest Fe concentrations of ~10µM at 1cm and decreased with depth throughout the core. Seagrass sediments had higher dissolved Fe than barren sediments in the south segment only ($p=0.011$) but dissolved Fe concentrations were not statistically different in the north and central segments between seagrass beds and barren areas ($p=0.053$).

Dissolved sulfide (Figure 9) averaged for summer and fall sampling periods (August, October 2012, 2013 and June 2013), had low (10-30µM) sulfide in the top 1cm, increasing sharply to ~100-250µM by 15cm. Average sulfide concentrations were significantly lower ($p=0.003$) in the seagrass sediments of the south segment, where nutrient loading is lower, than those in the north and central segments, while barren sediments were not significantly different across segments of the estuary ($p=0.484$). In both seagrass and barren sediments, sulfide concentrations began to increase below the depth where dissolved Fe peaked, with this increase occurring at shallower depths in the north segment (2-4cm) than in the central (5-7cm) and south (5cm) segments (indicated by the green dashed line on Figure 9).

Sulfide accumulation levels were variable in magnitude over the course of a year and higher sulfide levels were observed in March (Figure 10), after seagrass had died back for the winter. Profile shapes were similar to that described above for summer and fall, and sulfide increased with depth exponentially. H_2S concentrations in the top 5cm were similar in spring to those in summer/ fall (~0-50µM), but reached 400-600µM by 7-11cm sediment depth in the south and central segment sediments. In barren sediments, sulfide concentrations increased to ~2000µM at 15cm sediment depth.

B. *Sediments*

a. Organic Carbon and Nitrogen

Profiles of N and organic C (C_{org}) in the sediments are presented as the average and standard error of concentrations from October 2012/2013 and June 2013 (Figure 11). C_{org}:N molar ratios range from ~3-8 in all segments. It may be assumed that the top 5cm of sediment are the most recently impacted by eutrophication and best reflect the current conditions of the estuary. Therefore, I present average concentrations of N and C_{org} in the top 5cm ± 1 standard deviation to compare how eutrophication is preserved in the sediments and has changed through time. North (0.07 ± 0.03 wt%) and central (0.07 ± 0.03 wt%) segment seagrass sediments, where nutrient loading is greater, contained significantly more N (p=0.004) than in the south segment (0.04 ± 0.01 wt%). The north segment also appeared to have a greater C_{org} content (0.50 ± 0.24 wt%) in seagrass beds, than the central (0.33 ±0.22 wt%) and south (0.22 ± 0.12 wt%) segments, but this was not statistically significant (p=0.12). Nitrogen and C_{org} generally decreased slightly with depth in the sediment. Nitrogen contents range from ~0 to ~0.2 wt% and C_{org} decreased from about ~0.8 wt% at the surface to about ~0.2 wt% at 15cm. Nitrogen was also statistically different by segment in barren sediments (p=0.011), but C_{org} was not (p=0.45). Respectively, N and C_{org} concentrations in barren sediments were 0.03 ±0.01 wt% and 0.26 ± 0.11 wt% in the north, 0.03 ± 0.01 wt% and 0.21 ± 0.17 wt% in the central, and 0.05 ± 0.01 wt% and 0.16 ±0.03 wt% in the south. Seagrass beds had significantly more N (p=0.013) but similar amounts of C_{org} (p=0.57) than barren areas.

b. Sedimentary Iron and Sulfur

Profiles of Fe/Al ratios in the sediments are presented as the average and standard error of concentrations from October 2012/2013 and June 2013. Bulk Fe/Al ratios were relatively

constant with depth, but varied by segment of the estuary. The north segment had an Fe/Al ratio of ~0.55 wt%/wt% slightly elevated from the lithogenic background of average continental crust of 0.5 wt%/wt% (Taylor and McClennan 1985). In contrast, the central and south segments had lower Fe/Al ratios of ~0.4 and 0.35 respectively (Figure 12).

Seasonally averaged reactive Fe concentrations (the sum of $Fe(II)_{HCl}$, $Fe(III)_{HCl}$ and Fe_{py}) were somewhat variable across segments, with a general trend of more reactive Fe in the south than in the north and slightly more Fe in seagrass sediments than barren sediments, particularly in the top 5cm (Figure 13). North seagrass sediments had similar amounts $Fe(II)_{HCl}$ and $Fe(III)_{HCl}$. $Fe(III)_{HCl}$ decreased from ~0.10 wt% at the surface to ~0.04 wt% at 15cm. While there were similar concentrations of $Fe(III)_{HCl}$ at the surface and at 15cm, $Fe(II)_{HCl}$ had a minimum peak at 7cm of ~0.01 wt%, and then increased to 0.05 wt% by 15cm. Fe_{py} was elevated compared to Fe_{HCl} and had a similar shape to $Fe(II)_{HCl}$, showing a decrease from ~0.18 wt% at the surface to ~0.10 wt% at 9cm, and then an increase to ~0.13 wt% at 15cm. In contrast, $Fe(II)_{HCl}$ at the north barren site did not have a mid-depth minimum, and Fe_{py} increased throughout the profile from ~ 0.07 wt% at surface to ~0.10 wt% at 15cm. In the central segment, a decrease from ~0.08 to 0.05 wt% (seagrass) and ~ 0.05 to 0.03 wt% (barren) of $Fe(III)_{HCl}$ with depth was congruent with increases of both $Fe(II)_{HCl}$ and Fe_{py} from ~0.06 to 0.08 wt% (seagrass) and ~0.02 to 0.05 wt% (barren). Unlike the north segment, $Fe(II)_{HCl}$ and Fe_{py} had similar concentrations in the central segment. Sediments in the south also had decreasing $Fe(III)_{HCl}$ from ~0.10 to 0.05 wt% congruent with increasing Fe_{py} from ~0.15 to 0.23-0.35 wt% at both seagrass and barren sites. $Fe(II)_{HCl}$ in the south barren site had a mid-depth minimum at 11cm of 0.06 wt% and the south seagrass site had a minimum at 7cm and concentrations range from ~0.10-0.14 wt% throughout the core.

Solid phase S (Figure 13) displayed a similar trend to those described for Fe_{py} and there was more S in the south segment than in the central and north segments ($p=2.15x10^{-5}$). Generally, there was an increase in S with depth, with the exception of the north and south seagrass sites. Sulfur concentrations increased from ~0.05-0.1wt% at the surface to ~0.15-0.45wt% at 15cm. At the north seagrass site, S decreased throughout the entire core from ~0.3wt% at the surface to ~0.15wt% at 15cm. The south seagrass site showed a decrease in S in the top 7cm, from 0.45wt% to 0.15wt%, followed by an increase to 0.2wt% at 15cm.

c. Trace Metals

Trace metal concentrations are presented as metal to Al ratios in order to normalize concentrations to variable lithogenic inputs. Lithogenic ratios of average continental crust, based on Taylor and McClennan (1985) are indicated by the vertical line on each profile.

Mn/Al ratios were enriched above the lithogenic baseline of 119 ppm/wt% (Taylor and McClennan 1985) in the north segment but were depleted in the central and south segments (Figure 14). In the north segment and at the central barren site, Mn/Al increased in the surficial sediments, with a peak at 3-4cm followed by a decrease with depth throughout the rest of the core (indicated by the red dashed line on Figure 14). The central seagrass site and the south segment sediments decreased throughout the core.

U/Al ratios were enriched above the lithogenic baseline of 0.19 ppm/wt% (Taylor and McClennan 1985) at all sites (Figure 15). Greatest enrichment occurred in the north segment. U/Al displayed similar behavior at all sites. U/Al remained relatively constant or slightly increased in the surface and then increased sharply at depth. This increase occurred at a shallower depth in the north segment than in the central and south segments (indicated by the red dashed line in Figure 15). This increase occurred at 2cm at the north seagrass site, 4cm at

the north barren site, 4cm at the central seagrass site, 5cm at the south seagrass site, and 7cm at both the south seagrass and south barren sites.

Mo/Al ratios were also enriched above the lithogenic baseline of 0.15 ppm/wt% (Taylor and McClennan 1985) and again, greatest enrichment occurred in the north segment (Figure 16). With the exception of the north seagrass site, profiles were similar to those for U/Al, showing some increase in Mo/Al in the surface followed by a more pronounced subsurface increase that occurs around 4-7cm at all sites (indicated by the red dashed line on Figure 16). Unlike the other sites, Mo/Al in the north seagrass site decreased with depth. An initial, shallower, increase in Mo/Al was also found in the central barren, south seagrass, and south barren sites, at 2cm, 3cm, and 3cm, respectively (identified by the orange dashed line on Figure 16).

C. *Principal Component Analysis*

A scree plot (Figure 17) of the Principal component analysis (PCA) showed that principal component axes 1-4 are useful in describing the variance between samples. PCA showed that the 1st and 2nd principal components (PCs) account for 35.82% and 24.26% of the variability, respectively, in BBLEH and distinguished the three segments from one another (Figure 18). This separation best aligned with dissolved Fe^{2+}, Fe_{HCl}, Mn, Ti, and U, indicating that these factors cause the greatest difference in sediment conditions across segments of BBLEH. Sample depth also accounted for minor variability in the samples, as depicted by PC 3 (Figure 19), representing 12.27%, which is best aligned with greater concentrations of C_{org} and excess S, and lower concentrations of H_2S at shallow depths. PC 4 also contributed to the separation of shallow and deeper sediments, representing 6.39% of the variability. $Fe(III)_{HCl}$ and Fe_{py} also seem to explain some of the variation with depth, with more $Fe(III)_{HCl}$ and less Fe_{py} in the surface sediments. PCA

did not find a separation between seagrass sediments and barren sediments within a segment however. PCA analysis showed that sediments are variable with redox sensitive constituents describing most of the variation and indicating a difference in redox conditions throughout BBLEH.

VI. Discussion

The nutrient loading and eutrophication gradients in BBLEH make it a valuable target to investigate if and how water column eutrophication is translated into the sediments. Sediment conditions between seagrass beds and barren areas display similar effects of eutrophication within a segment. Sediment conditions in the north segment, where there is a longer history of eutrophication, display longer term effects of eutrophication on the sediments. In contrast, the central and south segments are more recently eutrophic and here I can investigate the shorter term effects of eutrophication on the sediments. Furthermore, I can investigate how the resultant sediment conditions (e.g. redox state and sulfide) may create unfavorable habitat for seagrass, thereby influencing seagrass decline.

A. *C_{org} and N in the Sediments*

Eutrophication fuels large algal and phytoplankton blooms, which increase the supply of organic matter to the sediments. C_{org}:N ratios can be used to decipher the origin of the C_{org}. In BBLEH, C_{org}:N are ~3-8, consistent with typical marine C_{org}:N ratios of 5-8 compared to terrestrial C_{org}:N ratios > 15 (Hastings et al. 2012), indicating that the organic carbon being deposited into the sediments of BBLEH is of marine origin, as would be expected in a eutrophic setting with intense local production. Sedimentary denitrification would cause a loss of N from the sediments and an increase in the C_{org}:N ratio, but as ratios are not elevated, this is evidence that

denitrification does not appear to be prominent in the BBLEH sediments. Research in the early 1990's on sediment nutrient fluxes in Barnegat Bay suggested that the sediments are a sink for nitrogen(Seitzinger and Isabel 1990). However, denitrification was not measured by Seitzinger and Isabel (1990). Limited (taken only in June 2013, Figure A8) dissolved nutrient data in the sediments collected in this study do not show characteristic NO_3 depth profiles and suggest that denitrification is limited.

Not surprisingly, N concentrations in the sediments align with the eutrophication gradient in BBLEH, with concentrations of 0.07wt% in the north and lower concentrations of 0.04wt% in the south because of differences in nutrient inputs from land in each segment (Figure 11) indicating that the sediments also reflect the eutrophication gradient that has been documented for the water column (Kennish et al. 2011; Fertig et al. 2013b). Organic carbon in the top 5cm, however, is similar for all segments, indicating that the amount of organic carbon may not be driving the redox condition differences between sites discussed below.

Seagrass help to trap algae and also themselves supply organic matter, suggesting that the sediments in seagrass beds would have more C_{org} supplied to them and therefore would have more C_{org} in them. However, there is no significant difference between seagrass beds and barren areas for C_{org}. As such, the lack of variation in sediment diagenesis and reducing conditions (e.g. dissolved H_2S, dissolved Fe, $Mn_{(s)}$ discussed below) between seagrass beds and barren areas within a segment are understandable because of the lack of difference in C_{org}. This is an indication that C_{org} is not limiting and there is some other sediment characteristic that is helping to control what areas are barren and what areas are vegetated.

B. *Pore Water Chemistry*

Pore water chemistry in BBLEH sediments suggests that all sites are reducing, with measurable dissolved Fe and H_2S even at shallow depths at all sites (Figure 9). In oxic environments, Fe is present as solid Fe-oxides. Under anoxic conditions, diagenetic reactions reduce Fe-oxides to dissolved Fe^{2+}. Therefore, the depth at which Fe begins to accumulate in the pore waters is an indication of the oxygen penetration, and signals the transition from suboxic to anoxic conditions. Under sulfidic conditions, dissolved Fe^{2+} reacts with sulfides, forming Fe-S minerals, and dissolved Fe is removed. Consequently, a peak in dissolved Fe^{2+} marks the transition zone from anoxic to sulfidic conditions (Figure 9; Canfield et al. 1993; Thamdrup et al. 1994). In BBLEH, dissolved Fe is present at 1cm depth at all sites suggesting that oxygen penetration is minimal and that the sediments become anoxic within millimeters. Shallow Fe peaks in the north (1-2cm) segment, central seagrass site (2cm), and south barren site (2cm) also suggest that the transition from anoxic to sulfidic sediments occurs at shallow depths across the entire estuary (see the blue dashed line on (Figure 9). A dissolved Fe peak occurs at slightly deeper depths at the south seagrass site (3cm) and relatively higher Fe concentrations (~12-40µM) to ~5cm suggests a wider anoxic zone.

Below the anoxic zone and Fe-reduction, sulfidic conditions occur through the production of H_2S in sulfate reduction. Low levels of H_2S can be present at the bottom of the anoxic zone and concentrations increase once dissolved Fe is depleted (Figure 20). In BBLEH, a noticeable difference in the depth at which H_2S concentrations increase is observed across segments of the estuary (refer to horizontal green dashed line in Figure 9). Generally, the depth of H_2S increase occurs below the Fe peak, in accord with the diagenetic sequence. In the north segment, H_2S increase begins at 2cm, providing further evidence that oxygen penetration is very shallow and the redox zonation is compressed (Figure 9). In the central segment and south

seagrass site, H_2S does not begin to increasing until ~5cm. The south barren site has sulfide increases beginning around 3-4cm, but dissolved Fe is still relatively high (10µM) until ~5cm. Thus, when combined with dissolved Fe data, it appears that the north segment has more reducing conditions, becoming sulfidic at shallower depths. This would be expected to expose seagrass roots to unfavorable habitats and sulfide poisoning. The central and south segments are anoxic, but not sulfidic until twice as deep, below 5cm, and therefore below the depth of most seagrass roots. The seagrass in the central and south therefore appear to have a more suitable habitat due to the lack of sulfide at shallow depth.

The presence of seagrass appears to have an effect on the sulfidic conditions of the sediments, as hypothesized. Although dissolved Fe levels and profile shapes with depth are similar between seagrass and barren sediments, H_2S accumulates deeper and is ~30% lower in seagrass beds. Seagrasses are known to supply oxygen to the sediments surrounding the roots to prevent the accumulation of toxic sulfide (Pedersen et al. 2004). Low peaks (about one third the concentration of the surface) in sulfide concentrations at 2cm and 4cm at the central seagrass site and at 2cm in the south seagrass site, which are absent from barren sites, suggest some sulfide oxidation at these depths facilitated by the seagrass (Figure 9). Though the presence of seagrass does not appear to completely remove sulfide, its presence is correlated with relatively low H_2S concentrations and I infer that it is likely working to protect itself and keep sulfide concentrations low. Furthermore, a lack of evidence for seagrass driven sulfide oxidation, as denoted by the lack of minimum peaks in sulfide concentrations in the north and overall higher sulfide concentrations is a suggestion of either generally higher sulfide production or a less healthy seagrass population that is unable to produce enough oxygen and transport it to the sediments.

Only low H_2S concentrations (10-30µM) in the top 5cm (the depth to which seagrass roots are generally present) are found in BBLEH sediments and even at depths below 5cm, concentrations only approach 100-200µM in both vegetated and barren sites. The sulfidic conditions in BBLEH appear not to be toxic to *Z. marina* yet, which has a tolerance level of up to 400µM sulfide (Goodman et al. 1995; Terrados et al. 1999), and remains present in all segments of the estuary. Recent research on seagrass biomass in BBLEH, however, has found a decrease in both above- and belowground seagrass biomass (8.7g/m^2/year between 2008 and 2010) and a decrease in blade length (from an average of 32cm in 2004 to 21cm in 2010) of *Z. marina (Fertig et al. 2013a)*. Blade length reduction is a known consequence of sulfide poisoning and a response observed by Terrados et al. (1999) at sulfide concentrations of less than 100µM. *Ruppia maritima*, which is dominantly present in the north segment due to lower salinity tolerance and is speculated to also have a lower H_2S tolerance (Pulich 1989), is exposed to shallower (accumulation beginning at 2cm versus 5cm in the south) sulfidic conditions in the north, with concentrations between 30 and 60µM in the top 5cm. Thus, *R. maritima* is likely more vulnerable to continued decline if sulfide concentrations remain or become elevated. Although seagrass response was not measured in this study and sulfide was not measured by Fertig et al. (2013a), it is plausible that seagrass in BBLEH is being harmed by the low levels of sulfide measured in this study.

In the spring, the anoxic zone is not as shallow (by about 1-2cm) and the redox zones are less compressed than in the summer and fall (Figure 10). Over winter, respiration rates and organic matter production decrease, allowing the sediments to become re-oxygenated. Winter storms may also help to mix the sediments and re-oxygenate them. If this occurs and sediments are less anoxic and sulfidic, re-establishment of seagrass is more likely. In the spring, in all but the north and central barren sites, dissolved Fe begins to accumulate between 1 and 2cm and is

near zero in the top 1cm of sediment. The lack of Fe at the surface indicates a deeper oxygen penetration in spring. Sulfidic conditions also occur at deeper depths in the spring than in summer and fall. Whereas sulfidic conditions began at ~1-2cm in the north, ~2cm in the central, and ~3-5cm in the south segments during summer and fall, in the spring, sulfidic conditions (as indicated by an increase in sulfide and denoted by the green dashed line in Figure 10) began at ~3-5cm in the north, ~5cm in the central, and ~4-7cm in the south segments getting progressively deeper to the south. The less compressed redox zonation observed in the spring suggests that the surface sediments of BBLEH are able to recover and become re-oxygenated over winter, rather than allowing sulfide to cumulatively build-up year after year. This may be related to increased storm activity in the winter which can help to mix the sediments (Schoellhamer 1995) and a lack of organic matter production as algal growth and seagrass growth cease for the winter.

High H_2S concentrations of ~400-600µM at 5-7cm and up to 2200µM at 15cm were present in the March 2013 sediments. This suggests that sulfide seasonally reaches and exceeds the tolerance levels of *Z. marina* (400µM; Goodman et al. 1995). Such high sulfide concentrations in the spring were surprising, especially when the surface sediments show signs of re-oxygenation. However, in the winter, seagrass dies back and this may have a two-pronged effect on the sediments. First, the dead seagrass adds more fresh organic carbon to be respired to the sediments. Second, the dormancy of seagrass during the winter limits the bioirrigation of the sediments which would decrease the oxygen supply through the plants' lacunae system. Thus, high spring sulfide concentrations at depth can be consistent with the seasonality of seagrass growth. Furthermore, in the spring, smaller plants may not oxidize sulfide as effectively as larger plants in the summer. Previous studies have shown that *Z. marina* seedlings are killed at concentrations above 680µM sulfide and areas with previous seagrass decline due to sulfide

lack re-colonization if sulfide levels remain elevated (Dooley et al. 2013). Data from this study in BBLEH show that, seasonally, toxic H_2S concentrations are reached. If toxic spring concentrations persist into summer and fall, or the sulfidic zone becomes shallower in spring, seedlings may not survive and seagrass recovery will be limited.

Diurnal cycles in sediment redox state are known to exist in shallow coastal seagrass areas and it is important to note that sampling in this study was conducted between the hours of 10am and 3pm. More oxic sediments are present during the day when seagrass is photosynthesizing and supplying oxygen to the sediments. At night, sediments become more reducing due to respiration (e.g. Lee and Dunton 2000; Pagès et al. 2012). Pagès et al. (2012) have observed a 5 to 10 fold increase of H_2S in *Z. capricorni* sediments in Australia, increasing from near-zero sulfide concentrations in daylight hours to low/moderate sulfide concentrations of 50-100µM at night. Hebert and Morse (2003) recorded a similar cyclic response in *Z. marina* sediments in Oregon for both H_2S and Fe with a 50% increase in H_2S at night, but did not observe a diurnal cycle in barren sediments that lacked daytime oxygen infusion by seagrass roots. I conclude that the low sulfide concentrations measured in BBLEH, particularly in the top centimeters of the seagrass beds reflect this daily redox cycle and record photosynthetically depleted sulfide concentrations. Using the rate of increase in H_2S at night observed by Herbert and Morse (2003), sulfide concentrations in surface sediments might approach ~200-300µM in seagrass beds, suggesting that toxic concentrations are probable at night.

Daily and seasonal effects on pore water chemistry means that any single pore water sample can only provide a short-term description of the redox conditions. Solid phase elemental abundances provide a more integrated long-term signal. Using the combination of both dissolved and sedimentary phase data, the impacts of eutrophication affecting the seasonal seagrass communities can be explored on both a short term basis and a long term basis. The

pore water data presented here suggest that sulfide is not accumulating to toxic levels currently. But, on a long term basis, wider implications for the future health and ability for the ecosystem to recover from the continued eutrophication and degradation of BBLEH can be understood by looking at sediment data.

C. *Sediment Solid Phase Chemistry and Redox Conditions*

Trace metals such as $Mn_{(s)}$, $U_{(s)}$, and $Mo_{(s)}$ are useful indicators of sediment redox state on longer time scales (e.g., Calvert and Pedersen 1993; McManus et al. 2006; Tribovillard et al. 2006). Diagenetic processes in the sediments occur via a sequence of respiration pathways using different electron acceptors to breakdown organic matter, moving from oxic to sulfidic conditions as each receptor is consumed in order of the energy yield from each process. The changing redox conditions also impact many trace metals through use in respiration or by authigenic reactions under varying redox states. The result is characteristic dissolved and solid-phase trace metal profiles across redox zones that provide evidence for the extent of the reducing conditions of the sediments (Figure 20). Unlike many divalent metals, Al is not affected by chemical processes, such as scavenging, redox processes, or biological uptake and behaves essentially conservatively. Normalizing the concentrations of trace metals to Al allow one to identify elemental enrichments or depletions relative to the lithogenic baseline, without the complication of source amount variation. Aluminum normalized metal concentrations can be used to identify authigenic alterations (McManus et al. 2006).

a. Solid Mn

Under low oxygen conditions, microbial Mn-reduction occurs following aerobic respiration and denitrification, making dissolved Mn an indication of sub-oxic conditions

(Canfield et al. 1993; Thamdrup et al. 1994). Microbial and abiotic Mn-reduction reduces solid phase Mn-oxides to dissolved Mn^{2+} and in the presence of Fe^{2+} and H_2S in anoxic and sulfidic conditions, Mn remains dissolved. Once dissolved, Mn^{2+} diffuses up towards the oxic layer where it re-precipitates as a stable $Mn_{(S)}$-oxide at the base of the oxic/denitrification boundary. Consequently, a shallow $Mn_{(s)}$ peak can mark the oxic/suboxic interface in the sediments. If sediments are anoxic at the sediment-water interface, dissolved Mn^{2+} diffuses out of the sediments and is lost to the seawater, resulting in relatively low sedimentary $Mn_{(S)}$. Thus, a depleted $Mn_{(S)}/Al_{(S)}$ ratio relative to a lithogenic $Mn_{(S)}/Al_{(S)}$ ratio of ~119 ppm/wt% (Taylor and McClennan 1985) suggest that Mn is being lost from the sediments.

In BBLEH, $Mn_{(S)}/Al_{(S)}$ ratios generally indicate a suboxic zone at or close to the sediment-water interface, as evidenced by $Mn_{(s)}/Al_{(s)}$ below the lithogenic background of 119ppm/wt%, and do not suggest a difference in the redox state between barren and seagrass sediments. The vertical profiles of $Mn_{(s)}/Al_{(s)}$ ratios are less obvious than for the other proxies discussed below, and identifying a suboxic transition depth is difficult. Nevertheless, $Mn_{(s)}/Al_{(s)}$ ratios can provide some useful information. In the central and south segments, low $Mn_{(S)}/Al_{(S)}$ (<100ppm/wt%) relative to lithogenic $Mn_{(S)}/Al_{(S)}$ throughout the entire core suggest that Mn is being lost from the sediment (Figure 14). If sediments are suboxic at the sediment/water interface, $Mn_{(S)}$-oxides are being reduced to dissolved Mn^{2+}, which is likely diffusing out of the sediments and produces the low $Mn_{(S)}/Al_{(S)}$ measured. Shallow peaks at ~4cm and 2cm at the central barren and south seagrass sites, and a general decrease in $Mn_{(S)}$ at the central seagrass and south barren sites (indicated by the red dashed line on Figure 14), which are characteristic for profile shapes (e.g. Figure 20) further support Mn-reduction and suboxic conditions. At the north seagrass site, depleted $Mn_{(S)}/Al_{(S)}$ (~100ppm/wt%) ratios at the sediment surface also suggest suboxic sediments and a loss of $Mn_{(S)}$ to the dissolved phase and from the sediments with a peak at 3cm.

Curiously however, $Mn_{(S)}/Al_{(S)}$ ratios below the top 1cm in the north seagrass site and in all of the north barren site are enriched (>130ppm/wt%), with no obvious explanation. It is worth noting though that $Mn_{(S)}/Al_{(S)}$ are variable across sampling periods and errors for these samples are relatively large and $Mn_{(S)}/Al_{(S)}$ are probably close to the lithogenic background.

The shallow suboxic zone suggested by $Mn_{(S)}/Al_{(S)}$ in the central and south segments and at the north seagrass site is generally in agreement with the redox zonation suggested by the pore water chemistry. $Mn_{(S)}/Al_{(S)}$ data suggests suboxic conditions in surface sediments, which is consistent with the very shallow anoxic zone indicated by dissolved Fe. However, $Mn_{(S)}/Al_{(S)}$ does not indicate that the sediments in the north are significantly more reducing than those in the south. Like dissolved Fe, and to some degree H_2S, $Mn_{(S)}/Al_{(S)}$ does not show much difference in the reducing conditions and transition depths of oxic to suboxic between seagrass beds and barren areas. It is possible that a high detrital background of Mn is making it hard to detect authigenic $Mn_{(S)}$ signal variations throughout BBLEH. There is an overlap between suggested suboxic conditions by $Mn_{(S)}/Al_{(S)}$ near the surface and anoxic conditions at the same depth suggested by dissolved Fe, but this is likely related to a spatial resolution in these samples that is too coarse to detect a very sharp transition (within 1-4cm) from oxic to suboxic to anoxic conditions. The sediments in BBLEH do however appear to have oxygen penetration depth of few millimeters to 1-2cm into the sediment.

b. Solid U

Sedimentary $U_{(S)}$ enrichments are frequently used as indicators of anoxic conditions (e.g., Cochran et al. 1986; Anderson et al. 1989; Barnes and Cochran 1993; McManus et al. 2006). In oxic seawater, U is soluble and dissolved U behaves conservatively. In the sediments, as conditions become reduced, U is reduced to uraninite, and sedimentary enrichments occur,

especially below the depth of bioturbation where introduced oxygen could re-oxidize the U. Additionally, U is frequently complexed by organic matter and adsorbed onto particles, resulting in a close coupling between $U_{(S)}$ and C_{org} (Cochran et al. 1986; Anderson et al. 1989; Shaw et al. 1990; Brumsack 2006; McManus et al. 2006). The reduction of U from U(VI) to U(IV) occurs in the zone between Fe-reduction and sulfate reduction (Figure 20), causing $U_{(S)}$ enrichments to occur below $Mn_{(S)}$-oxide peaks, and concentrations to increase with depth.

All sites in BBLEH show some $U_{(S)}$ enrichment, with $U_{(S)}/Al_{(S)}$ ratios of ~0.3-1.2 ppm/wt% that generally increase with depth in the core and are well above the $U_{(S)}/Al_{(S)}$ lithogenic baseline of 0.19 ppm/wt% (Figure 15; (Taylor and McClennan 1985; McManus et al. 2006), with no discernable difference between seagrass beds and barren areas. Organic carbon loading caused by eutrophication is a plausible mechanism for the observed enrichment. The increased input of C_{org} to the sediments from large algal blooms could also increase the flux of $U_{(S)}$ into the sediments through complexation by the C_{org}. $U_{(S)}/Al_{(S)}$ concentrations are higher overall in the north that the south, where eutrophication and, potentially C_{org} are greater. The tendency for U to associate with C_{org} can explain this trend; however, there is no significant correlation between authigenic $U_{(S)}$ and C_{org} in the BBLEH samples ($r^2 < 0.5$; Figure 21). McManus et al. (2006) showed that there is a trend between C_{org} burial rate and authigenic $U_{(S)}$, rather than C_{org} concentration that have not been normalized to mass accumulation rates, which may explain the lack of correlation in BBLEH.

The depth profiles of $U_{(S)}/Al_{(S)}$ concentrations do provide information about the vertical redox structure of the sediments though. At all sites, $U_{(S)}/Al_{(S)}$ concentrations are relatively lower at the surface compared to depth (by about 30-60%). A prominent increase occurs at depth at each site, indicating U reduction and enrichment. The increase in $U_{(s)}/Al_{(S)}$ occurs at increasingly deeper depths towards the south of the estuary at (refer to the red dashed line on Figure 15):

2cm at the north seagrass site, at 4cm at the north barren site, at 4-5cm in the central segment, and at 7cm in the south segment. The enrichment at these depths is consistent with U chemistry and reductions under anoxic conditions The depth of anoxia suggested by $U_{(S)}/Al_{(S)}$is below that indicated by the Mn-reduction zone in most sites, and occurs close to the transition to sulfidic conditions suggested by the pore water chemistry. Congruent with dissolved Fe and H_2S, $U_{(S)}/Al_{(S)}$ indicates that the sediments in the north are more reduced at shallower sediment depths than sediments in the south. Thus, the north has a more compressed anoxic zone than the south.

c. *Solid Mo*

Molybdenum and U are similarly affected by redox conditions, but unlike U, Mo removal is closely coupled to H_2S, and is therefore used as a proxy for sulfidic conditions. Under oxic conditions, Mo is dissolved. Under reduced conditions, dissolved Mo is scavenged by sulfide and incorporated into Fe-S minerals, resulting in $Mo_{(s)}$ enrichments. Thus, while $U_{(S)}$ enrichment occurs independent of the presence of sulfide, enrichment of $Mo_{(S)}$ typically occurs only under sulfidic conditions (Shaw et al. 1990; McManus et al. 2006; Tribovillard et al. 2006) and can therefore be used to separate the anoxic and sulfidic zones (Figure 20).

The northern and central segments are generally more enriched in $Mo_{(S)}$ ($Mo_{(s)}/Al_{(s)}$ ~0.5ppm/wt%) than those in the southern segment ($Mo_{(s)}/Al_{(s)}$ ~ 0.4ppm/wt%), but all sites are enriched above lithogenic values ($Mo_{(S)}/Al_{(S)}$=0.15 ppm/wt%; (Taylor and McClennan 1985), suggesting reduced conditions everywhere but more so in the north. In agreement with $Mn_{(s)}$ and $U_{(s)}$, $Mo_{(s)}$ also does not show a difference between seagrass and barren sediments. The lack of difference between seagrass and barren sediments observed suggests that the amount of eutrophication is more important in controlling sediment redox state than the presence or

absence of seagrass beds. Though the role of sediment redox state may not be the primary control on seagrass survival, the environmental redox state does not recover to more oxic conditions in the absence of seagrass. Sedimentary $Mo_{(S)}$ enrichments with depth are expected as sediments get more reducing and are indeed observed at all sites except for northern seagrass site (Figure 16). This enrichment occurs at shallower depths in the northern (3cm) and central (4-7cm) segments compared to in the southern (7cm) sites, consistent with more reduced conditions, a more compressed redox zonation, and more sulfidic conditions described thus far by dissolved Fe, dissolved H_2S, $Mn_{(S)}/Al_{(S)}$, and $U_{(S)}/Al_{(S)}$.

The mechanisms controlling the enrichment of Mo were also looked at. Under sulfidic conditions, a correlation may be expected between Mo and reduced S (i.e. dissolved H_2S or solid Fe-sulfides). However, in BBLEH these correlations are not found. Increases in $Mo_{(S)}$ concentration occur at similar depths to sulfide accumulation, but there is no significant correlation between $Mo_{(S)}/Al_{(S)}$and H_2S ($r^2<0.5$). Correlations also do not exist with reduced S (i.e., the S bound in Fe-sulfide minerals; see below for calculation; Figure 22) or Fe_{py} (Figure 23), though visual inspection of depth profile appears to suggest similar depth tends. Molybdenum can also be scavenged by $Mn_{(S)}$-oxides, causing transient $Mo_{(S)}$ enrichments near the sediment surface under sub-oxic conditions, but as $Mn_{(S)}$-oxides are buried and reduced, the associated $Mo_{(S)}$ is re-released and eventually gets scavenged by sulfides (McManus et al. 2006). In the south segment and at the central barren site, there is an initial, shallower increase in $Mo_{(S)}/Al_{(S)}$ enrichment, at 3cm and 2cm respectively (denoted by the orange dashed lines in Figure 16). There also appears to be small increases in $Mn_{(S)}/Al_{(S)}$ at the same depth in (Figure 14), and suggesting that these $Mo_{(S)}/Al_{(S)}$ enrichments may be a result of scavenging by $Mn_{(S)}$-oxides, as previously shown by McManus et al. (2006). However, there also is no significant correlation between $Mo_{(S)}$ and $Mn_{(S)}$ ($r^2<0.5$) in these segments, indicating that $Mn_{(S)}$ sorption is not the

dominant uptake mechanism of $Mo_{(S)}$. It is possible that insufficient sampling resolution and the long vs. short term proxies of solid-phase vs. pore waters discussed in this study are not sufficient enough to identify any significant correlations. However, these results can provide insight into trends for future study in BBLEH and suggest at least some connection between $Mo_{(S)}$ enrichment and H_2S and $Mn_{(S)}$.

The sedimentary trace metal distributions described here suggest that the north segment is more reducing than the south segment (Figure 24). This observation is consistent with pore water observations, which show that the north also has a more compressed redox zonation transitioning to anoxic and sulfidic sediments within the top 3cm. In contrast, the south segment has a less compressed redox zonation and doesn't become sulfidic until 5-7cm. While the $Mn_{(S)}$ data is somewhat ambiguous, trace metal data further support a more compressed redox zonation in the north, illustrated by greater enrichments in the north than in the south. Prolonged eutrophication in the north appears to have produced these conditions and perhaps future increased nutrient loading in the south will produce more reducing sediments there as well. Trace metals also illustrate similar redox regimes for seagrass and barren sediments, suggesting that eutrophication is a primary control on the sediment state and not the presence or absence of seagrass.

D. *Fe-S Dynamics*

a. Fe/Al

The enrichment or depletion of $Fe_{(S)}/Al_{(S)}$ relative to the lithogenic baseline is another measure of redox conditions. Under oxic conditions, when $Fe(III)_{(S)}$ is present mostly in insoluble $Fe_{(S)}$-oxides, $Fe_{(S)}/Al_{(S)}$ ratios should be close to the lithogenic baseline (0.5 wt%/wt%; (Taylor and McClennan 1985). As oxygen concentrations decrease (under sub-oxic to anoxic conditions), Fe-

reduction coupled to organic matter respiration directly by bacteria or indirectly by sulfide generated from bacterial sulfate reduction will cause a reduction of $Fe(III)_{(S)}$ to soluble Fe^{2+}. If this occurs close to the sediment-water interface, an Fe^{2+} flux out of the sediments results (Canfield et al. 1993; Thamdrup et al. 1994), thereby lowering the $Fe_{(S)}/Al_{(S)}$ ratio. Severmann et al. (2010) have shown that dissolved Fe^{2+} fluxes increase exponentially at 60-80µM bottom water dissolved oxygen, making high Fe^{2+} efflux a sensitive indicator for hypoxia. As conditions become more reducing, dissolved Fe^{2+} flux out of the sediments may decrease again as Fe becomes scavenged by sulfides that can trap Fe in the sediments as pyrite and FeS. An elevated $Fe_{(S)}/Al_{(S)}$ implies that reactive Fe already present in the sediments has become trapped and that reactive Fe from the water column is being actively scavenged and added to the sediments (Wijsman et al. 2001). This is a process that only occurs if bottom waters are sulfidic (Lyons and Severmann 2006).

$Fe_{(S)}/Al_{(S)}$ ratios (Figure 12) in BBLEH that are ~0.05 above the lithogenic background of 0.5wt%/wt% in the north and ~0.05-0.2 below the lithogenic baseline in the central and south also suggest that the northern segment sediments are more reducing than the southern segment sediments. The southern and central segment sediments have higher (by~20-30%) $Fe(III)_{HCl}$ (indicative of more Fe-oxides) and higher dissolved Fe (~2x the concentration) in the top few centimeters than the northern segment does (Figure 13). In the southern and central segments, reduction of $Fe(III)_{(S)}$ is producing the high measured dissolved Fe and suggests low to no oxygen near the sediment-water interface. The high dissolved Fe^{2+} produced at the surface is probably fluxing out of the sediments and lowers the $Fe_{(S)}/Al_{(S)}$ ratios. In contrast, the north segment sediments have likely surpassed the oxygen threshold described by Severmann et al. (2010), and Fe is being scavenged by sulfide causing the lower dissolved Fe^{2+} concentrations, $Fe_{(S)}$ precipitation, and a flux into the sediments, resulting in the slightly enriched $Fe_{(S)}/Al_{(S)}$ ratios

observed. Thus, there is further evidence that the north is more reducing than the south, and Fe dynamics vary spatially in BBLEH.

There is no difference in Fe/Al between seagrass and barren sediments. The lack of difference is in agreement with the lack of difference shown by Mn, U, Mo. This is a further indication that something besides redox state is causing the barren sediments to be barren and not be re-established by seagrass.

b. Reactive Fe and Sulfur

Reactive Fe is a critical geochemical mechanism for the removal of the toxic H_2S from the pore waters and prevention of sulfidic conditions (Jorgensen 1977; Thamdrup et al. 1994; Ruiz-Halpern et al. 2008). Barren and seagrass sediments have similar trends within a segment. However, barren areas generally have less reactive Fe than seagrass sediments. Seagrass help to trap particles, including fine sediment containing Fe, from the water column. The lower reactive Fe in barren areas is likely a result of this because the barren areas are no longer supplied with Fe as readily. PCA of the solid sediment and pore water data shows the importance of reactive Fe (Figure 18; Figure 19), suggesting that H_2S and responses of the sediments to eutrophication are largely driven by reactive Fe in BBLEH. Reactive Fe-oxyhydroxides can dissolve quickly (on the order of mintues to hours; Poulton et al. 2004) in the presence of H_2S. The result is the production of dissolved Fe that then reacts with H_2S. Fe-sulfide minerals form via a chain of reactions (equations 1-3 discussed above) to form FeS and then FeS_2, ultimately removing dissolved sulfide to a solid phase (Rickard 2012). Thus the amount of Fe in the sediments (particularly the amount of Fe in oxides and FeS, i.e. in this study Fe_{HCl}) dictates the sulfide buffering capacity of the sediments, i.e. is titrated by reaction with Fe(II) before it accumulates in the pore waters. As such, sulfide trapping by reactive iron is an important mechanism to

protect seagrass and understand stress from sulfide on seagrass. Once reactive Fe is depleted, there is more sulfide that seagrass needs to oxidize by itself.

$Fe(III)_{HCl}$ does not become fully exhausted, down to the sampled depth (~15cm) in the sediments of BBLEH at any of the sites (Figure 13). This makes the presence of H_2S somewhat puzzling, and may suggest that the Fe(III) is less reactive and is only slowly reduced by sulfide. This discrepancy could also be caused by a number of other factors. It could be a reflection of short-term pore water chemistry and longer-term sediment records that do not allow for direct comparison on the same time scale. The long term average of pore water chemistry may better match the sediment record. Additionally, this discrepancy may be an analytical artifact due to partial re-oxidation of wet sediments, or due to heterogeneous sediments with oxic conditions surrounding seagrass roots and sulfidic conditions further away, whereas pore waters taken in situ will not have this heterogeneity. Regardless, there is a general decreasing trend with depth of $Fe(III)_{HCl}$ that loosely parallels H_2S accumulation and supports the buffering reactions discussed above.

Solid phase $Fe(II)_{HCl}$ is more variable with depth across sites and suggests varying degrees of pyrite formation and buffering capacity across segments (Figure 13). In the north, low $Fe(II)_{HCl}$ (<0.1 wt%) in parallel with low $Fe(III)_{HCl}$ (<0.1 wt%) suggests that there is little Fe left to react with H_2S. Most of the Fe-oxides have already been reduced and reacted with sulfide to form FeS and the FeS has also reacted with additional sulfide to form Fe_{py}. This suggests that the north segment has a decreased ability to remove H_2S via reactions with Fe. The presence of significantly higher (~100 µM vs 45µM) dissolved sulfide at depth in the seagrass sediments of the north segment than the south is possible because of this lack of Fe_{HCl} (0.05-0.18 wt%). In contrast, in the central and south, I suggest that $Fe(III)_{HCl}$ has been, or is being, reduced, and some has reacted with H_2S to form FeS, shown by the down-core increase in and overall higher

concentrations of $Fe(II)_{HCl}$. The presence of $Fe(II)_{HCl}$ further suggests that not all of the FeS has reacted to form pyrite yet unlike in the north, resulting in the lower H_2S concentrations measured in the central and south. Giordani et al. (2008) have shown that sulfide removal slows with repeated sulfide additions because Fe-oxides and FeS are being used up through reduction and conversion to pyrite. The buffering capacity is lowered and residual sulfide concentrations increase in magnitude and become more persistent and create more reducing sediments over time. The northern segment of BBLEH has experienced eutrophication, and likely sulfide accumulation, for a longer period of time than the central and southern segments, and it is therefore not surprising then that the northern segment sediments have less Fe_{HCl}. Lower total reactive Fe ($Fe_{HCl} + Fe_{Py}$) in the northern segment also indicates that the sediments in that region have a lower buffering potential. A greater or longer exposure to H_2S has continually driven reactions 1 and 2 to form pyrite through the reduction of the available Fe_{HCl}, and resulted in the lowered buffering capacity observed in the north.

I use the reactive Fe data to calculate how much of the S in the sediments is present as reduced (S_{red}), that is, the S bound in Fe-sulfide minerals. $Fe(II)_{HCl}$ is likely to be FeS, which consumes one mole of S while Fe_{py} consumes two moles of S, and S_{red} can be calculated as:

$$S_{red} = Fe(II)_{HCl} + 2*Fe_{py} \quad [5]$$

By subtracting S_{red} from the total S measured, the location of any excess S can be determined. This is the S that has not formed Fe-sulfide minerals and is likely present as S of higher oxidation state, such as elemental S^0 (Figure 25). Presence of elemental S^0 can provide further insight into the buffering capacity of the sediments.

Elemental $S^{0\ likely}$ formed from either the oxidation of S_{red} coupled to Fe(III) (equation 1), or more likely, elemental S is from active oxidation of H_2S by the seagrass. Once Fe-(oxyhydr)oxides and the sedimentary buffering capacity become exhausted, sulfide can no

longer be sequestered into Fe-sulfides, and the seagrass will need to rely entirely on actively removing sulfide to avoid poisoning. The supply of oxygen by seagrass to the root zone can oxidize sulfide completely back to sulfate (equation 6). However, in eutrophic estuaries, it is more likely that low oxygen concentrations and decreased photosynthetic ability from increased epiphyte growth and decreased irradiance (Burkholder et al. 2007; McGlathery et al. 2007) yields incomplete oxidation, and sulfide is oxidized incompletely to elemental S^0 (equation 7).

$$H_2S + 2O_2 \rightarrow SO_4^{2-}{}_{(aq)} + 2H^+ \quad [6]$$

$$H_2S + ½O_2 \rightarrow S^o{}_{(s)} + H_2O \quad [7]$$

Excess S data is presented as the average excess S calculated for all periods sampled (Oct. 2012,2013 and June 2013; Figure 25). Negative excess S values in all cores are confounding and indicate that Fe_{py} may be overestimated. However, these overestimates are probably a function of Fe-extraction methodology and therefore all samples should be impacted similarly. Though the actual amount of excess S may vary in magnitude, the trend of more excess S in the north and in barren areas observed likely still exists.

Seagrass sediments have small peaks of S^0 that coincide with root presence and may have been caused by active H_2S oxidation by the plant (circled in red on Figure 25), which barren sediments do not have. Thus, the seagrass in BBLEH appears to be actively protecting itself from H_2S exposure, allowing it to persist under the eutrophic conditions of BBLEH. Barren sediments have elevated S^0, through reaction of Fe-(oxyhydr)oxides with H_2S and active oxidation by seagrass when these areas were still vegetated, and is more pronounced in the northern segment . It is the elevated S^0 in barren sediments that best illustrates the lowered buffering capacity and the biggest driver of difference between seagrass and barren sediments. Sedimentary S^0 provides a historical record of H_2S exposure and subsequent H_2S oxidation throughout the estuary, illustrating greater H_2S exposure, greater reducing conditions, and a

prevalence of exhausted buffering capacity in the north where eutrophication has been occurring for longer. PCA (Figure 18; Figure 19) identify excess S as a main variant between the north and south and between seagrass and barren sediments within a segment, indicating further that an exhausted buffering capacity is an important driver of sediment conditions throughout the estuary. Thus, the north and barren areas are more vulnerable to future H_2S accumulation, and therefore greater seagrass loss.

VII. Synthesis and Conclusions

In this study, how eutrophication impacts the sediment geochemistry of BBLEH has been investigated. The focus is on the redox conditions, sulfide accumulation, and Fe-sulfide dynamics in particular. I have considered both short-term impacts of eutrophication documented by pore water chemistry and long-term impacts documented by solid-phase sediment chemistry. I have explored how these properties influence seagrass decline and recovery in BBLEH.

Trace metal and sulfur results presented in this study demonstrate that eutrophication of BBLEH has worsened reducing conditions in the sediments that become anoxic and sulfidic at shallow sediment depths. Little difference in reducing conditions is observed between seagrass and barren sediments, suggesting that it is not the primary factor influencing where seagrass is surviving. The results of this research suggest that the buffering capacity is the key difference between seagrass and barren sediments in BBLEH. Seagrass has two lines of defense against sulfide – passive sediment buffering by reactive Fe-(oxyhydr)oxides and active oxidation by oxygen pumped down into the roots. Barren areas only have the former as a defense. Fe-oxyhydroxides can be regenerated through the re-oxidation of dissolved Fe and FeS, which will replenish the buffering capacity. But, this requires healthy plants and infauna that can drive

bioturbation and bioirrigation to pump oxygen down into the sediments. This buffering regeneration can occur on a daily or seasonal level, but once the FeS is converted to pyrite, it cannot easily be regenerated and the "effective" reactive Fe pool decreases. Additionally, accumulation of S^0 suggests that the natural Fe-oxide buffer capacity has been exhausted and although elemental sulfur is probably not harmful to seagrass, these conditions make it harder for seagrass to become re-established. Fe chemistry in BBLEH shows that most of the effective reactive Fe pool in barren areas and in the north in general has been used and converted to pyrite and the buffering capacity has been exhausted. Although there is some minor evidence for oxidation by seagrass as a defense mechanism, such as lower accumulation of H_2S in the pore waters at seagrass sites compared to barren sites, it appears that, especially in the north, but also in barren areas throughout, conditions are not conducive to seagrass recovery and re-establishment.

Eutrophication is not uniform throughout the estuary and neither are the resultant reducing conditions of the sediments. Together, $Mn_{(S)}$, dissolved Fe, dissolved H_2S, $U_{(S)}$, and $Mo_{(S)}$ as redox proxies show that the northern segment, which undergoes more eutrophication, has a more compressed redox zonation and has sulfidic conditions occurring at shallower sediment depths. Although sedimentary $Mn_{(S)}$ data are less straightforward, the metal redox proxies suggest that all sediments become suboxic within the top millimeters to 1-2cm of the sediment. However, a finer sampling resolution and dissolved Mn^{2+} and NO_3^- data are necessary to determine the exact depth limit of oxygen penetration in the sediments. Dissolved Fe data further suggest suboxic to anoxic conditions at very shallow depths, with measurable Fe in the top 1cm at all sites. The transition to anoxic conditions suggested by dissolved Fe occurs at 1-2cm in the north, but not until 3-4cm in the central and south. Authigenic $U_{(S)}$ enrichments also suggests a transition to anoxic conditions at shallower depths and an overall more reducing

state (based on a greater $U_{(S)}/Al_{(S)}$ enrichment) in the north. Following the anoxic zone, sediments in all segments become sulfidic as indicated by dissolved H_2S and authigenic $Mo_{(S)}$ enrichments. In the north segment, this is shallow, within 3-4cm's, at a depth where seagrass roots are still present and can be impacted by the sulfide. In the central and south, sulfidic conditions do not begin until ~5-7cms, at the lower limits of seagrass root presence. The long-term record of $Mo_{(s)}$ enrichments places the sulfidic transition at a shallower depth in the north, more eutrophic region. The difference in depths of these redox transitions between the north and south segments demonstrate that continued eutrophication has caused reduced sediments that have a very compressed and shallow redox zonation, which has contributed to the accumulation of toxic sulfide and probably influences seagrass decline.

Sulfide concentrations are elevated in the north compared to the south as well, but despite the differences in eutrophication and the resultant organic matter production, C_{org} does not vary systematically along the eutrophication gradient. Therefore, organic carbon does not appear to be what is limiting or accelerating dissolved H_2S accumulation. This suggests that C_{org} is in excess in all segments and the amount of it is not having a large impact on the reducing conditions. Instead, I find that Fe is more important in controlling sulfide buildup, and reactive Fe cycling and depletion has occurred over longer time frames and under continued eutrophication.

Seagrass is not preventing sulfide accumulation as sulfide is produced and accumulates to similar concentrations in the sediment pore waters of both seagrass beds and barren areas in the estuary. However, summer and fall (when seagrass is present) sulfide concentrations are approaching only 100-250µM, and have not yet reached reported toxicity levels. But, higher dissolved H_2S in the north, more eutrophic region suggests that if eutrophication continues,

suggests that reducing conditions will become more prevalent and dissolved H_2S will reach higher concentrations.

Seagrass helps to capture fine particles that contain much of the Fe supply. If seagrass is unable to re-establish itself in barren areas, it will be harder to replenish sediments with reactive Fe once it has been converted to pyrite and sulfide can continually build up, allowing for more and more toxic concentrations. In the north, it appears that re-establishment of seagrass beds is less likely. Thus, though sulfide is not currently toxic to the seagrass in BBLEH, if eutrophication continues, seagrass is lost due to other stressors (e.g. epiphyte growth), and the buffering capacity declines, shallow sulfide accumulation will likely become more prevalent, particularly in barren and north segment sediments that are already more susceptible. If the current conditions in the north are an indication of future conditions in the central and south that are now becoming more eutrophic, less favorable habitat, increased, shallower sulfide, and more seagrass loss seem likely there as well. The longer-term response of the sediments indicates that the sediments have been and are continually impacted by eutrophication, creating harmful conditions for seagrass that worsen as eutrophication continues. Thus, sediment condition should be considered and monitored to a greater extent in future eutrophication studies, particularly as it relates to the health and survival of seagrass. In BBLEH, as in other eutrophic estuaries, the loss of seagrass removes the numerous services provided by these ecosystems (e.g. habitats for commercial fisheries). Understanding the complete threat to the valuable seagrass ecosystems is key to understanding how the ecosystem may change and impact the socio-ecological relationship between humans and the estuary.

VIII. References

Aller, R.C. 1990. Bioturbation and Manganese Cycling in Hemipelagic Sediments. *Philosophical Transactions of the Royal Society a-Mathematical Physical and Engineering Sciences* 331: 51-68.

Aller, R.C., and J.Y. Aller. 1998. The effect of biogenic irrigation intensity and solute exchange on diagenetic reaction rates in marine sediments. *Journal of Marine Research* 56: 905-936.

Aller, R.C., and N.E. Blair. 1996. Sulfur diagenesis and burial an the Amazon shelf: Major control by physical sedimentation processes. *Geo-Marine Letters* 16: 3-10.

Aller, R.C., C. Heilbrun, C. Panzeca, Z. Zhu, and F. Baltzer. 2004. Coupling between sedimentary dynamics, early diagenetic processes, and biogeochemical cycling in the Amazon–Guianas mobile mud belt: coastal French Guiana. *Marine Geology* 208: 331-360.

Anderson, R.F. 1987. Redox Behavior of Uranium in an Anoxic Marine Basin. *Uranium* 3: 145-164.

Anderson, R.F., M.Q. Fleisher, and A.P. LeHuray. 1989. Concentration, oxidation state, and particulate flux of uranium in the Black Sea. *Geochimica et Cosmochimica Acta* 53: 2215-2224.

Bai, J. 1997. Estimation of a Change Point in Multiple Regression Models. *Review of Economics and Statistics* 79: 551-563.

Banks, J.L., D.J. Ross, M.J. Keough, B.D. Eyre, and C.K. Macleod. 2012. Measuring hypoxia induced metal release from highly contaminated estuarine sediments during a 40 day laboratory incubation experiment. *Science of The Total Environment* 420: 229-237.

Barnes, C.E., and J.K. Cochran. 1993. Uranium geochemistry in estuarine sediments: Controls on removal and release processes. *Geochimica et Cosmochimica Acta* 57: 555-569.

Barry, D., and J.A. Hartigan. 1993. A Bayesian Analysis for Change Point Problems. *Journal of the American Statistical Association* 88: 309-319.

Berner, R.A. 1970. Sedimentary pyrite formation. *American Journal of Science* 268: 1-23.

Bricker, S.B., B. Longstaff, W.C. Dennison, A. Jones, K. Boicourt, C. Wicks, and J. Woerner. 2007. Effects of Nutrient Enrichment in the Nation's Estuaries: a Decade of Change, 156. Silver Spring, MD.

Brumsack, H.-J. 2006. The trace metal content of recent organic carbon-rich sediments: Implications for Cretaceous black shale formation. *Palaeogeography, Palaeoclimatology, Palaeoecology* 232: 344-361.

Burkholder, J.M., D.A. Tomasko, and B.W. Touchette. 2007. Seagrasses and eutrophication. *Journal of Experimental Marine Biology and Ecology* 350: 46-72.

Cai, W.-J. 2011. Estuarine and coastal ocean carbon paradox: CO_2 sinks or sites of terrestrial carbon incineration? *Annual Review of Marine Science* 3: 123-145.

Calleja, M.L., N. Marba, and C.M. Duarte. 2007. The relationship between seagrass (*Posidonia oceanica*) decline and sulfide porewater concentration in carbonate sediments. *Estuarine Coastal and Shelf Science* 73: 583-588.

Calvert, S.E., and T.F. Pedersen. 1993. Geochemistry of Recent oxic and anoxic marine sediments: Implications for the geological record. *Marine Geology* 113: 67-88.

Canfield, D.E., B.B. Jorgensen, H. Fossing, R. Glud, J. Gundersen, N.B. Ramsing, B. Thamdrup, J.W. Hansen, L.P. Nielsen, and P.O.J. Hall. 1993. Pathways of Organic-Carbon Oxidation in 3 Continental-Margin Sediments. *Marine Geology* 113: 27-40.

Canfield, D.E., R. Raiswell, and S. Bottrell. 1992. The Reactivity of Sedimentary Iron Minerals toward Sulfide. *American Journal of Science* 292: 659-683.

Carlson, P.R., L.A. Yarbro, and T.R. Barber. 1994. Relationship of Sediment Sulfide to Mortality of Thalassia-Testudinum in Florida Bay. *Bulletin of Marine Science* 54: 733-746.

Cline, J.D. 1969. Spectrophotometric determination of hydrogen sulfide in natural waters. *Limnology and Oceanography* 14: 454-458.

Cochran, J.K., A.E. Carey, E.R. Sholkovitz, and L.D. Surprenant. 1986. The geochemistry of uranium and thorium in coastal marine sediments and sediment pore waters. *Geochimica et Cosmochimica Acta* 50: 663-680.

Crusius, J., and J. Thomson. 2000. Comparative Behavior of Authigenic Re, U, and Mo during reoxidation and Subsequent Long-term Burial in Marine Sediments. *Geochimica et Cosmochimica Acta* 64: 2233-2242.

Diaz, R.J., and R. Rosenberg. 2008. Spreading dead zones and consequences for marine ecosystems. *Science* 321: 926-929.

Dickens, G.R., M. Koelling, D.C. Smith, L. Schnieders, and I.e. scientists. 2007. Rhizon sampling of pore waters on scientific drilling expeditions: an example from the IODP Expedition 302, Arctic Coring Expedition (ACEX). *Scientific Drilling* 4: 22-25.

Dooley, F.D., S. Wyllie-Echeverria, M.B. Roth, and P.D. Ward. 2013. Tolerance and response of Zostera marina seedlings to hydrogen sulfide. *Aquatic Botany* 105: 7-10.

Duarte, C.M. 2002. The future of seagrass meadows. *Environmental Conservation* 29: 192-206.

Fertig, B., M.J. Kennish, and G.P. Sakowicz. 2013a. Changing eelgrass (*Zostera marina* L.) characteristics in a highly eutrophic temperate coastal lagoon. *Aquatic Botany* 104: 70-79.

Fertig, B., M.J. Kennish, G.P. Sakowicz, and L.K. Reynolds. 2013b. Mind the Data Gap: Identifying and Assessing Drivers of Changing Eutrophication Condition. *Estuaries and Coasts*.

Giordani, G., R. Azzoni, and P. Viaroli. 2008. A Rapid Assessment of the Sedimentary Buffering Capacity Towards Free Sulphides. *Hydrobiologia* 611: 55-66.

Goodman, J.L., K.A. Moore, and W.C. Dennison. 1995. Photosynthetic Responses of Eelgrass (*Zostera-Marina* L) to Light and Sediment Sulfide in a Shallow Barrier-Island Lagoon. *Aquatic Botany* 50: 37-47.

Hastings, R.H., M.A. Goni, R.A. Wheatcroft, and J.C. Borgeld. 2012. A terrestrial organic matter depocenter on a high-energy margin: The Umpqua River system, Oregon. *Continental Shelf Research* 39-40: 78-91.

Hebert, A.B., and J.W. Morse. 2003. Microscale effects of light on H_2S and Fe^{2+} in vegetated (*Zostera marina*) sediments. *Marine Chemistry* 81: 1-9.

Helz, G.R., and J.M. Adelson. 2013. Trace Element Profiles in Sediments as Proxies of Dead Zone History; Rhenium Compared to Molybdenum. *Environmental Science & Technology* 47: 1257-1264.

Hemminga, M.A. 1998. The root/rhizome system of seagrasses: an asset and a burden. *Journal of Sea Research* 39: 183-196.

Holmer, M., and E.J. Bondgaard. 2001. Photosynthetic and growth response of eelgrass to low oxygen and high sulfide concentrations during hypoxic events. *Aquatic Botany* 70: 29-38.

Howarth, R., F. Chan, D.J. Conley, J. Garnier, S.C. Doney, R. Marino, and G. Billen. 2011. Coupled biogeochemical cycles: eutrophication and hypoxia in temperate estuaries and coastal marine ecosystems. *Frontiers in Ecology and the Environment* 9: 18-26.

Huerta-Diaz, M.A., and J.W. Morse. 1990. A quantitative method for determination of trace metal concentrations in sedimentary pyrite. *Marine Chemistry* 29: 119-144.

Hunchak-Kariouk, K., and R.S. Nicholson. 2001. Waterhsed contributions of nutrients and other nonpoint source contaminants to the Barnegat Bay-Little Egg Harbor Estuary. *Journal of Coastal Research* SI 32: 28-81.

Jorgensen, B.B. 1977. The sulfur cycle of a coastal marine sediment (Limfjorden, Denmark). *Limnol. Oceanogr* 22: 814-831.

Kaufmann, G.J., and C. Cruz-Ortiz. 2012. Economic value of the Barnegat Bay watershed, 56: Barnegat Bay Partnership.

Kennish, M.J. 2001. Physical description of the Barnegat Bay-Little Egg Harbor estuarine system. *Journal of Coastal Research* SI 32: 13-27.

Kennish, M.J. 2009. Eutrophication of Mid-Atlantic Coastal Bays. *Bulletin of the New Jersey Academy of Science* 54: 5-12.

Kennish, M.J., S.B. Bricker, W.C. Dennison, P.M. Glibert, R.J. Livingston, K.A. Moore, R.T. Noble, H.W. Paerl, J.M. Ramstack, S. Seitzinger, D.A. Tomasko, and I. Valiela. 2007. Barnegat Bay-Little Egg Harbor Estuary: Case study of a highly eutrophic coastal bay system. *Ecological Applications* 17: S3-S16.

Kennish, M.J., B. Fertig, and G.P. Sakowicz. 2011. Benthic macroalgal blooms as an indicator of system eutrophy in the Barnegat Bay-Little Egg Harbor Estuary. *Bulletin of the New Jersey Academy of Science* 56: 1-5.

Kennish, M.J., S.M. Haag, and G.P. Sakowicz. 2008. Seagrass habitat characterization in estuarine waters of the Jacques Cousteau National Estuarine Research Reserve. *Journal of Coastal Research* SI 55: 171-179.

Kennish, M.J., S.M. Haag, and G.P. Sakowicz. 2010. Seagrass decline in New Jersey coastal lagoons: a response to increasing eutrophication. In *Coastal Lagoons: Critical Habitats of Environmental Change*, ed. M.J. Kennish and H.W. Paerl, 167-201. Boca Raton, FL: Taylor and Francis Publishers.

Lathrop, R.G., and S.M. Haag. 2007. Assessment of Land Use Change and Riparian Zone Status in the Barnegat Bay and Little Egg Harbor Watershed: 1995-2002-2006. New Brunswick, NJ: Rutgers University, Grant F. Walton Center for Remote Sensing and Spatial Analysis.

Lathrop, R.G., R.M. Styles, S.P. Seitzinger, and J.A. Bognar. 2001. Use of GIS mapping and modeling approaches to examine the spatial distribution of seagrasses in Barnegat Bay, New Jersey. *Estuaries* 24: 904-916.

Lee, K.-S., and K.H. Dunton. 2000. Diurnal changes in pore water sulfide concentrations in the seagrass< i> Thalassia testudinum</i> beds: the effects of seagrasses on sulfide dynamics. *Journal of experimental marine biology and ecology* 255: 201-214.

Lyons, T.W., and S. Severmann. 2006. A critical look at iron paleoredox proxies: New insights from modern euxinic marine basins. *Geochimica Et Cosmochimica Acta* 70: 5698-5722.

McGlathery, K.J., K. Sundback, and I.C. Anderson. 2007. Eutrophication in shallow coastal bays and lagoons: the role of plants in the coastal filter. *Marine Ecology Progress Series* 348: 1-18.

McManus, J., W.M. Berelson, G.P. Klinkhammer, K.S. Johnson, K.H. Coale, R.F. Anderson, N. Kumar, D.J. Burdige, D.E. Hammond, H.J. Brumsack, D.C. McCorkle, and A. Rushdi. 1998. Geochemistry of barium in marine sediments: implications for its use as a paleoproxy. *Geochimica et Cosmochimica Acta* 62: 3453-3473.

McManus, J., W.M. Berelson, S. Severmann, R.L. Poulson, D.E. Hammond, G.P. Klinkhammer, and C. Holm. 2006. Molybdenum and uranium geochemistry in continental margin sediments: Paleoproxy potential. *Geochimica Et Cosmochimica Acta* 70: 4643-4662.

Morford, J.L., and S. Emerson. 1999. The geochemistry of redox sensitive trace metals in sediments. *Geochimica et Cosmochimica Acta* 63: 1735-1750.

Mortimer, R.J.G., J.T. Davey, M.D. Krom, P.G. Watson, P.E. Frickers, and R.J. Clifton. 1999. The Effect of Macrofauna on Porewater Profiles and Nutrient Fluxes in the Intertidal Zone of the Humber Estuary. *Estuarine, Coastal and Shelf Science* 48: 683-699.

Orth, R.J., T.J.B. Carruthers, W.C. Dennison, C.M. Duarte, J.W. Fourqurean, K.L. Heck, A.R. Hughes, G.A. Kendrick, W.J. Kenworthy, S. Olyarnik, F.T. Short, M. Waycott, and S.L. Williams. 2006. A Global Crisis for Seagrass Ecosystems. *BioScience* 56: 987-996.

Pagès, A., D.T. Welsh, D. Robertson, J.G. Panther, J. Schäfer, R.B. Tomlinson, and P.R. Teasdale. 2012. Diurnal shifts in co-distributions of sulfide and iron(II) and profiles of phosphate and ammonium in the rhizosphere of Zostera capricorni. *Estuarine, Coastal and Shelf Science* 115: 282-290.

Pedersen, O., T. Binzer, and J. Borum. 2004. Sulphide intrusion in eelgrass (*Zostera marina* L.). *Plant Cell and Environment* 27: 595-602.

Poulton, S.W., M.D. Krom, and R. Raiswell. 2004. A revised scheme for the reactivity of iron (oxyhydr)oxide minerals towards dissolved sulfide. *Geochimica Et Cosmochimica Acta* 68: 3703-3715.

Pulich, W.M.J. 1989. Effects of rhizosphere macronutrients and sulfide levels on the growth physiology of *Halodule wrightii* Aschers. and *Ruppia maritima* L. s.l. *Journal of Experimental Marine Biology and Ecology* 127: 69-80.

Rabalais, N.N., R.E. Turner, R.J. Diaz, and D. Justic. 2009. Global change and eutrophication of coastal waters. *Ices Journal of Marine Science* 66: 1528-1537.

Rabalais, N.N., R.E. Turner, and W.J. Wiseman. 2002. Gulf of Mexico hypoxia, aka "The dead zone". *Annual Review of Ecology and Systematics* 33: 235-263.

Raiswell, R., and D.E. Canfield. 1998. Sources of iron for pyrite formation in marine sediments. *American Journal of Science* 298: 219-245.

Rickard, D. 2012. *Sulfidic Sediments and Sedimentary Rocks*. London: Elsevier Science.

Ruiz-Halpern, S., S.A. Macko, and J.W. Fourqurean. 2008. The effects of manipulation of sedimentary iron and organic matter on sediment biogeochemistry and seagrasses in a subtropical carbonate environment. *Biogeochemistry* 87: 113-126.

Schoellhamer, D.H. 1995. Sediment Resuspension Mechanisms in Old Tampa Bay, Florida. *Estuarine, Coastal and Shelf Science* 40: 603-620.

Seeberg-Elverfeldt, J., M. Schluter, T. Feseker, and M. Kolling. 2005. Rhizon sampling of porewaters near the sediment-water interface of aquatic systems. *Limnology and Oceanography-Methods* 3: 361-371.

Seitzinger, S., and I.E. Pilling. 1993. Eutrophication and nutrient loading in Barnegat Bay: sediment water phosphorus dynamics. Philadelphia, PA: The Academy of Natural Sciences.

Seitzinger, S., R.M. Styles, and I.E. Pilling. 2001. Benthic microalgal and phytoplankton production in Barnegat Bay, New Jersey (USA): Microcosm experiments and data synthesis. *Journal of Coastal Research* SI 32: 144-162.

Seitzinger, S.P.P., and E. Isabel. 1990. Eutrophication and nutrient loading in Barnegat Bay: importance of sediment-water nutrient interactions: year II. Philadelphia, PA: The Academy of Natural Sciences.

Severmann, S., J. McManus, W.M. Berelson, and D.E. Hammond. 2010. The continental shelf benthic iron flux and its isotope composition. *Geochimica Et Cosmochimica Acta* 74: 3984-4004.

Shaw, T.J., J.M. Gieskes, and R.A. Jahnke. 1990. Early diagenesis in differing depositional environments: The response of transition metals in pore water. *Geochimica et Cosmochimica Acta* 54: 1233-1246.

Short, F., and C. McRoy. 1984. Nitrogen uptake by leaves and roots of the seagrass *Zostera marina* L. *Botanica Marina* 27: 547-556.

Shotbolt, L. 2010. Pore water sampling from lake and estuary sediments using Rhizon samplers. *Journal of Paleolimnology* 44: 695-700.

Stookey, L.L. 1970. Ferrozine-A new spectrophotometric reagent for iron. *Analytical Chemistry* 42: 779-781.

Taylor, S.R., and S.M. McClennan. 1985. *The continental crust: its composition and evolution*: Blackwell Scientific Publication,.

Terrados, J., C.M. Duarte, L. Kamp-Nielsen, N.S.R. Agawin, E. Gacia, D. Lacap, M.D. Fortes, J. Borum, M. Lubanski, and T. Greve. 1999. Are seagrass growth and survival constrained by the reducing conditions of the sediment? *Aquatic Botany* 65: 175-197.

Thamdrup, B., H. Fossing, and B.B. Jorgensen. 1994. Manganese, Iron, and Sulfur Cycling in a Coastal Marine Sediment, Aarhus Bay, Denmark. *Geochimica Et Cosmochimica Acta* 58: 5115-5129.

Tribovillard, N., T.J. Algeo, T. Lyons, and A. Riboulleau. 2006. Trace metals as paleoredox and paleoproductivity proxies: An update. *Chemical Geology* 232: 12-32.

Viaroli, P., M. Bartoli, G. Giordani, M. Naldi, S. Orfanidis, and J.M. Zaldivar. 2008. Community shifts, alternative stable states, biogeochemical controls and feedbacks in eutrophic coastal lagoons: a brief overview. *Aquatic Conservation-Marine and Freshwater Ecosystems* 18: S105-S117.

Viollier, E., P. Inglett, K. Hunter, A. Roychoudhury, and P. Van Cappellen. 2000. The ferrozine method revisited: Fe (II)/Fe (III) determination in natural waters. *Applied geochemistry* 15: 785-790.

Wheatcroft, R.A., and C.K. Sommerfield. 2005. River sediment flux and shelf sediment accumulation rates on the Pacific Northwest margin. *Continental Shelf Research* 25: 311-332.

Wieben, C.M., and R.J. Baker. 2009. Contributions of nitrogren to the Barnegat Bay-Little Egg Harbor Estuary: Updated Loading Estimates. In *Barnegat Bay Partnership State of the Bay Technical Report*, 19.

Wijsman, J.W., J.J. Middelburg, and C.H. Heip. 2001. Reactive iron in Black Sea sediments: implications for iron cycling. *Marine Geology* 172: 167-180.

IX. List of Tables

Table 1. % Accuracy from total digestions of Standard Reference Materials: NRS Estuarine Sediment 1646; USGS MAG-1 Marine Mud; USGS SCO-1 Cody Shale for both ignited and un-ignited samples. Al, Ca, Ti, Fe are in weight % and Mn, Co, Ni, Cu, Mo, and U are in ppm ± 1std dev.

	EST 1646			EST 1646-Ignited		
Metal	**Certified Value**	**Measured Value**	**Accuracy(%)**	**Certified Value**	**Measured Value**	**Accuracy (%)**
Al	6.25 ± 0.2	5.79 ± 0.90	92.64	6.25 ± 0.2	5.90 ± 0.58	94.40
Ca	0.83 ± 0.03	0.76 ± 0.13	91.57	0.83 ± 0.03	0.78 ± 0.06	93.98
Ti	0.51	0.49 ± 0.08	96.08	0.51	0.50 ± 0.02	98.04
Mn	375 ± 20	346.16 ± 53.82	92.31	375 ± 20	349.68 ± 19.78	93.25
Fe	3.35 ± 0.10	3.17 ± 0.49	94.63	3.35 ± 0.10	3.21 ± 0.18	95.82
Co	10.5 ± 1.3	9.43 ± 1.517	89.81	10.5 ± 1.3	9.54 ± 0.75	90.86
Ni	32 ± 3	28.76 ± 4.27	89.88	32 ± 3	29.14 ± 2.08	91.06
Cu	18 ± 3	15.45 ± 3.54	85.83	18 ± 3	20.67 ± 2.04	114.83
Mo	2.0	1.84 ± 0.28	92.00	2.0	1.96 ± 0.02	98.00
U	NA	2.65 ± 0.38	NA	NA	2.67 ± 0.02	NA
Average			91.64			96.69

	MAG-1			MAG-1 Ignited		
Metal	**Certified Value**	**Measured Value**	**Accuracy(%)**	**Certified Value**	**Measured Value**	**Accuracy (%)**
Al	8.68 ± 0.16	7.06 ± 1.06	81.34	8.68 ± 0.16	7.76 ± 0.54	89.40
Ca	0.98 ± 0.07	0.88 ± 0.04	89.80	0.98 ± 0.07	0.88 ± 0.04	89.80
Ti	0.45 ± 0.04	0.43 ± 0.01	95.56	0.45 ± 0.04	0.41 ± 0.01	91.11
Mn	759 ± 70	735.68 ± 24.84	96.84	759 ± 70	711.79 ± 24.84	93.70
Fe	4.76 ± 0.42	4.70 ± 0.11	98.74	4.76 ± 0.42	4.54 ± 0.11	95.38
Co	20 ± 1.6	20.99 ± 0.78	104.95	20 ± 1.6	20.78 ± 0.78	103.90
Ni	53 ± 8	49.60 ± 2.64	93.58	53 ± 8	48.53 ± 1.39	91.57
Cu	30 ± 3	25.21 ± 0.69	83.73	30 ± 3	27.22 ± 0.69	90.73
Mo	1.6	1.63 ± 0.05	101.88	1.6	1.61 ± 0.05	100.63
U	2.7 ± 0.3	2.71 ± 0.07	100.37	2.7 ± 0.3	2.58 ± 0.07	95.56
Average			94.68			94.18

	SCO-1			SCO-1 Ignited		
Metal	**Certified Value**	**Measured Value**	**Accuracy(%)**	**Certified Value**	**Measured Value**	**Accuracy(%)**
Al	7.25 ± 0.11	6.36 ± 0.39	87.72	7.25 ± 0.11	6.48 ± 0.20	89.38
Ca	1.87 ± 0.14	1.55 ± 0.02	82.89	1.87 ± 0.14	1.47 ± 0.04	78.61
Ti	0.38 ± 0.04	0.34 ± 0.00	89.47	0.38 ± 0.04	0.32 ± 0.00	84.21
Mn	410 ± 30	367.39 ± 3.39	89.61	410 ± 30	348.57 ± 4.22	85.02
Fe	3.59 ± 0.13	3.37 ± 0.03	93.87	3.59 ± 0.13	3.17 ± 0.04	88.30
Co	11 ± 0.8	10.29 ± 0.09	93.55	11 ± 0.8	10.22 ± 0.14	92.91
Ni	27 ± 4	25.07 ± 0.22	92.85	27 ± 4	24.09 ± 0.27	89.22
Cu	29 ± 2	24.86 ± 0.63	85.72	29 ± 2	24.51 ± 0.09	84.52
Mo	1.4 ± 0.2	1.17 ± 0.08	83.57	1.4 ± 0.2	1.81 ± 0.09	129.29
U	NA	2.84 ± 0.04	NA	NA	2.63 ± 0.03	NA
Average			88.81			91.27

Table 2. % Accuracies from CNS analysis of Standard Reference Materials: Sulfanilamide, NRS Estuarine Sediment 1646; USGS MAG-1 Marine Mud; USGS SCO-1 Cody Shale for un-ignited samples. Concentrations are in weight % ± 1 std dev.

	Sulfanilamide			EST 1646		
Element	**Certified Value**	**Measured Value**	**Accuracy(%)**	**Certified Value**	**Measured Value**	**Accuracy(%)**
C	41.84 +- 2.09	42.69 +- 1.09	102.03	NA	1.63 +- 0.00	NA
N	16.27 +- 0.81	16.8 +- 1.41	103.26	NA	0.17 +- 0.01	NA
S	18.62 +- 0.93	18.36 +- 3.41	98.60	0.96	0.87 +- 0.02	90.63

	MAG-1			SCO-1		
Element	**Certified Value**	**Measured Value**	**Accuracy(%)**	**Certified Value**	**Measured Value**	**Accuracy(%)**
C	2.15	2.21 +- 0.03	102.79	NA	1.04 +- 0.11	NA
N	NA	0.28 +- 0.02	NA	NA	0.037 +- 0.00	NA
S	0.39	0.30 +- 0.05	76.92	0.063 +- 0.009	0.041 +- 0.05	65.08

X. List of Figures

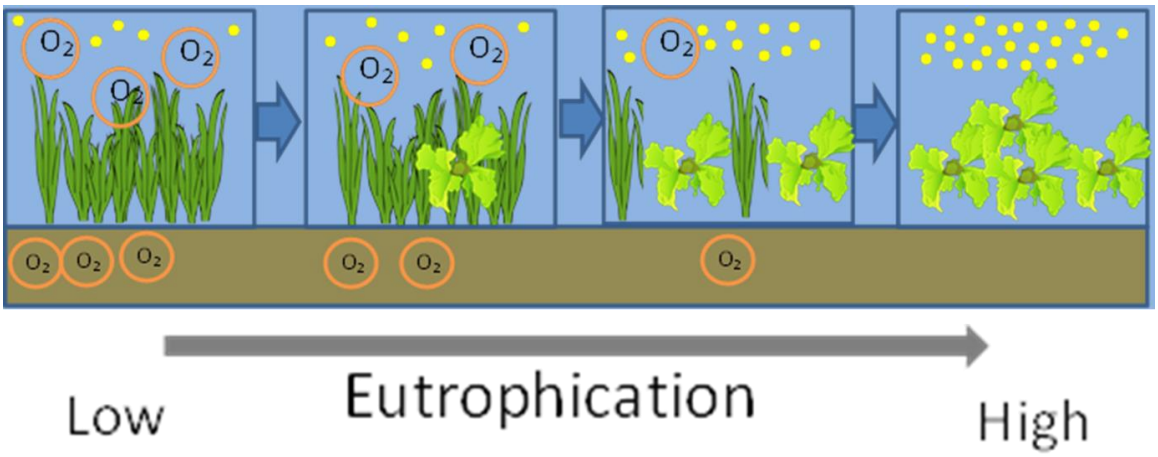

Figure 1. Non- and low- Eutrophic ecosystems are dominated by seagrass, are well oxygenated, and have little micro and macro algae. As eutrophication increases the ecosystems shifts to one dominated by macro and micro algae, have low water column and sediment oxygen, and no seagrass.

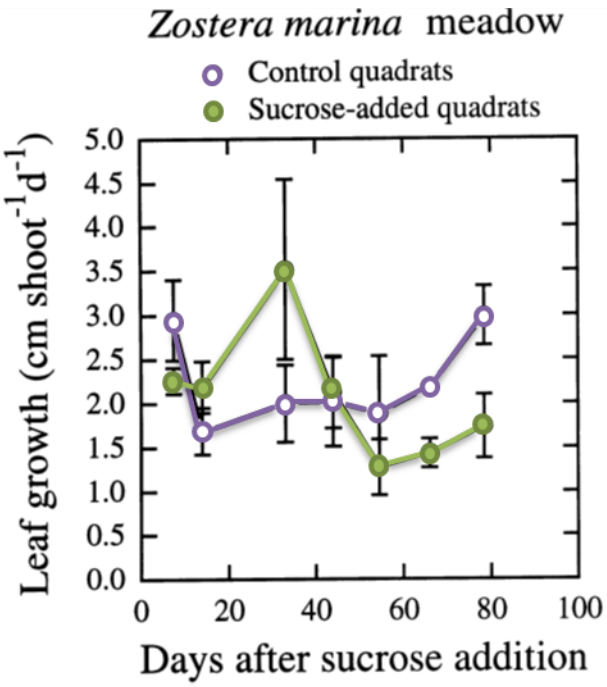

Figure 2. Leaf growth rate of Z. marina was found to slightly decrease after the addition of sucrose. The addition of sucrose was associated with stimulation of anaerobic respiration and a measured increase in pore water sulfide concentrations (Terrados et al. 1999).

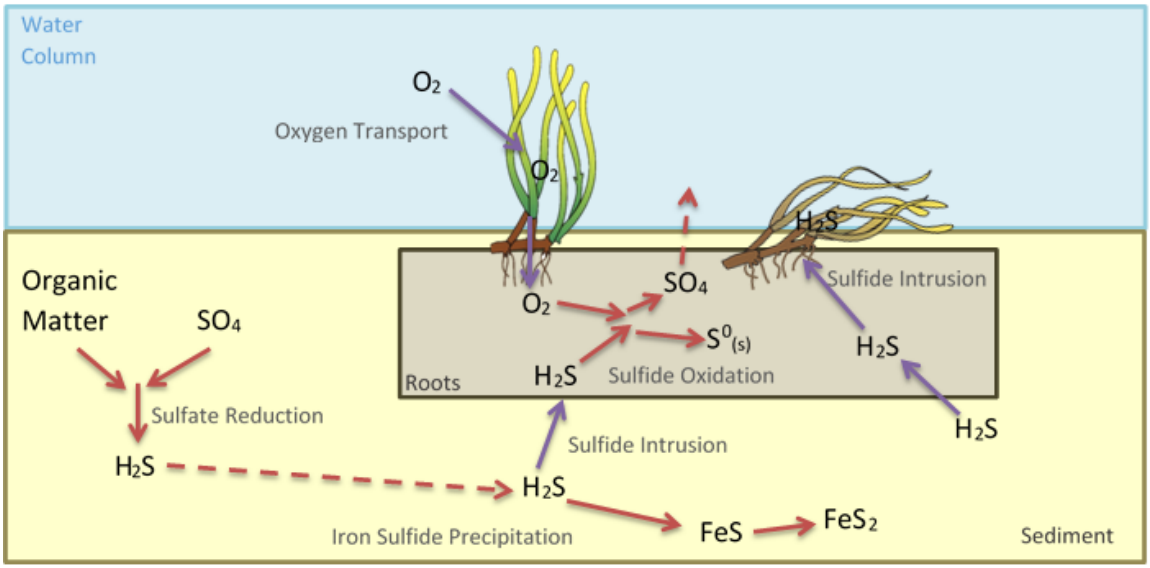

Figure 3. Sulfide is produced through sulfate reduction coupled with organic matter decomposition. Sulfide can intrude into seagrass roots when oxygen transport slows down or ceases. If oxygen is transported to the roots, sulfide can be oxidized. In the absence of oxygen transport, sulfide can intrude into the seagrass blades. Sulfide can also be oxidized with oxygen in the sediment/water column or can precipitate as solid FeS and FeS2.

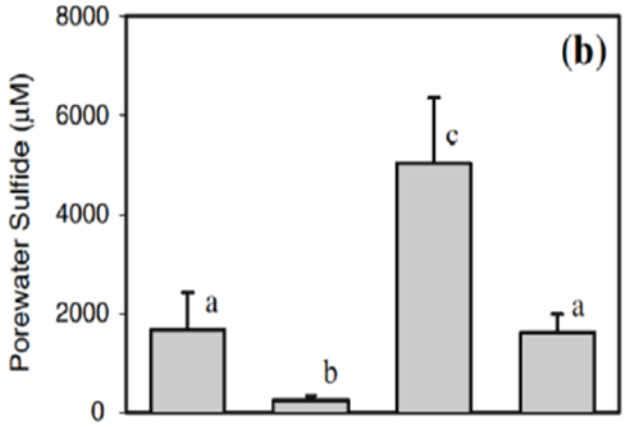

Figure 4. Pore water sulfide concentrations in sediments with (a) no addition of reactive iron oxides or organic matter, (b) iron additions, (c) organic matter additions, and (d) both iron and organic matter additions. The presence of iron lowers dissolved sulfide concentrations, while adding organic matter increases sulfide concentrations (Ruiz-Halpern et al. 2008).

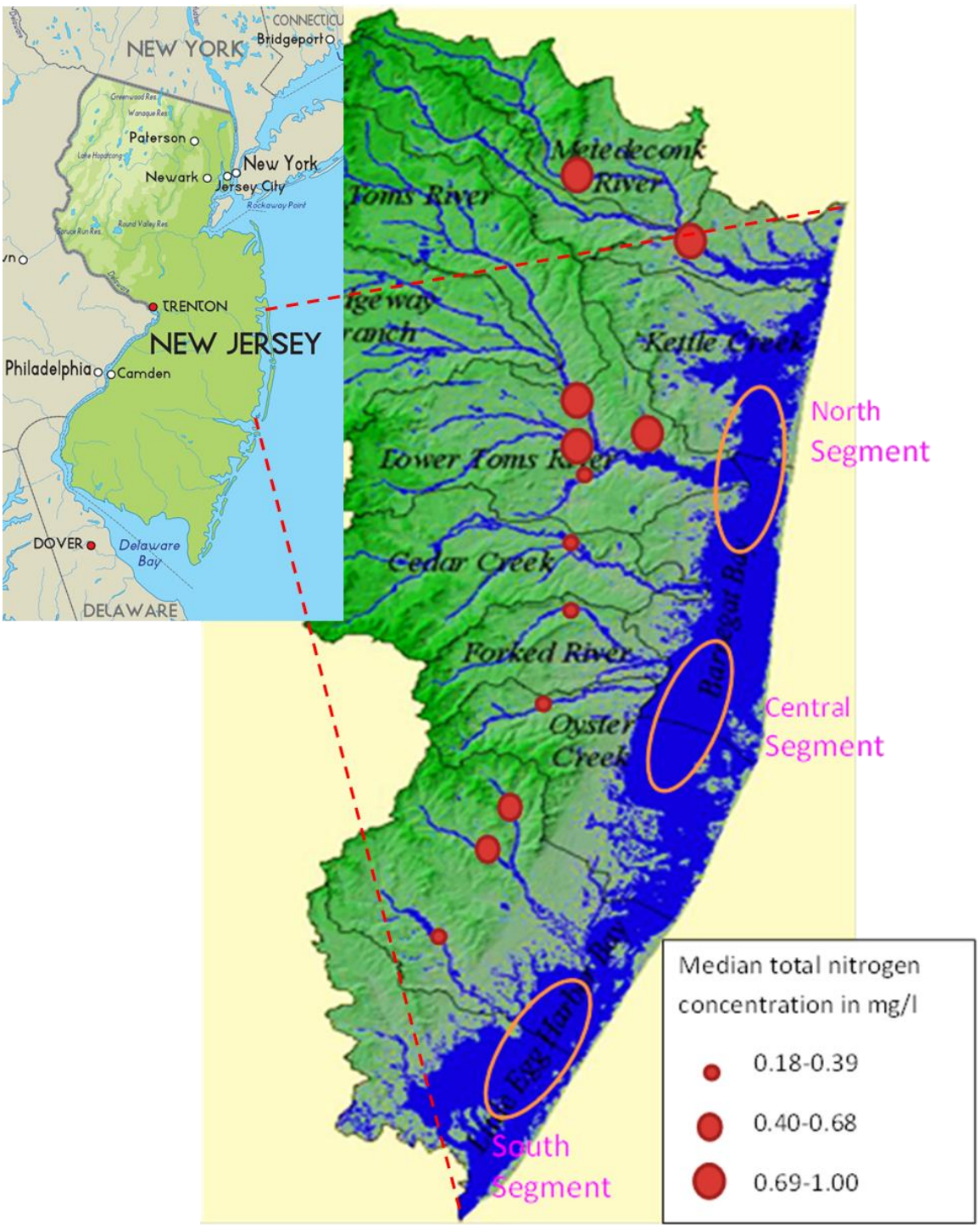

Figure 5. Median nitrogen concentrations into Barnegat Bay-Little Egg Harbor along the 3 segments of the estuary from 1987-2008. Total nitrogen includes ammonia, nitrate, nitrite, ammonia, and other organic N forms. Highest concentrations are seen in the northern watershed, with lower concentrations in the central and southern watershed (nitrogen data from Wieben and Baker 2009; map from www.nj.gov).

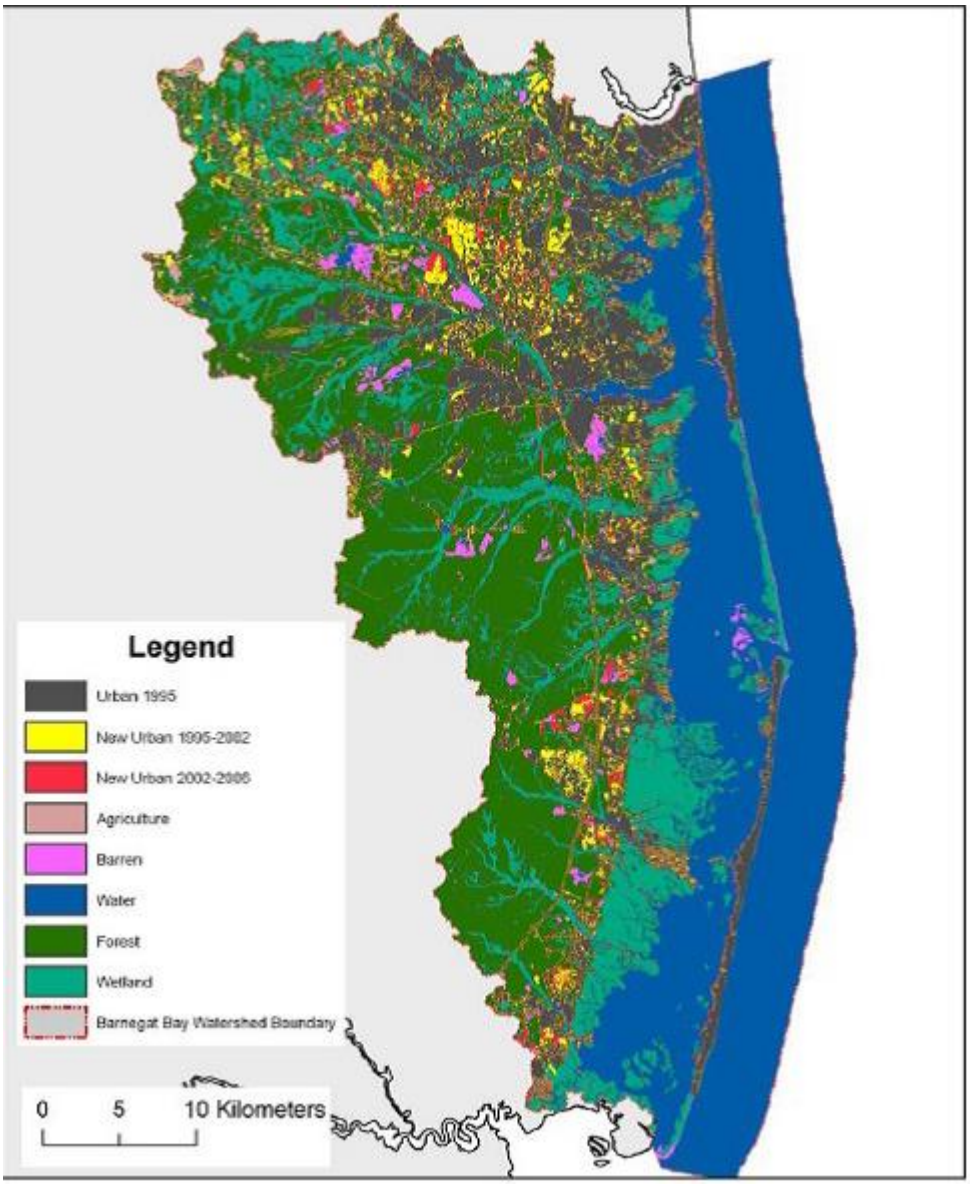

Figure 6. Land use in the Barnegat Bay-Little Egg Harbor watershed in 2006 (Lathrop and Haag 2007). The north region, surrounding the Toms River area are highly urbanized with little to no wetlands and forests. In contrast, the south region of the watershed has some urbanized land, but has also has a significant amount of forests and wetlands.

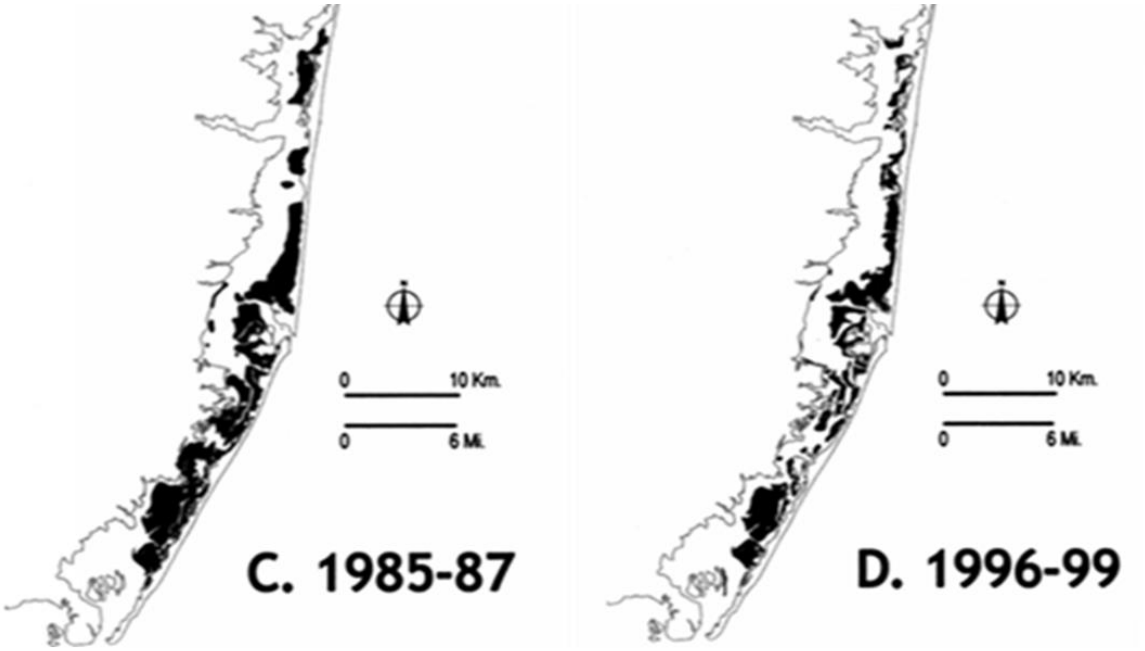

Figure 7. Historic seagrass distribution in Barnegat Bay-Little Egg Harbor from the 1960's through the 1990's. There has been a decline in seagrass throughout the entire estuary of approximately 30-35%, with greatest loss in the northern and central regions (Lathrop et al. 2001).

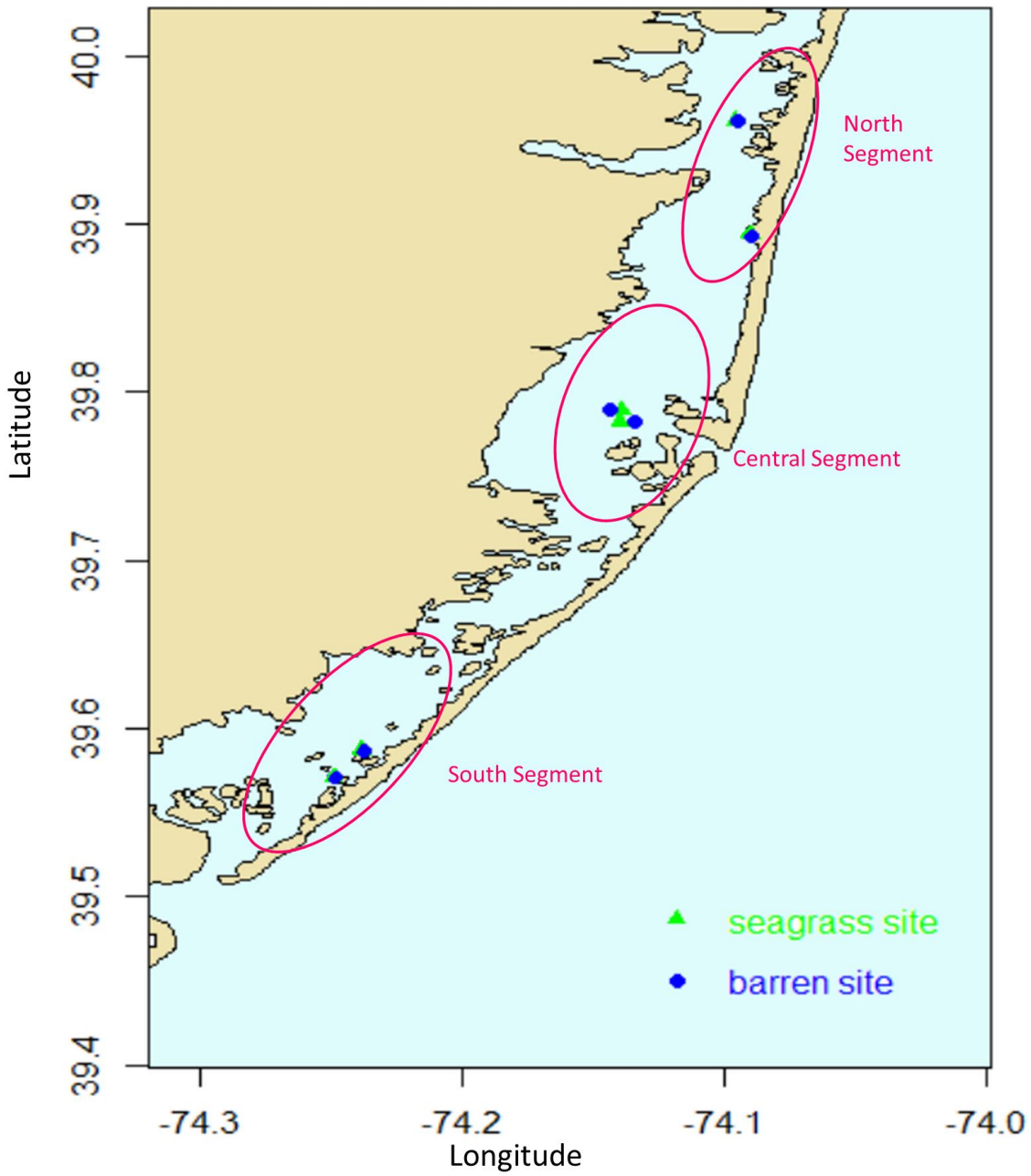

Figure 8. Locations of sampling sites in BBLEH. Sediments and pore waters were collected from seagrass beds and adjacent barren areas. Green triangles indicate seagrass sites and blue circles indicate barren sites. 2 seagrass sites and 2 barren areas were sampled in each segment of BBLEH.

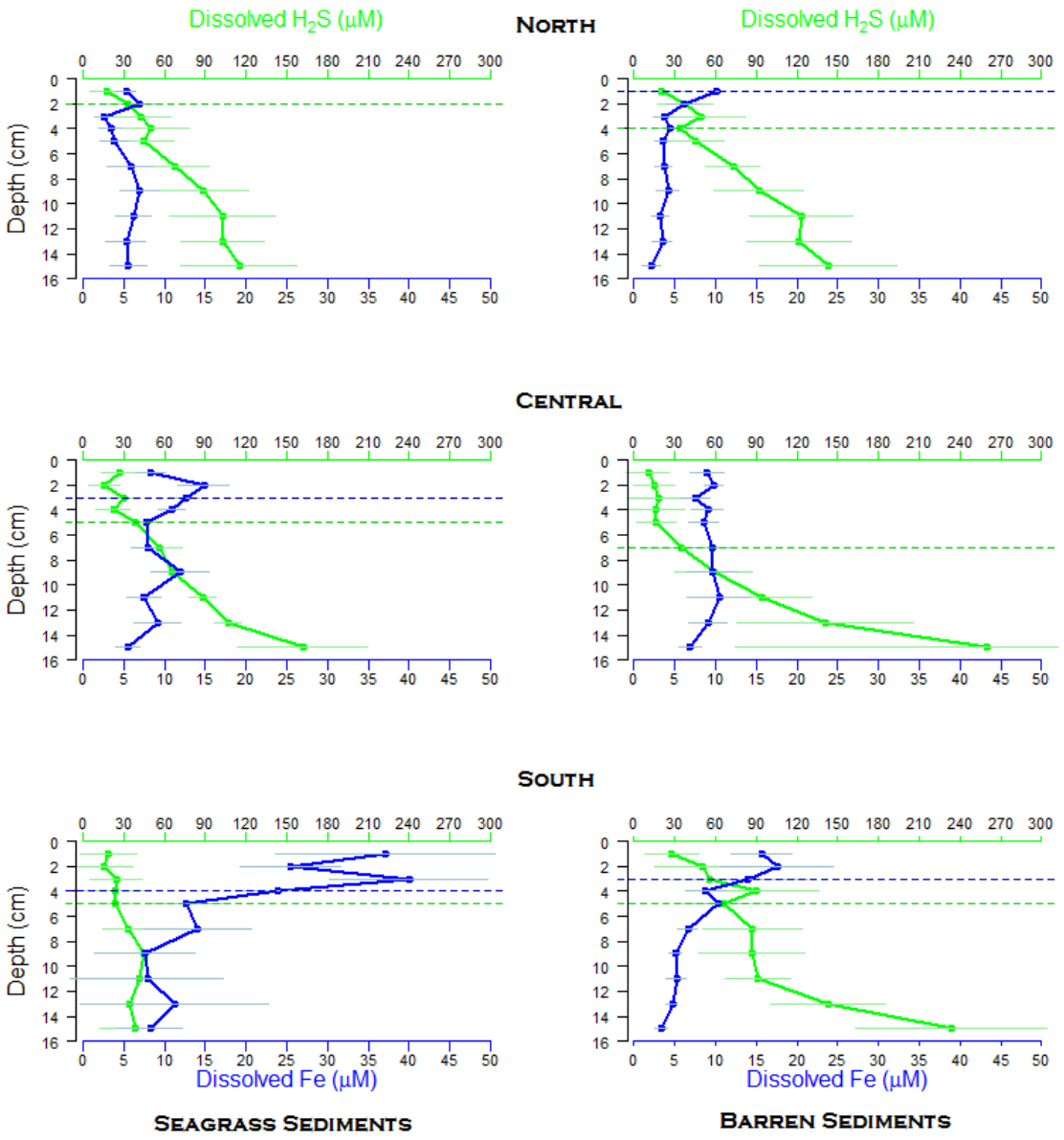

Figure 9. Average summer/fall dissolved sulfide (green) and dissolved iron (blue) with standard error in BBLEH. Porewaters were analyzed in June, August, and October 2012 and 2013. The blue dashed line represents the suggested transition from suboxic to anoxic conditions as indicated by depletion of iron and the green dashed line represents the suggested transition from anoxic to sulfidic conditions as indicated by the accumulation of sulfide (both determined using change point analysis).

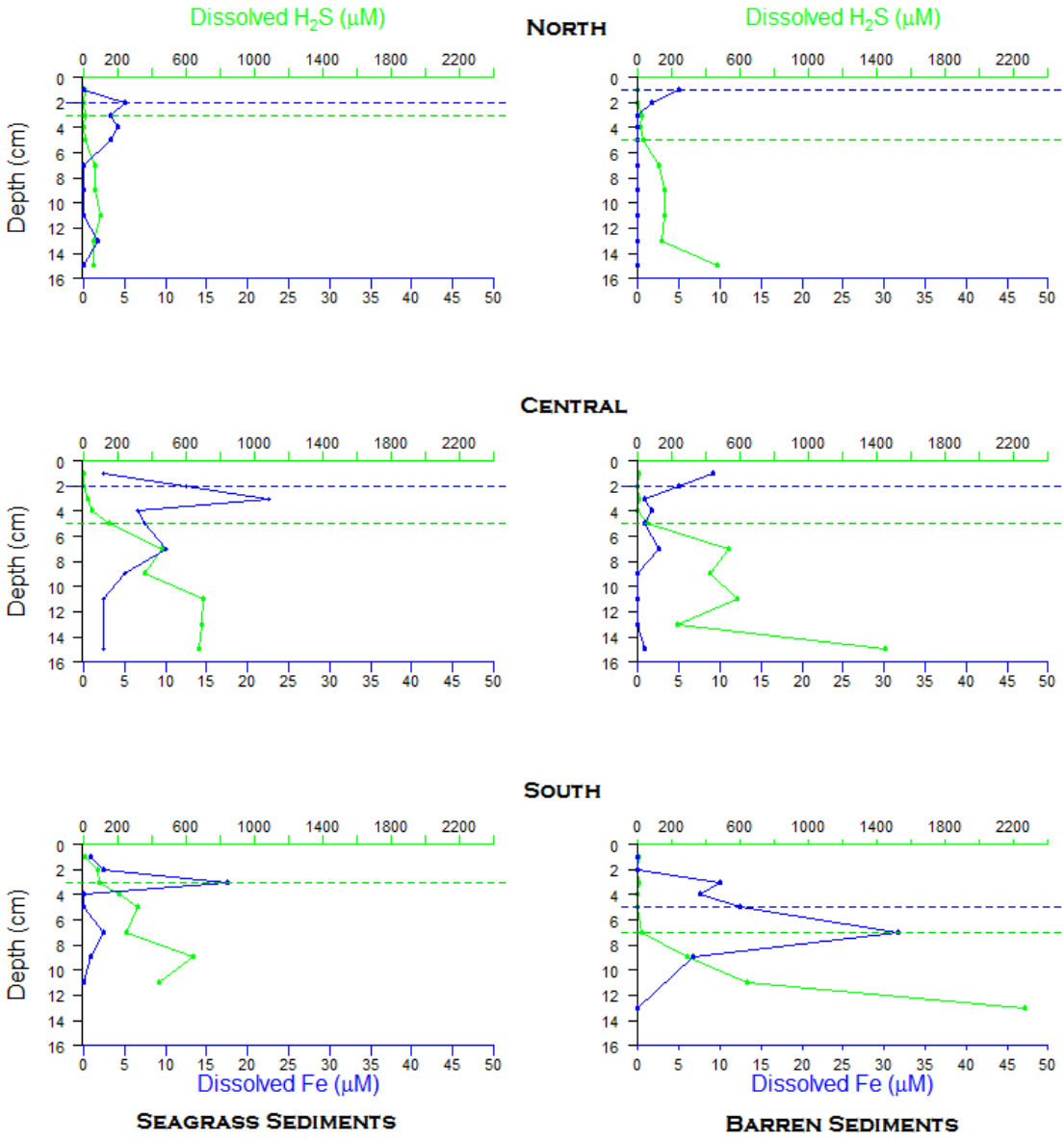

Figure 10. March 2013 dissolved sulfide (green) and dissolved iron (blue) in BBLEH. The blue dashed line represents the suggested transition from suboxic to anoxic conditions as indicated by depletion of iron and the green dashed line represents the suggested transition from anoxic to sulfidic conditions as indicated by the accumulation of sulfide (both determined using change point analysis).

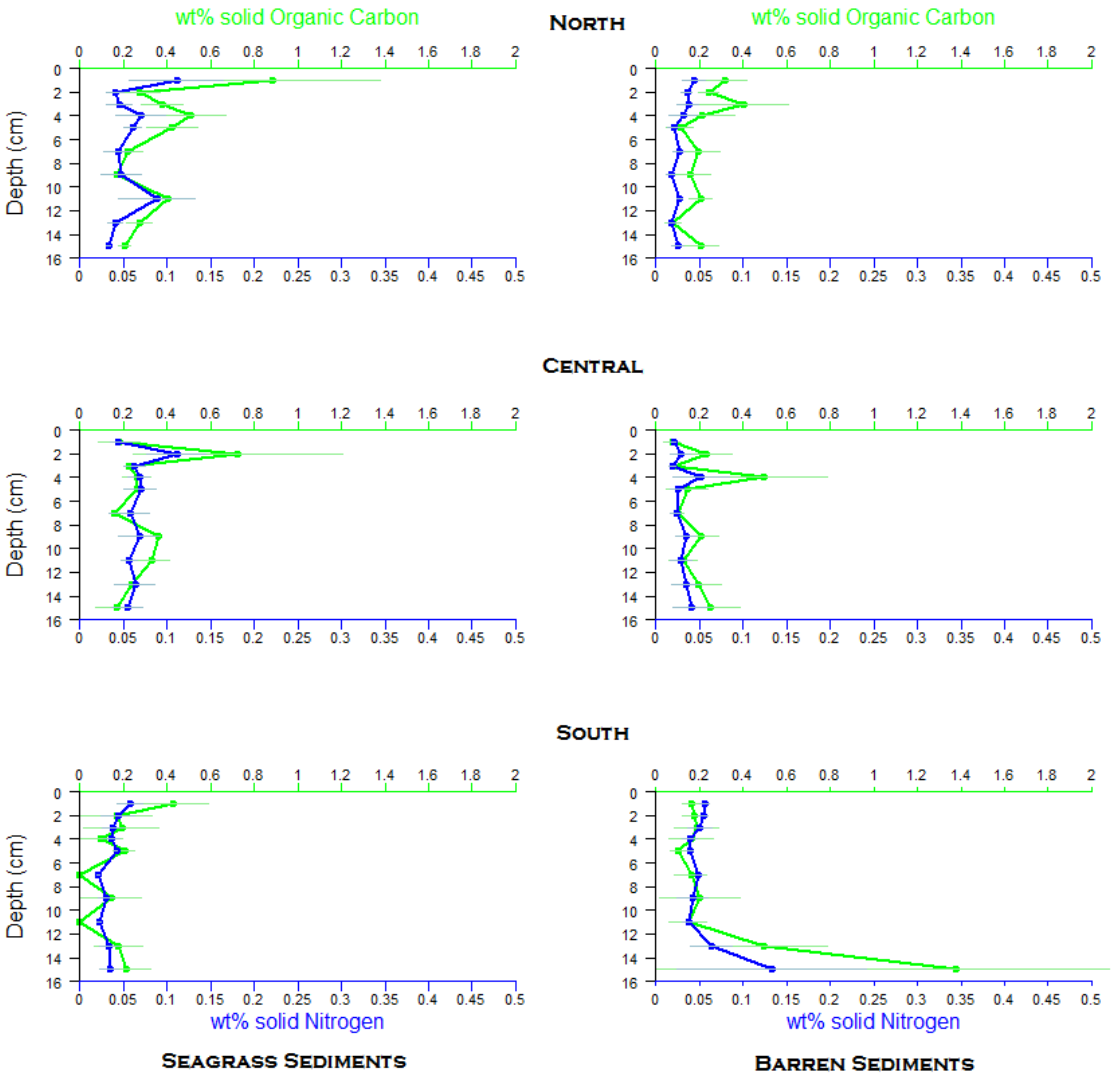

Figure 11. Average Organic Carbon (green) and Total Nitrogen (blue) with standard error in the sediments of BBLEH. Samples were analyzed in Oct 2012 and 2013 and June 2013.

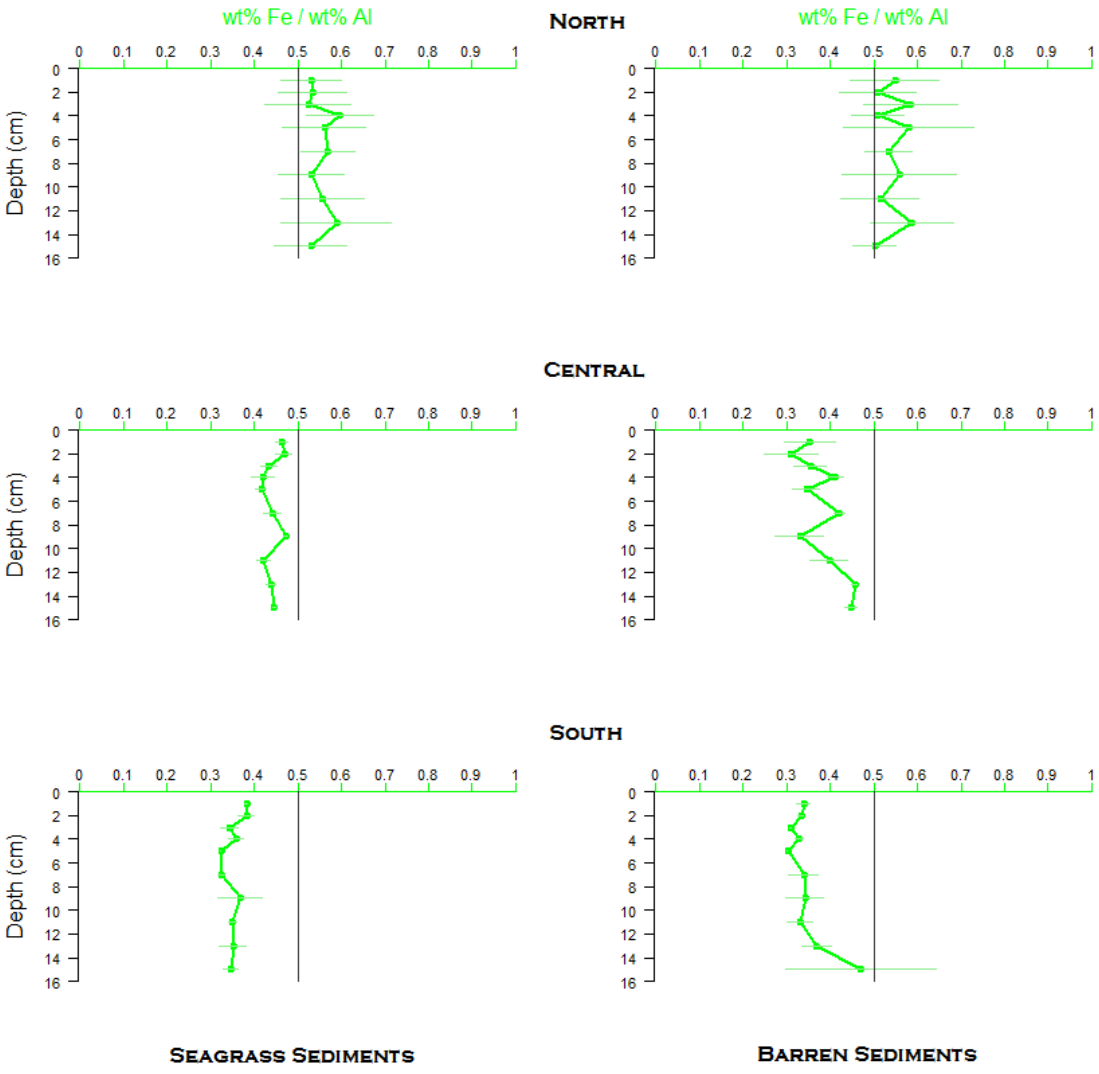

Figure 12. Average Fe/Al ratios with standard error in the sediments of BBLEH. Samples were analyzed in Oct 2012 and 2013 and June 2013. The vertical gray line represents the lithogenic baseline of average continental crust of 0.5wt%/wt% (Taylor and McLennan 1985).

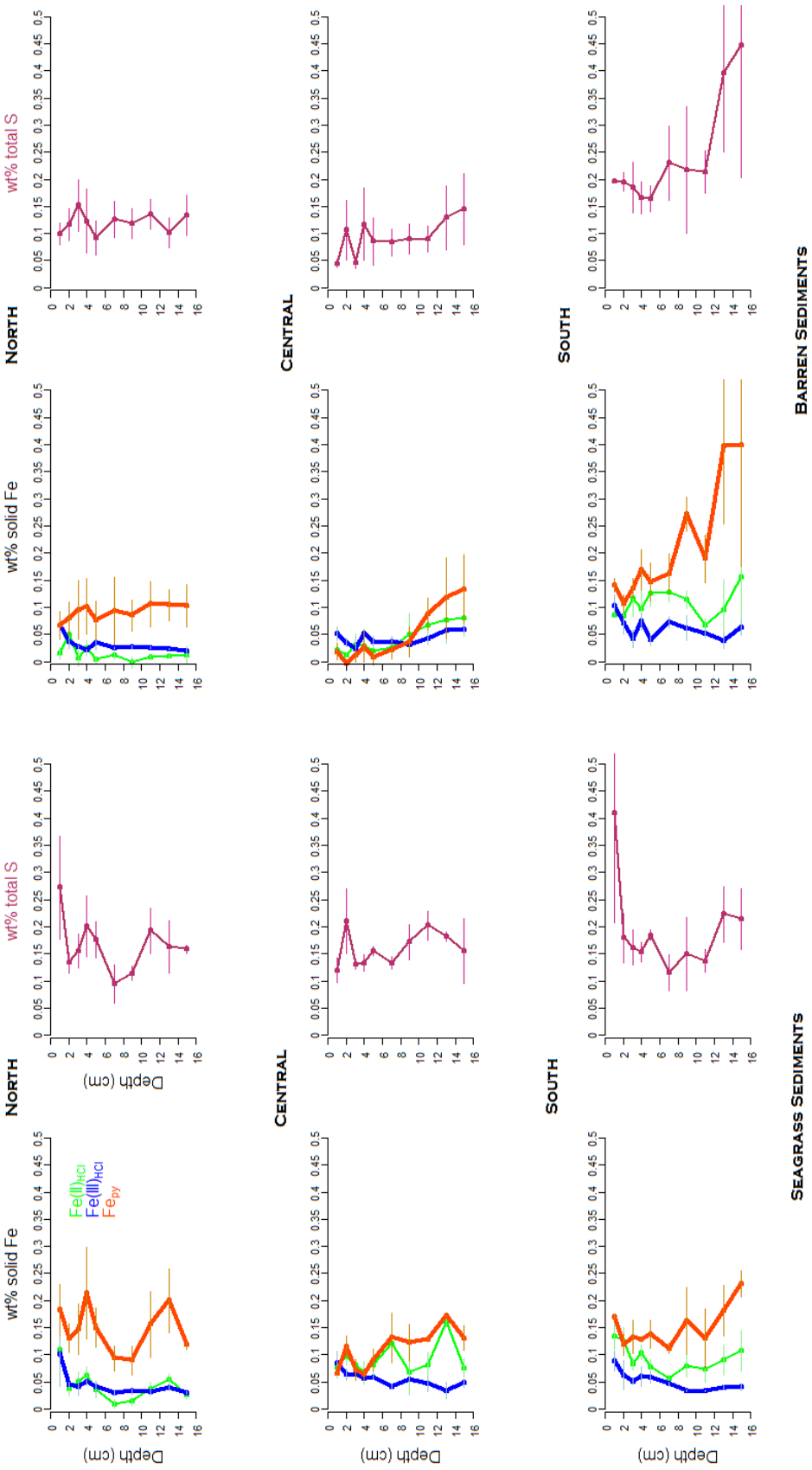
Seagrass Sediments
Barren Sediments
North
Central
South
wt% solid Fe
wt% total S
Depth (cm)
Fe(II)HCl
Fe(III)HCl
FePY

Figure 13. Average Fe(II)HCl (green), Fe(III)HCl (blue), Pyrite-Fe (orange), and Total S (maroon) with standard error in the sediments of BBLEH. Sediments were analyzed in October 2012,2013 and June 2013.

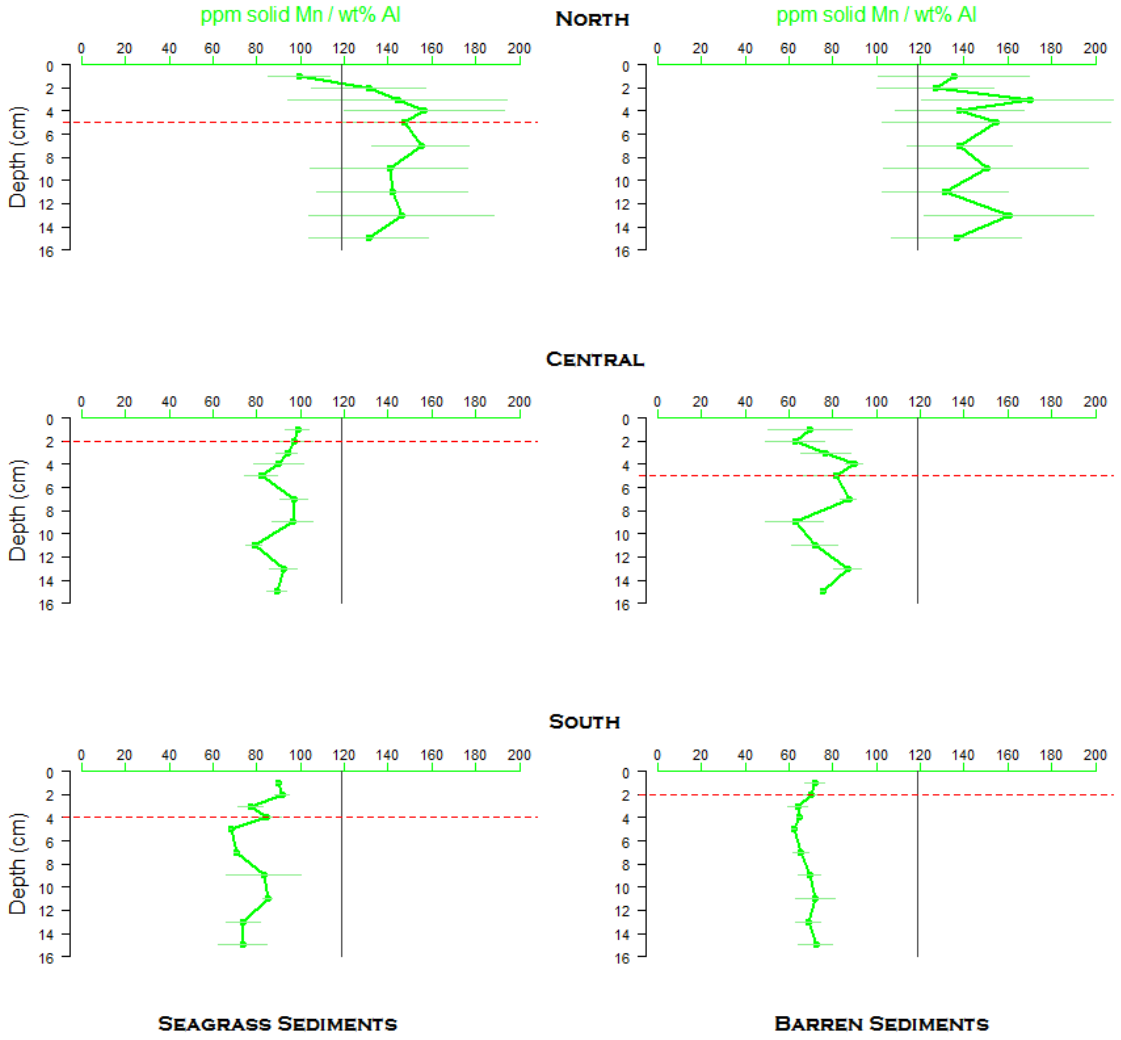

Figure 14. Average Mn/Al with standard error in the sediments of BBLEH. Samples were analyzed in Oct 2012, 2013 and June 2013. The vertical gray line represents the lithogenic baseline of average continental crust of 119 ppm/wt% (Taylor and McClennen 1985). The red dashed line represents the suggested transition to suboxic conditions, as indicated by a decrease in Mn (determined using change point analysis).

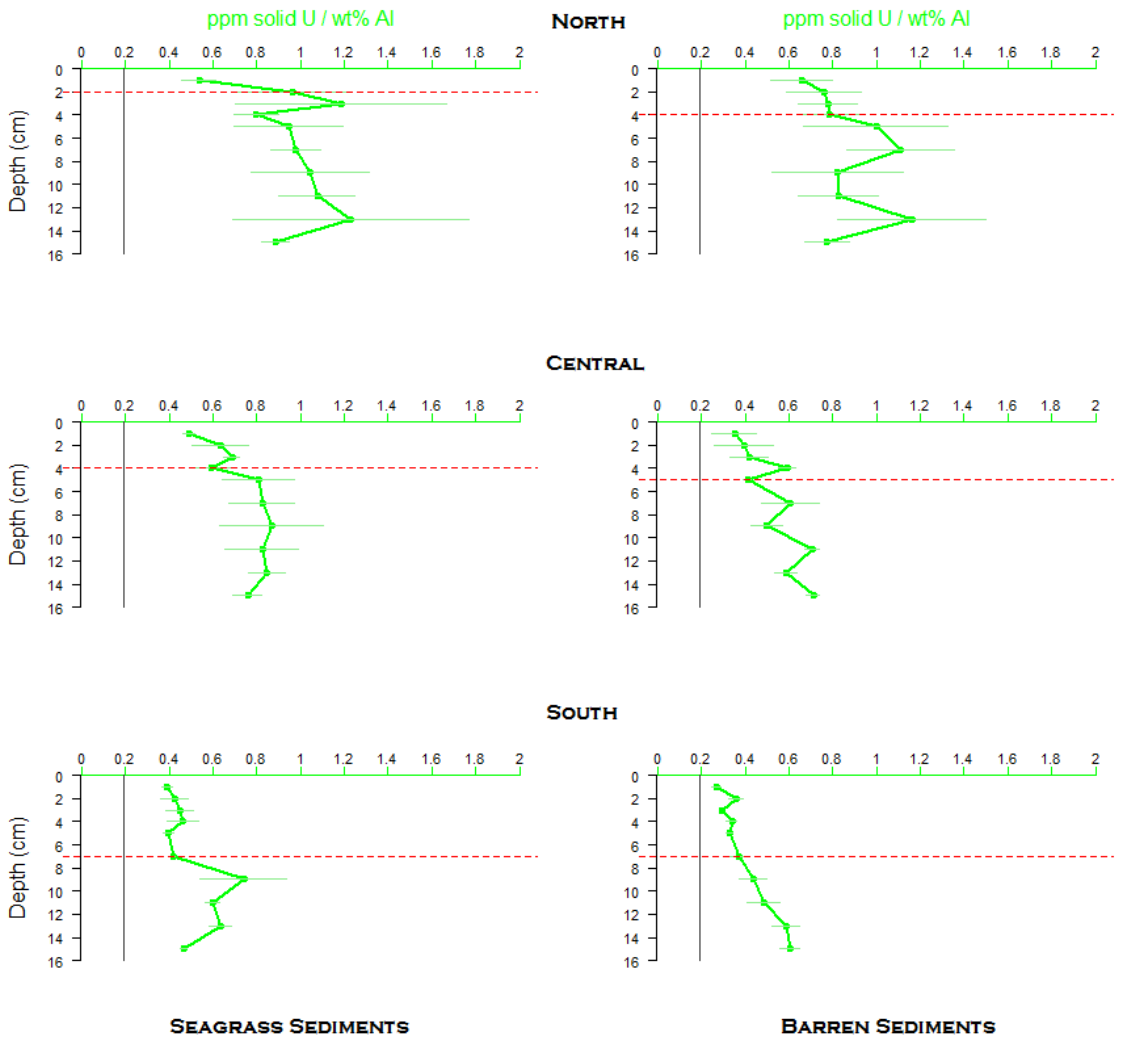

Figure 15. Average U:Al with standard error in the sediments of BBLEH. Samples were analyzed in Oct 2012, 2013 and June 2013. The vertical gray line represents the lithogenic baseline of average continental crust of 0.19 ppm/wt% (Taylor and McLennan 1985). The red dashed line represents the suggested transition to anoxic/sulfidic conditions, as indicated by a sharp increase in U (determined using change point analysis).

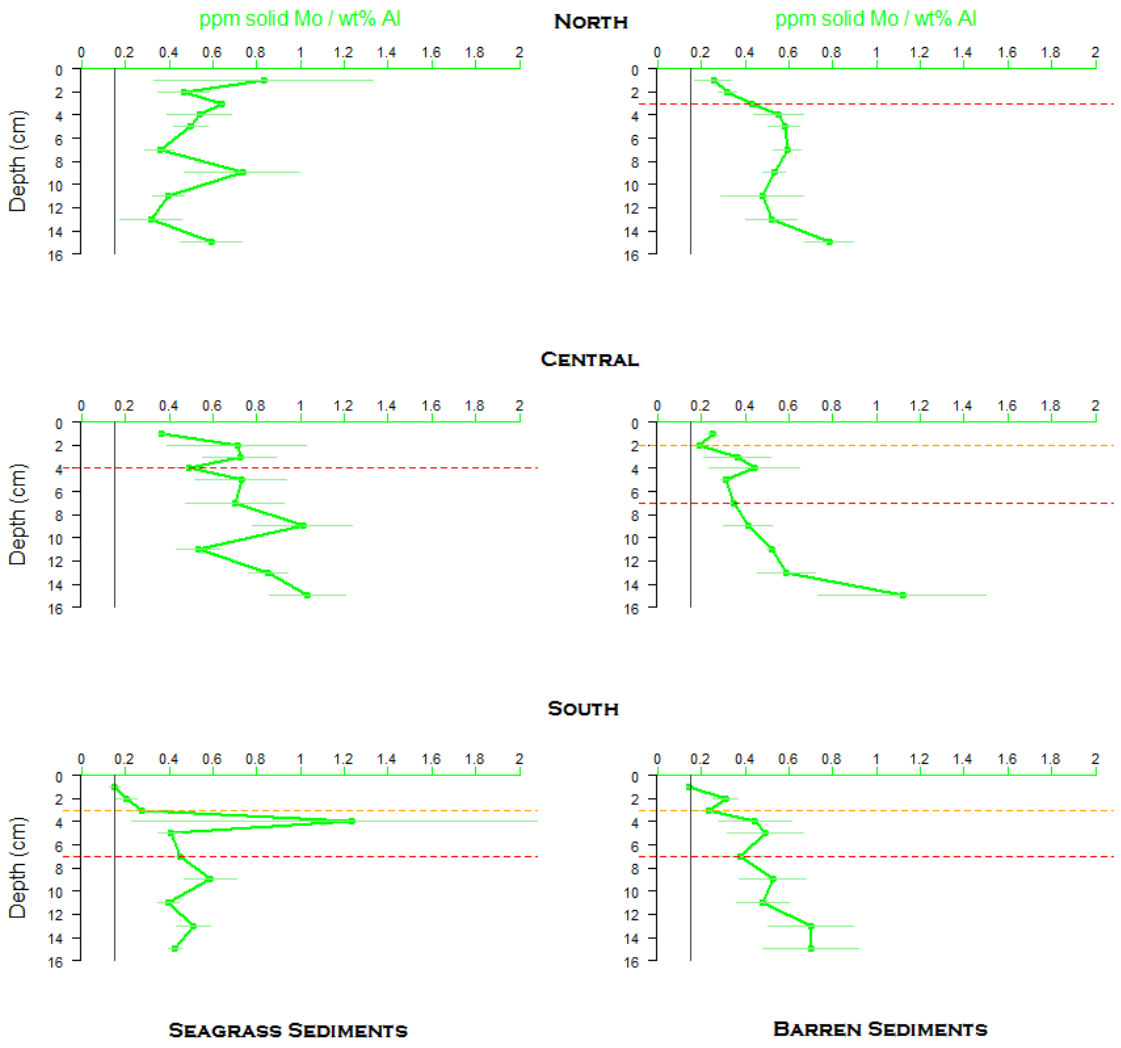

Figure 16. Average Mo/Al with standard error in the sediments of BBLEH. Samples were analyzed in Oct 2012, 2013 and June 2013. The vertical gray line represents the lithogenic baseline of average continental crust of 0.15 ppm/wt% (Taylor and McLennan 1985). The red dashed line represents the suggested transition to sulfidic conditions, as indicated by a sharp increase in Mo and the orange dashed line represents a suggested enrichment due to scavenging by Mn (both determined using change point analysis).

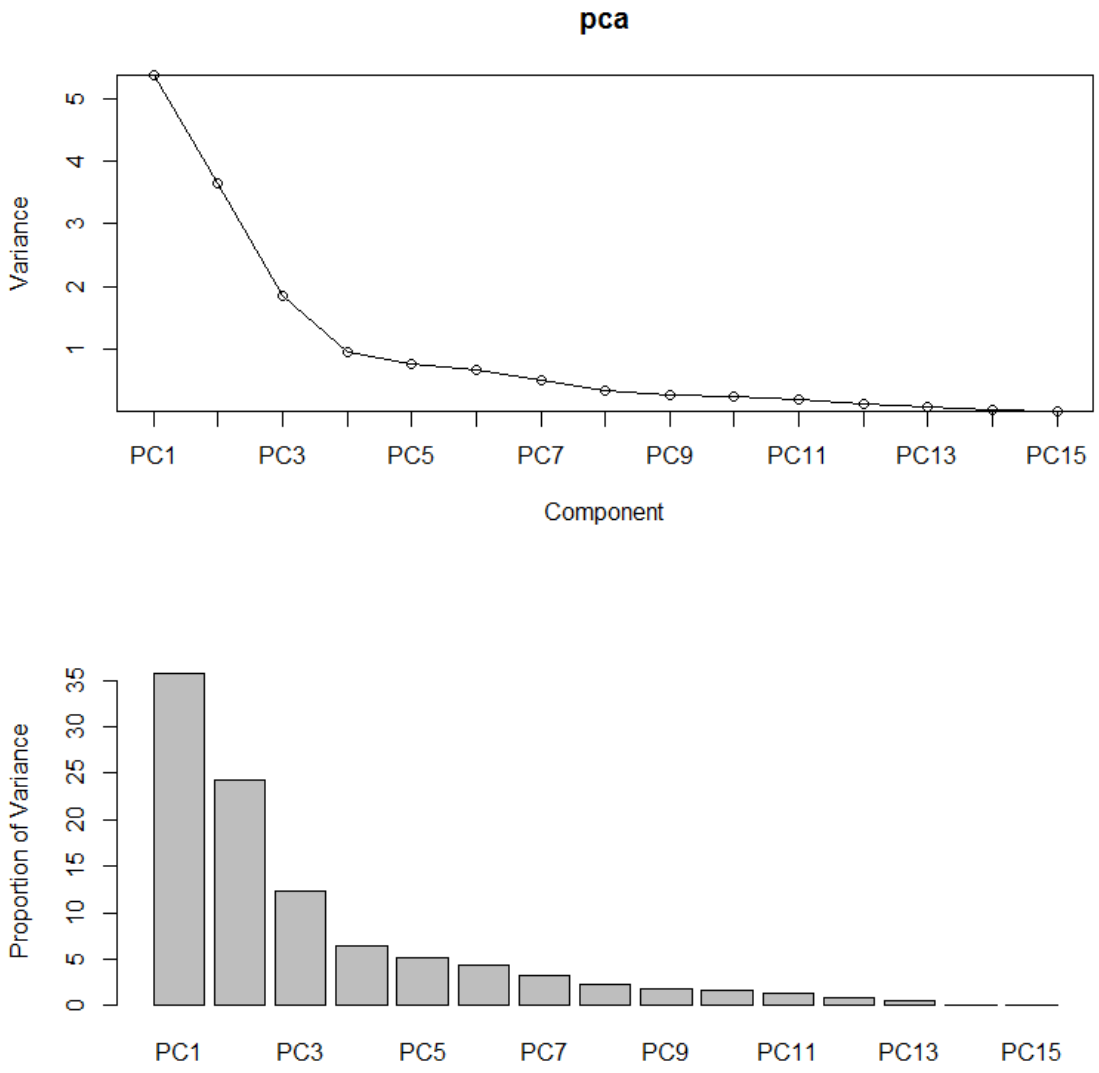

Figure 17. A) Scree plot of the variance represented by each component in Princial Component Analysis; and B) the proportion of the variance represented by each component (b).

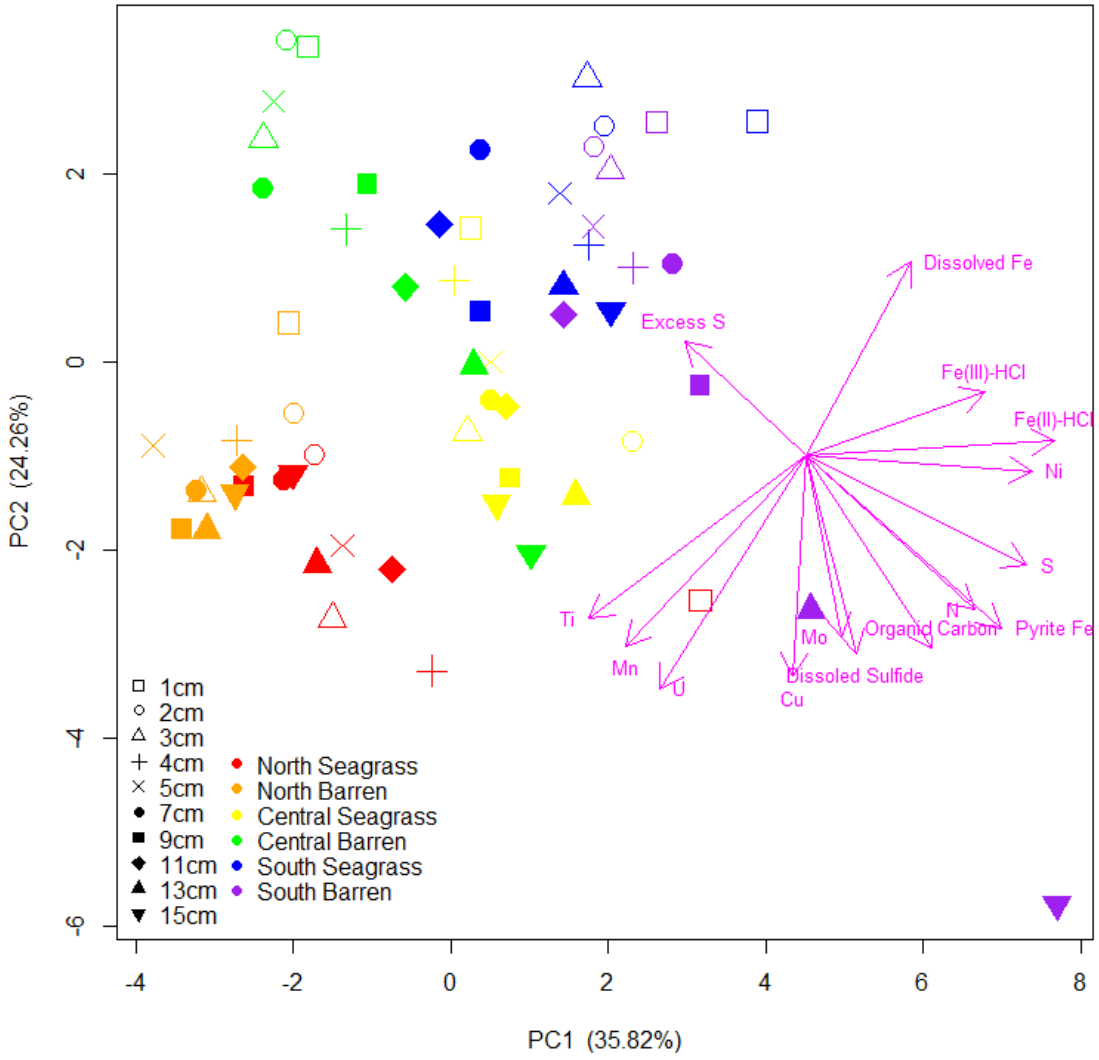

Figure 18. Principal components 1 and 2 from principal component analysis of dissolved sulfide, dissolved iron, solid-phase reactive iron, total nitrogen and sulfur, organic carbon, and trace metals normalized to Al in the sediments of BBLEH.

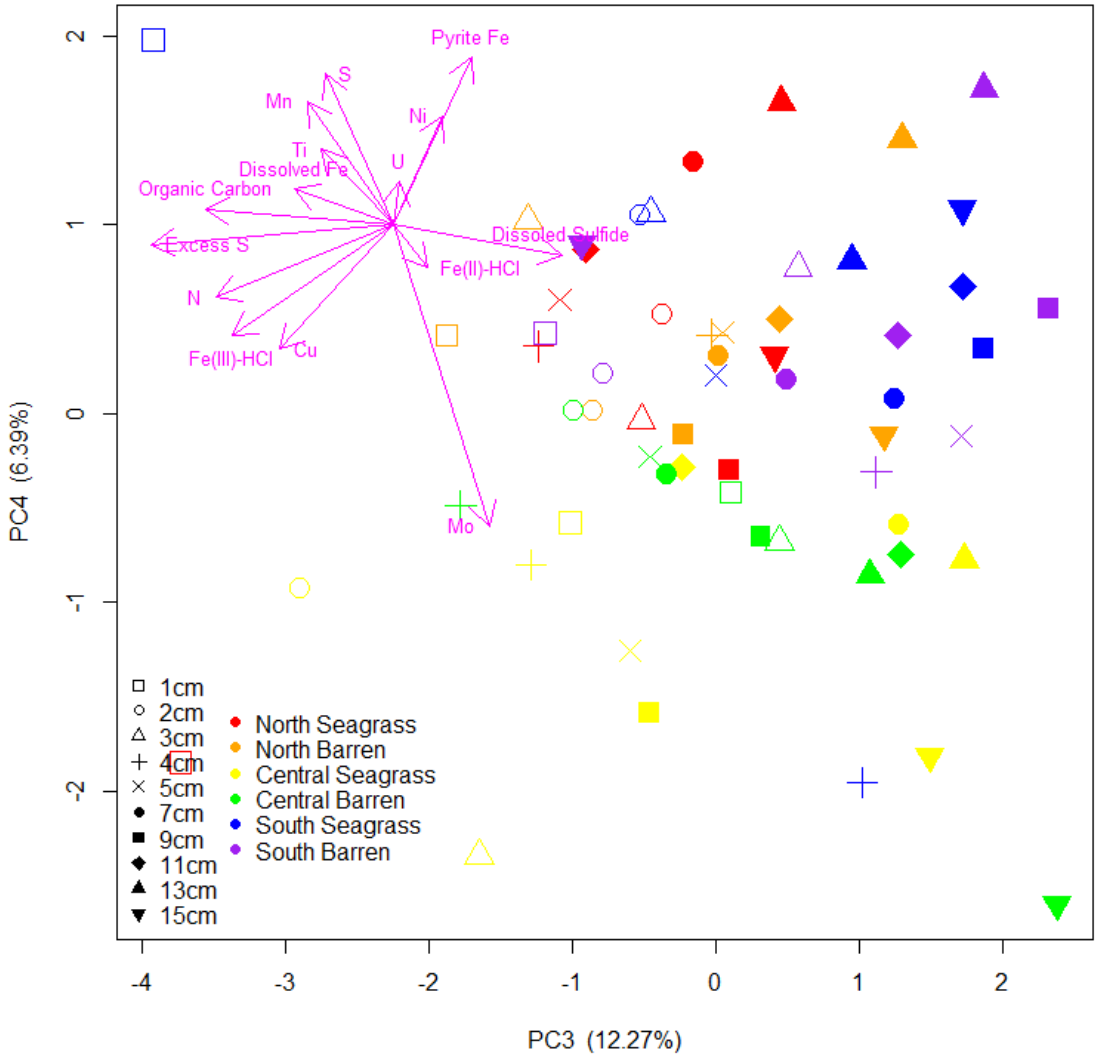

Figure 19. Principal components 3 and 4 from principal component analysis of dissolved sulfide, dissolved iron, solid-phase reactive iron, total nitrogen and sulfur, organic carbon, and trace metals normalized to Al in the sediments of BBLEH.

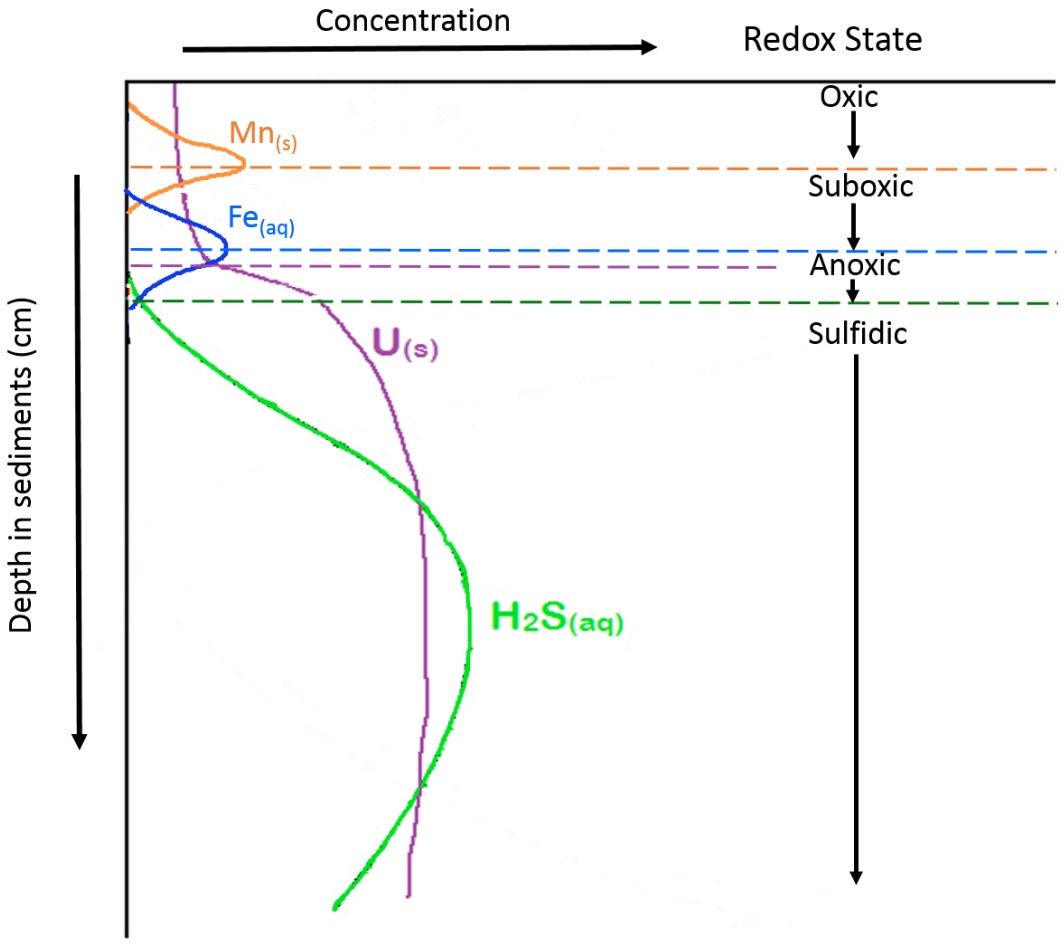

Figure 20. Schematic of idealized depth profiles in marine sediments with redox state zonations of Mn(s), U(s), Fe(aq), and H2S(aq). The orange dashed line represents where Mn reduction begins to occur in the suboxic zone; the purple dashed line represents where a sharp increase in U occurs at the anoxic boundary; and the blue and green dashed line represents where iron is depleted and sulfide begins to accumulate at the transition to anoxic conditions (similar to those on figures 8, 18, and 19). (Adapted from Libes Fig 12.13).

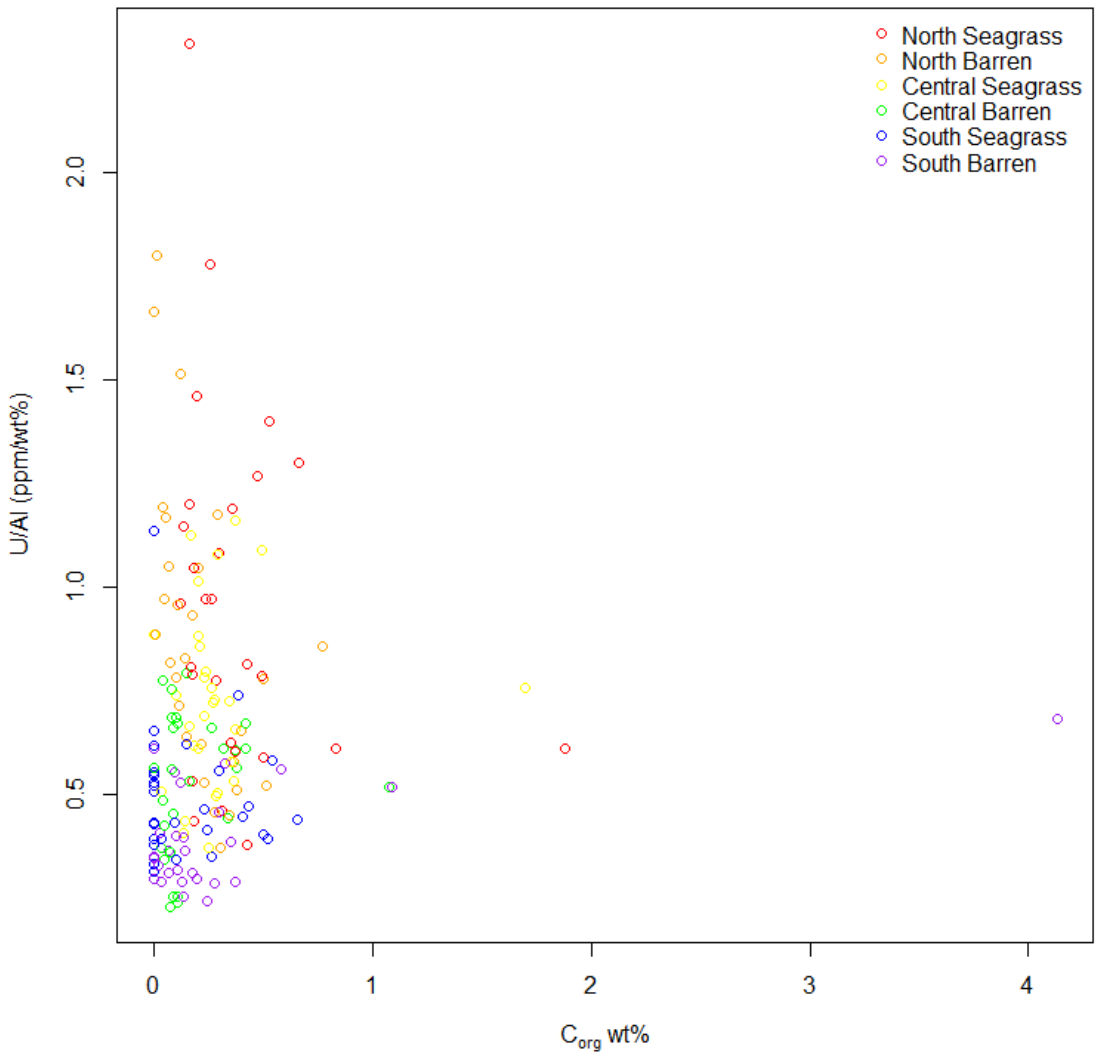

Figure 21. No significant correlation is identified between organic carbon and U/Al in the sediments of BBLEH. R-squared < 0.5.

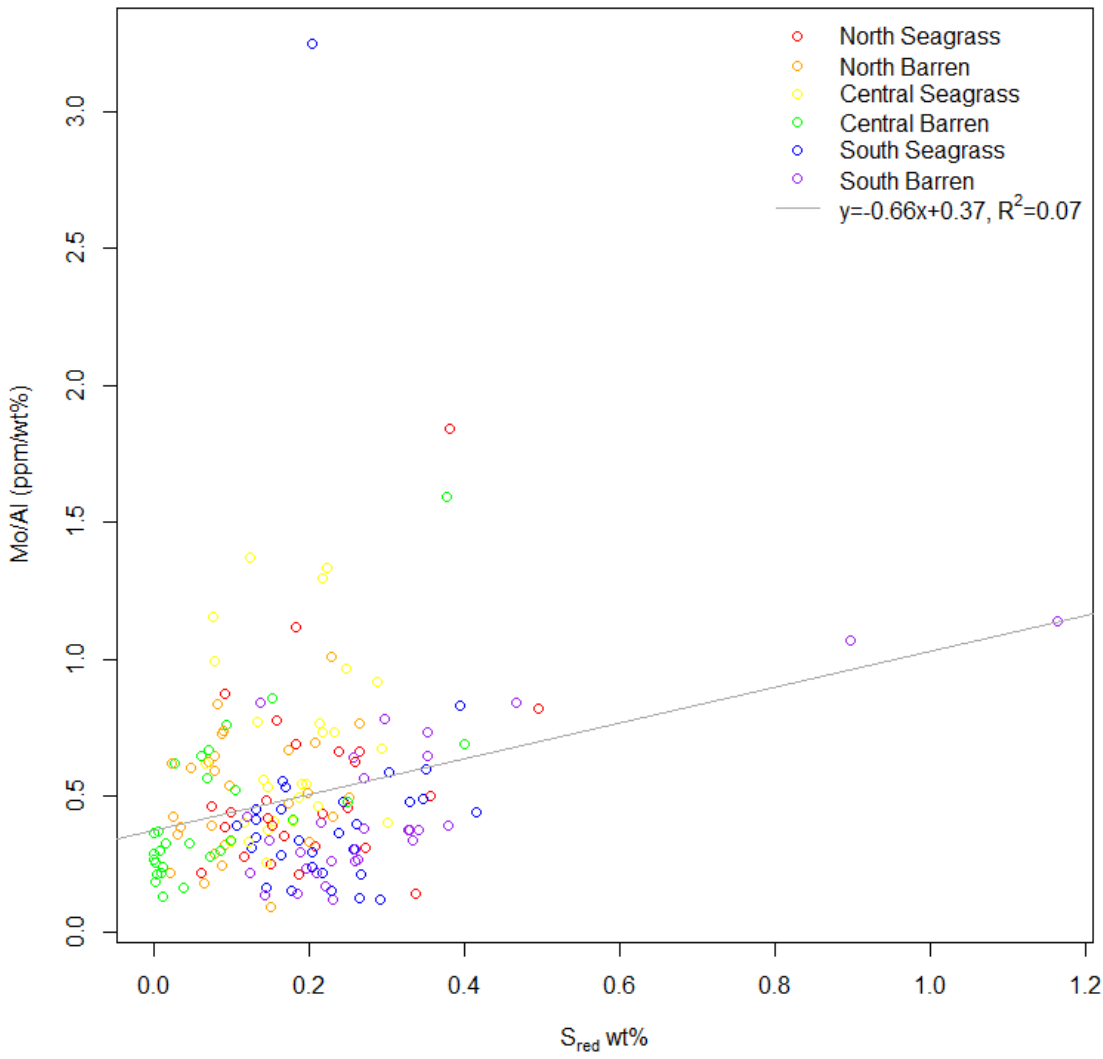

Figure 22. No significant correlation is identified between reduced S and Mo/Al in the sediments of BBLEH. R-squared < 0.5.

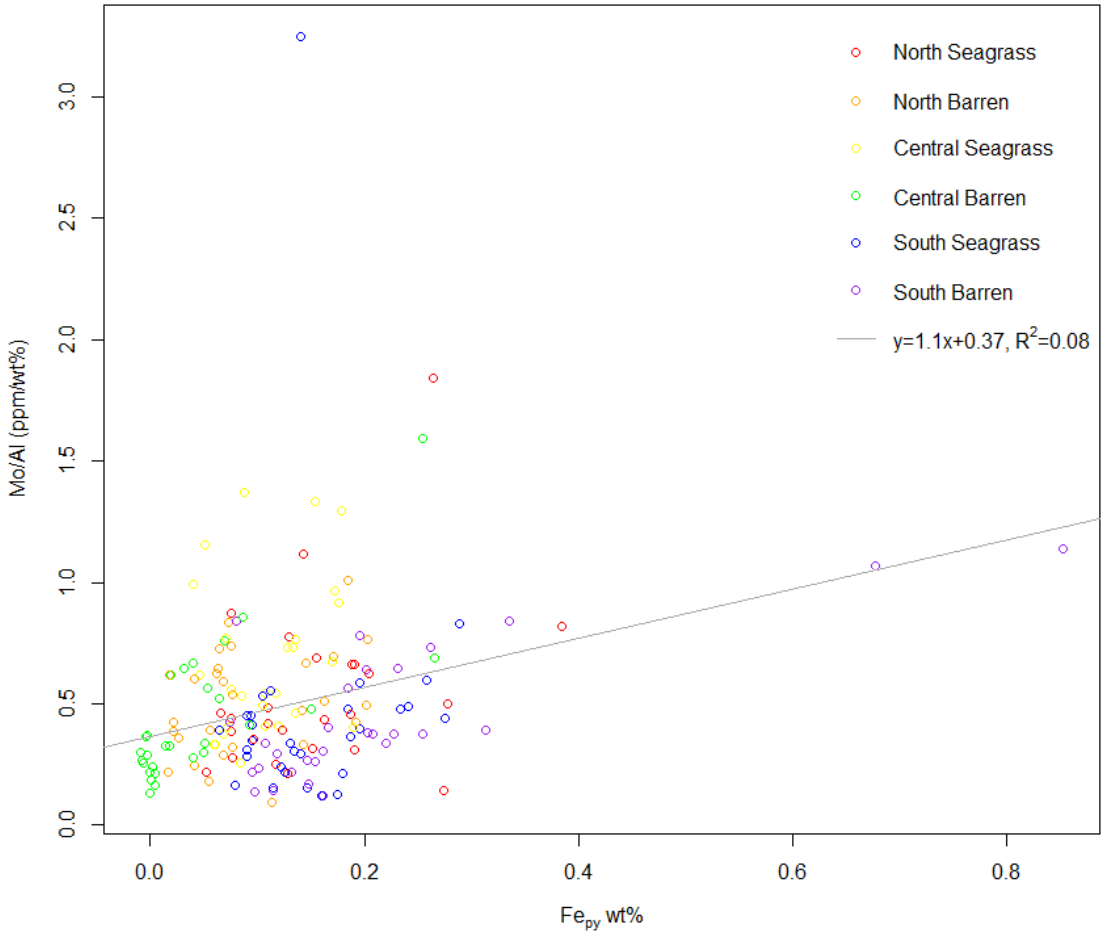

Figure 23. No significant correlation exists between Fepy and Mo/Al in BBLEH. R-squared = 0.08.

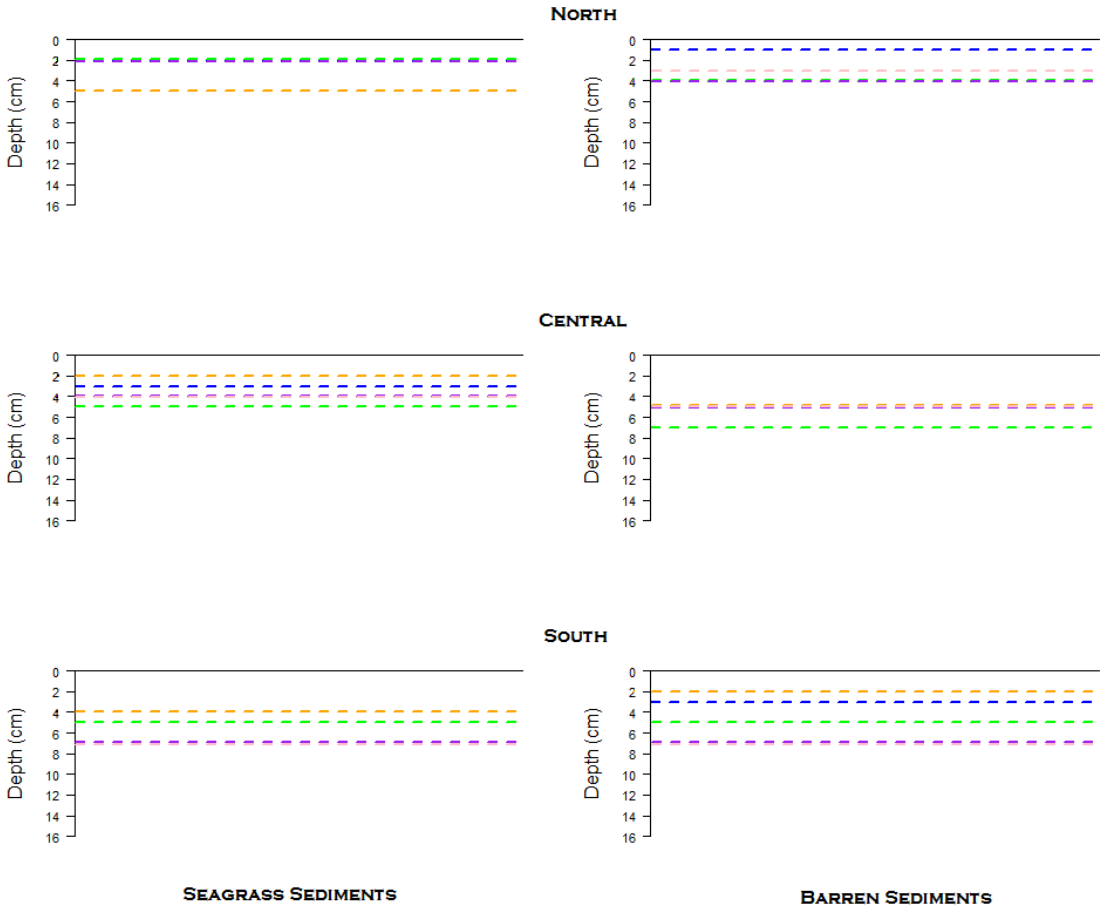

Figure 24. Sediment redox state in BBLEH sediments. The orange dashed line is where Mn(s) indicates sediments transition to suboxic. The blue and purple dashed lines are where dissolved Fe and U(s) indicate sediments become anoxic, respectively. The green and pink dashed lines are where dissolved H2S and Mo(s) indicate sediments become sulfidic,respectivel. The north segment sediments become anoxic and sulfidic at shallower sediment depths than the south segment sediments.

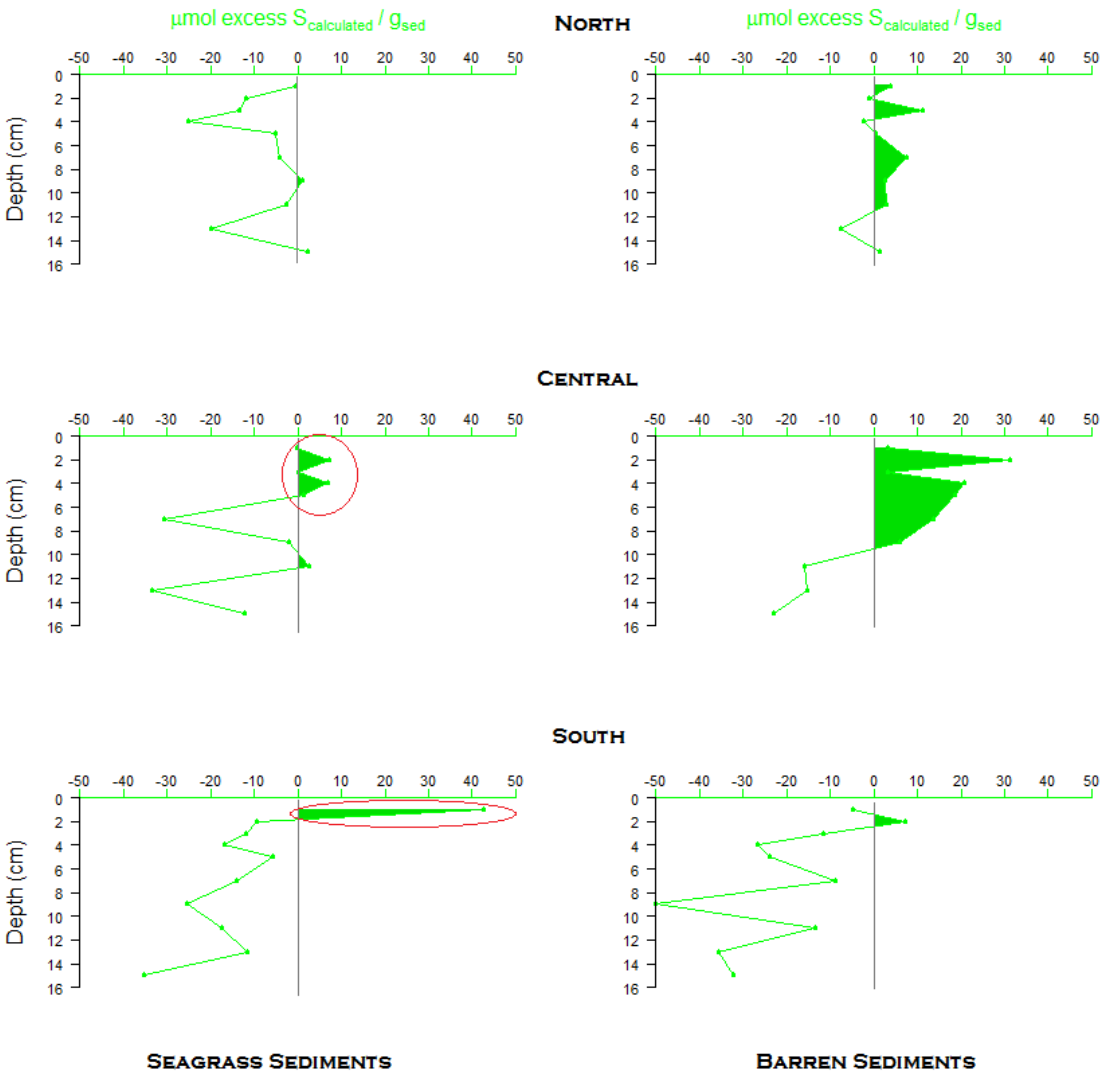

*Figure 25. The difference between Sred (calculated on a molar basis as Fe(II)HCl plus 2*Fepy) and total S indicates how much excess S is in the sediments that is not represented as Fe-sulfide. This excess S most likely represents S0. Average excess S for all all months samples (Oct 2012,2013, June 2013) show excess S primarily in the barren sediments in the more eutrophic regions of BBLEH. Additionally, excess S is seen in the seagrass root-zone, circled in red.*

XI. Appendix

Table A1. Pore water and sediment data collected in BBLEH. Sample locations are abbreviated with the segment letter N (North), C (Central), S (South) followed by either 'S' for seagrass or 'B' for barren sediments. 'NA' denotes "not available" due to no data for that point. Solid phase analysis was only completed on cores in October 2012, June 2013, and October 2013.

Sample Period	Site	Depth (cm)	Dissolved Fe (μM)	Dissolved H_2S (μM)	Total C (wt%)	C_{org} (wt%)	N (wt%)	Total S (wt%)	S_{red} (wt%)	$Fe(II)_{HCl}$ (wt%)	$Fe(III)_{HCl}$ (wt%)	Fe_{py} (wt%)
Aug-12	NS	1	1.5	3.9	NA	NA	NA	NA	NA	NA	NA	NA
Aug-12	NS	2	0.09	15	NA	NA	NA	NA	NA	NA	NA	NA
Aug-12	NS	3	0	57	NA	NA	NA	NA	NA	NA	NA	NA
Aug-12	NS	4	0	74	NA	NA	NA	NA	NA	NA	NA	NA
Aug-12	NS	5	0	46	NA	NA	NA	NA	NA	NA	NA	NA
Aug-12	NS	7	0	78	NA	NA	NA	NA	NA	NA	NA	NA
Aug-12	NS	9	0	75	NA	NA	NA	NA	NA	NA	NA	NA
Aug-12	NS	11	0	55	NA	NA	NA	NA	NA	NA	NA	NA
Aug-12	NS	13	0	60	NA	NA	NA	NA	NA	NA	NA	NA
Aug-12	NS	15	0	55	NA	NA	NA	NA	NA	NA	NA	NA
Aug-12	NB	1	7.9	7.2	NA	NA	NA	NA	NA	NA	NA	NA
Aug-12	NB	2	0.09	55	NA	NA	NA	NA	NA	NA	NA	NA
Aug-12	NB	3	0	35	NA	NA	NA	NA	NA	NA	NA	NA
Aug-12	NB	4	0	43	NA	NA	NA	NA	NA	NA	NA	NA
Aug-12	NB	5	0.09	39	NA	NA	NA	NA	NA	NA	NA	NA
Aug-12	NB	7	0	50	NA	NA	NA	NA	NA	NA	NA	NA
Aug-12	NB	9	0	51	NA	NA	NA	NA	NA	NA	NA	NA
Aug-12	NB	11	0	39	NA	NA	NA	NA	NA	NA	NA	NA
Aug-12	NB	13	0	21	NA	NA	NA	NA	NA	NA	NA	NA
Aug-12	NB	15	0	11	NA	NA	NA	NA	NA	NA	NA	NA
Aug-12	CS	1	5.2	22	NA	NA	NA	NA	NA	NA	NA	NA

Sample Period	Site	Depth (cm)	Dissolved Fe (µM)	Dissolved H_2S (µM)	Total C (wt%)	C_{org} (wt%)	N (wt%)	Total S (wt%)	S_{red} (wt%)	$Fe(II)_{HCl}$ (wt%)	$Fe(III)_{HCl}$ (wt%)	Fe_{py} (wt%)
Aug-12	CS	2	12	21	NA	NA	NA	NA	NA	NA	NA	NA
Aug-12	CS	3	9.4	29	NA	NA	NA	NA	NA	NA	NA	NA
Aug-12	CS	4	8.0	16	NA	NA	NA	NA	NA	NA	NA	NA
Aug-12	CS	5	3.8	32	NA	NA	NA	NA	NA	NA	NA	NA
Aug-12	CS	7	3.0	37	NA	NA	NA	NA	NA	NA	NA	NA
Aug-12	CS	9	3.8	59	NA	NA	NA	NA	NA	NA	NA	NA
Aug-12	CS	11	4.5	91	NA	NA	NA	NA	NA	NA	NA	NA
Aug-12	CS	13	3.8	78	NA	NA	NA	NA	NA	NA	NA	NA
Aug-12	CS	15	3.0	37	NA	NA	NA	NA	NA	NA	NA	NA
Aug-12	CB	1	6.6	11	NA	NA	NA	NA	NA	NA	NA	NA
Aug-12	CB	2	14	9.3	NA	NA	NA	NA	NA	NA	NA	NA
Aug-12	CB	3	10	15	NA	NA	NA	NA	NA	NA	NA	NA
Aug-12	CB	4	13	17	NA	NA	NA	NA	NA	NA	NA	NA
Aug-12	CB	5	6.6	25	NA	NA	NA	NA	NA	NA	NA	NA
Aug-12	CB	7	6.6	25	NA	NA	NA	NA	NA	NA	NA	NA
Aug-12	CB	9	7.3	25	NA	NA	NA	NA	NA	NA	NA	NA
Aug-12	CB	11	6.6	25	NA	NA	NA	NA	NA	NA	NA	NA
Aug-12	CB	13	5.9	26	NA	NA	NA	NA	NA	NA	NA	NA
Aug-12	CB	15	4.5	34	NA	NA	NA	NA	NA	NA	NA	NA
Aug-12	SS	1	14	11	NA	NA	NA	NA	NA	NA	NA	NA
Aug-12	SS	2	13	11	NA	NA	NA	NA	NA	NA	NA	NA
Aug-12	SS	3	39	16	NA	NA	NA	NA	NA	NA	NA	NA
Aug-12	SS	4	20	32	NA	NA	NA	NA	NA	NA	NA	NA
Aug-12	SS	5	20	39	NA	NA	NA	NA	NA	NA	NA	NA
Aug-12	SS	7	17	38	NA	NA	NA	NA	NA	NA	NA	NA
Aug-12	SS	9	10	70	NA	NA	NA	NA	NA	NA	NA	NA

Sample Period	Site	Depth (cm)	Dissolved Fe (µM)	Dissolved H_2S (µM)	Total C (wt%)	C_{org} (wt%)	N (wt%)	Total S (wt%)	S_{red} (wt%)	$Fe(II)_{HCl}$ (wt%)	$Fe(III)_{HCl}$ (wt%)	Fe_{py} (wt%)
Aug-12	SS	11	10	69	NA	NA	NA	NA	NA	NA	NA	NA
Aug-12	SS	13	14	38	NA	NA	NA	NA	NA	NA	NA	NA
Aug-12	SS	15	9.6	40	NA	NA	NA	NA	NA	NA	NA	NA
Aug-12	SB	1	8.9	36	NA	NA	NA	NA	NA	NA	NA	NA
Aug-12	SB	2	8.1	18	NA	NA	NA	NA	NA	NA	NA	NA
Aug-12	SB	3	4.6	90	NA	NA	NA	NA	NA	NA	NA	NA
Aug-12	SB	4	4.6	80	NA	NA	NA	NA	NA	NA	NA	NA
Aug-12	SB	5	6.7	140	NA	NA	NA	NA	NA	NA	NA	NA
Aug-12	SB	7	5.3	110	NA	NA	NA	NA	NA	NA	NA	NA
Aug-12	SB	9	5.3	100	NA	NA	NA	NA	NA	NA	NA	NA
Aug-12	SB	11	6.0	130	NA	NA	NA	NA	NA	NA	NA	NA
Aug-12	SB	13	5.3	160	NA	NA	NA	NA	NA	NA	NA	NA
Aug-12	SB	15	6.0	260	NA	NA	NA	NA	NA	NA	NA	NA
Oct-12	NS	1	5.4	33	2.02	1.88	0.22	0.46	0.38	0.136	0.219	0.264
Oct-12	NS	2	14	31	0.57	0.47	0.06	0.17	0.18	0.0106	0.0541	0.155
Oct-12	NS	3	0.14	26	0.38	0.26	0.04	0.17	0.26	0.0859	0.765	0.178
Oct-12	NS	4	3.3	30	0.52	0.43	0.06	0.16	0.21	0.0597	0.0599	0.152
Oct-12	NS	5	2.6	22	0.39	0.3	0.04	0.12	0.09	0.00992	0.0313	0.0755
Oct-12	NS	7	16	38	0.2	0.12	0.03	0.05	NA	NA	NA	NA
Oct-12	NS	9	14	58	0.23	0.14	0.03	0.1	0.09	0.00868	0.0351	0.0750
Oct-12	NS	11	11	90	0.68	0.53	0.07	0.18	0.15	0.0268	0.0425	0.118
Oct-12	NS	13	14	130	0.24	0.16	0.03	0.1	NA	NA	NA	NA
Oct-12	NS	15	13	130	NA	NA	NA	NA	NA	NA	NA	NA
Oct-12	NB	1	10	12	0.6	0.5	0.07	0.13	0.08	0.000	0.0979	0.0684
Oct-12	NB	2	5.4	42	0.27	0.18	0.04	0.09	0.07	0.0178	0.0232	0.0559
Oct-12	NB	3	5.1	43	0.88	0.77	0.06	0.21	0.08	0.000	0.0336	0.0678

Sample Period	Site	Depth (cm)	Dissolved Fe (µM)	Dissolved H_2S (µM)	Total C (wt%)	C_{org} (wt%)	N (wt%)	Total S (wt%)	S_{red} (wt%)	$Fe(II)_{HCl}$ (wt%)	$Fe(III)_{HCl}$ (wt%)	Fe_{py} (wt%)
Oct-12	NB	4	3.7	86	0.23	0.11	0.03	0.09	0.1	0.0167	0.0172	0.0771
Oct-12	NB	5	3.3	69	0.21	0.12	0.02	0.07	0.08	0.0105	0.0612	0.0631
Oct-12	NB	7	5.1	110	0.24	0.13	0.03	0.1	NA	NA	NA	NA
Oct-12	NB	9	4.4	120	NA	NA	NA	NA	0.08	0.000	0.0318	0.0735
Oct-12	NB	11	3.0	130	0.19	0.1	0.02	0.08	0.07	0.00601	0.0244	0.0547
Oct-12	NB	13	1.9	160	0.18	0.07	0.02	0.08	0.09	0.00732	0.0249	0.0762
Oct-12	NB	15	0.0	170	0.16	0.07	0.02	0.08	0.07	0.000	0.0279	0.0621
Oct-12	CS	1	15	2.0	0.32	0.03	0.03	0.13	0.12	0.0586	0.129	0.0725
Oct-12	CS	2	24	0.0	2.04	1.7	0.17	0.33	0.22	0.0790	0.0819	0.154
Oct-12	CS	3	17	40	0.46	0.23	0.05	0.12	0.08	0.0584	0.0811	0.0398
Oct-12	CS	4	10	25	0.62	0.37	0.07	0.16	0.07	0.0249	0.654	0.0461
Oct-12	CS	5	12	53	0.46	0.21	0.05	0.14	0.08	0.0327	0.0630	0.0512
Oct-12	CS	7	11	85	0.44	0.17	0.04	0.16	NA	NA	NA	NA
Oct-12	CS	9	10	91	0.59	0.37	0.07	0.23	0.22	0.0211	0.0669	0.179
Oct-12	CS	11	7.2	110	0.69	0.5	0.06	0.26	0.15	0.0309	0.0720	0.119
Oct-12	CS	13	7.9	110	0.39	0.21	0.04	0.18	NA	NA	NA	NA
Oct-12	CS	15	8.6	240	0.19	0	0.02	0.05	0.12	0.0405	0.0576	0.0879
Oct-12	CB	1	12	0.0	0.17	0.11	0.02	0.03	0.01	0.000	0.0432	0.00466
Oct-12	CB	2	10	0.0	0.45	0.38	0.04	0.18	0	0.00536	0.0465	0.000
Oct-12	CB	3	13	0.0	0.16	0.09	0.02	0.03	0	0.000	0.0439	0.000
Oct-12	CB	4	14	0.0	1.14	1.08	0.12	0.25	0	0.00384	0.0633	0.000246
Oct-12	CB	5	16	0.0	0.4	0.34	0.04	0.17	0	0.000	0.0512	0.000
Oct-12	CB	7	18	0.0	0.23	0.15	0.02	0.12	0.02	0.000	0.0467	0.0139
Oct-12	CB	9	22	14	0.47	0.37	0.05	0.12	0.03	0.00810	0.0292	0.0189
Oct-12	CB	11	26	35	0.19	0.04	0.02	0.08	0.07	0.0123	0.0555	0.0536

Sample Period	Site	Depth (cm)	Dissolved Fe (µM)	Dissolved H_2S (µM)	Total C (wt%)	C_{org} (wt%)	N (wt%)	Total S (wt%)	S_{red} (wt%)	$Fe(II)_{HCl}$ (wt%)	$Fe(III)_{HCl}$ (wt%)	Fe_{py} (wt%)
Oct-12	CB	13	18	37	0.37	0.11	0.02	0.1	0.09	0.0221	0.0782	0.0700
Oct-12	CB	15	12	17	NA	NA	NA	NA	0.16	0.0490	0.0740	0.114
Oct-12	SS	1	28	7.3	0.91	0.52	0.09	0.23	0.27	0.106	0.127	0.180
Oct-12	SS	2	35	1.8	0.87	0.51	0.08	0.27	0.26	0.179	0.113	0.135
Oct-12	SS	3	75	7.5	0.86	0.54	0.06	0.23	0.26	0.0649	0.0612	0.195
Oct-12	SS	4	38	13	0.66	0.3	0.06	0.19	0.21	0.0773	0.0991	0.140
Oct-12	SS	5	1.8	1.8	0.54	0.27	0.04	0.18	0.24	0.0555	0.0708	0.185
Oct-12	SS	7	0.0	10	0.16	0	0.02	0.05	0.13	0.0421	0.0418	0.0942
Oct-12	SS	9	0.0	11	0.14	0	0.02	0.04	0.13	0.0397	0.0393	0.0955
Oct-12	SS	11	0.0	7.0	0.18	0	0.02	0.12	0.13	0.0420	0.0353	0.0897
Oct-12	SS	13	0.0	7.6	0.12	0	0.01	0.12	0.13	0.0394	0.0489	0.0951
Oct-12	SS	15	0.0	4.5	0.13	0	0.01	0.1	0.24	0.0429	0.0426	0.187
Oct-12	SB	1	19	0.0	0.6	0.25	0.06	0.2	0.23	0.0800	0.146	0.161
Oct-12	SB	2	26	0.0	0.61	0.28	0.06	0.23	0.21	0.102	0.107	0.132
Oct-12	SB	3	9.7	0.0	0.72	0.37	0.07	0.25	0.26	0.165	0.0533	0.147
Oct-12	SB	4	13	0.0	0.24	0	0.02	0.11	0.33	0.140	0.0915	0.220
Oct-12	SB	5	5.8	0.0	0.39	0.07	0.04	0.15	0.26	0.145	0.0481	0.154
Oct-12	SB	7	6.1	0.0	0.36	0.04	0.04	0.15	0.23	0.0925	0.0921	0.154
Oct-12	SB	9	2.6	3.8	0.17	0	0.02	0.03	0.34	0.0837	0.102	0.255
Oct-12	SB	11	3.3	8.6	0.48	0.1	0.04	0.2	0.27	0.0666	0.0646	0.202
Oct-12	SB	13	3.3	13	0.57	0.27	0.05	0.31	0.26	0.0471	0.0347	0.201
Oct-12	SB	15	3.7	11	0.36	0	0.03	0.22	0.27	0.103	0.0834	0.185
Mar-13	NS	1	0.0	5.2	NA	NA	NA	NA	NA	NA	NA	NA
Mar-13	NS	2	5.0	4.1	NA	NA	NA	NA	NA	NA	NA	NA
Mar-13	NS	3	3.3	4.7	NA	NA	NA	NA	NA	NA	NA	NA
Mar-13	NS	4	4.2	0.0	NA	NA	NA	NA	NA	NA	NA	NA

Sample Period	Site	Depth (cm)	Dissolved Fe (µM)	Dissolved H_2S (µM)	Total C (wt%)	C_{org} (wt%)	N (wt%)	Total S (wt%)	S_{red} (wt%)	$Fe(II)_{HCl}$ (wt%)	$Fe(III)_{HCl}$ (wt%)	Fe_{py} (wt%)
Mar-13	NS	5	3.3	9.1	NA	NA	NA	NA	NA	NA	NA	NA
Mar-13	NS	7	0.0	65	NA	NA	NA	NA	NA	NA	NA	NA
Mar-13	NS	9	0.0	68	NA	NA	NA	NA	NA	NA	NA	NA
Mar-13	NS	11	0.0	97	NA	NA	NA	NA	NA	NA	NA	NA
Mar-13	NS	13	1.7	61	NA	NA	NA	NA	NA	NA	NA	NA
Mar-13	NS	15	0.0	62	NA	NA	NA	NA	NA	NA	NA	NA
Mar-13	NB	1	5.0	0.0	NA	NA	NA	NA	NA	NA	NA	NA
Mar-13	NB	2	1.7	0.0	NA	NA	NA	NA	NA	NA	NA	NA
Mar-13	NB	3	0.0	25	NA	NA	NA	NA	NA	NA	NA	NA
Mar-13	NB	4	0.0	15	NA	NA	NA	NA	NA	NA	NA	NA
Mar-13	NB	5	0.0	33	NA	NA	NA	NA	NA	NA	NA	NA
Mar-13	NB	7	0.0	120	NA	NA	NA	NA	NA	NA	NA	NA
Mar-13	NB	9	0.0	150	NA	NA	NA	NA	NA	NA	NA	NA
Mar-13	NB	11	0.0	160	NA	NA	NA	NA	NA	NA	NA	NA
Mar-13	NB	13	0.0	140	NA	NA	NA	NA	NA	NA	NA	NA
Mar-13	NB	15	0.0	460	NA	NA	NA	NA	NA	NA	NA	NA
Mar-13	CS	1	2.5	1.9	NA	NA	NA	NA	NA	NA	NA	NA
Mar-13	CS	2	13	4.1	NA	NA	NA	NA	NA	NA	NA	NA
Mar-13	CS	3	23	23	NA	NA	NA	NA	NA	NA	NA	NA
Mar-13	CS	4	6.7	47	NA	NA	NA	NA	NA	NA	NA	NA
Mar-13	CS	5	7.5	150	NA	NA	NA	NA	NA	NA	NA	NA
Mar-13	CS	7	10	460	NA	NA	NA	NA	NA	NA	NA	NA
Mar-13	CS	9	5.0	360	NA	NA	NA	NA	NA	NA	NA	NA
Mar-13	CS	11	2.5	700	NA	NA	NA	NA	NA	NA	NA	NA
Mar-13	CS	13	NA	700	NA	NA	NA	NA	NA	NA	NA	NA
Mar-13	CS	15	2.5	680	NA	NA	NA	NA	NA	NA	NA	NA

Sample Period	Site	Depth (cm)	Dissolved Fe (µM)	Dissolved H_2S (µM)	Total C (wt%)	C_{org} (wt%)	N (wt%)	Total S (wt%)	S_{red} (wt%)	$Fe(II)_{HCl}$ (wt%)	$Fe(III)_{HCl}$ (wt%)	Fe_{py} (wt%)
Mar-13	CB	1	9.2	3.0	NA	NA	NA	NA	NA	NA	NA	NA
Mar-13	CB	2	5.0	0.0	NA	NA	NA	NA	NA	NA	NA	NA
Mar-13	CB	3	0.83	0.78	NA	NA	NA	NA	NA	NA	NA	NA
Mar-13	CB	4	1.7	0.0	NA	NA	NA	NA	NA	NA	NA	NA
Mar-13	CB	5	0.83	59	NA	NA	NA	NA	NA	NA	NA	NA
Mar-13	CB	7	2.5	530	NA	NA	NA	NA	NA	NA	NA	NA
Mar-13	CB	9	0.0	420	NA	NA	NA	NA	NA	NA	NA	NA
Mar-13	CB	11	0.0	580	NA	NA	NA	NA	NA	NA	NA	NA
Mar-13	CB	13	0.0	230	NA	NA	NA	NA	NA	NA	NA	NA
Mar-13	CB	15	0.83	1400	NA	NA	NA	NA	NA	NA	NA	NA
Mar-13	SS	1	0.83	9.7	NA	NA	NA	NA	NA	NA	NA	NA
Mar-13	SS	2	2.5	81	NA	NA	NA	NA	NA	NA	NA	NA
Mar-13	SS	3	18	90	NA	NA	NA	NA	NA	NA	NA	NA
Mar-13	SS	4	0.0	210	NA	NA	NA	NA	NA	NA	NA	NA
Mar-13	SS	5	0.0	320	NA	NA	NA	NA	NA	NA	NA	NA
Mar-13	SS	7	2.5	250	NA	NA	NA	NA	NA	NA	NA	NA
Mar-13	SS	9	0.83	640	NA	NA	NA	NA	NA	NA	NA	NA
Mar-13	SS	11	0.0	440	NA	NA	NA	NA	NA	NA	NA	NA
Mar-13	SS	13	NA	NA	NA	NA	NA	NA	NA	NA	NA	NA
Mar-13	SS	15	NA	NA	NA	NA	NA	NA	NA	NA	NA	NA
Mar-13	SB	1	0.0	1.9	NA	NA	NA	NA	NA	NA	NA	NA
Mar-13	SB	2	0.0	0.0	NA	NA	NA	NA	NA	NA	NA	NA
Mar-13	SB	3	10	1.3	NA	NA	NA	NA	NA	NA	NA	NA
Mar-13	SB	4	7.5	0.0	NA	NA	NA	NA	NA	NA	NA	NA
Mar-13	SB	5	13	0.0	NA	NA	NA	NA	NA	NA	NA	NA
Mar-13	SB	7	32	21	NA	NA	NA	NA	NA	NA	NA	NA

Sample Period	Site	Depth (cm)	Dissolved Fe (µM)	Dissolved H_2S (µM)	Total C (wt%)	C_{org} (wt%)	N (wt%)	Total S (wt%)	S_{red} (wt%)	$Fe(II)_{HCl}$ (wt%)	$Fe(III)_{HCl}$ (wt%)	Fe_{py} (wt%)
Mar-13	SB	9	6.7	290	NA	NA	NA	NA	NA	NA	NA	NA
Mar-13	SB	11	NA	640	NA	NA	NA	NA	NA	NA	NA	NA
Mar-13	SB	13	0.0	2300	NA	NA	NA	NA	NA	NA	NA	NA
Mar-13	SB	15	NA	NA	NA	NA	NA	NA	NA	NA	NA	NA
Jun-13	NS	1	8.6	0.0	0.49	0.36	0.05	0.16	0.17	0.101	0.0691	0.0965
Jun-13	NS	2	8.6	0.0	0.3	0.17	0.03	0.11	0.12	0.0500	0.0477	0.0770
Jun-13	NS	3	5.2	0.0	0.3	NA	0.02	0.1	0.07	0.0231	0.0277	0.0535
Jun-13	NS	4	8.6	0.0	0.37	0.27	0.03	0.13	0.15	0.0344	0.0564	0.110
Jun-13	NS	5	8.6	0.0	0.78	0.66	0.07	0.24	0.25	0.0618	0.0669	0.187
Jun-13	NS	7	5.6	0.0	0.45	0.36	0.03	NA	0.08	0.000	0.0368	0.0655
Jun-13	NS	9	3.6	0.0	0.28	0.2	0.02	0.11	0.06	0.00243	0.0461	0.0529
Jun-13	NS	11	8.6	0.0	0.27	0.18	0.02	0.13	0.1	0.0215	0.0279	0.0761
Jun-13	NS	13	3.6	3.0	0.38	0.28	0.03	0.14	0.19	0.0700	0.0467	0.128
Jun-13	NS	15	3.6	4.7	0.36	0.24	0.03	0.17	0.15	0.0366	0.0346	0.109
Jun-13	NB	1	6.9	0.0	0.24	0.15	0.02	0.06	0.04	0.0181	0.0679	0.0219
Jun-13	NB	2	5.2	0.0	0.3	0.2	0.02	0.08	0.09	0.0688	0.0620	0.0417
Jun-13	NB	3	3.6	0.0	0.14	0.05	0.01	0.06	0.02	0.0598	0.0199	0.0166
Jun-13	NB	4	10	0.0	0.1	0.01	0.01	0.04	0.03	0.00354	0.0208	0.0260
Jun-13	NB	5	3.6	0.0	0.1	0	0.01	0.05	0.03	0.000	0.0197	0.0219
Jun-13	NB	7	5.2	38	0.18	0.06	0.01	0.09	0.02	0.00347	0.0225	0.0179
Jun-13	NB	9	3.6	35	0.17	0.04	0.01	0.08	0.05	0.000	0.0198	0.0413
Jun-13	NB	11	5.2	130	0.42	0.29	0.03	0.18	0.08	0.000	0.0236	0.0726
Jun-13	NB	13	5.2	110	0.12	0.02	0.01	0.07	0.09	0.00558	0.0207	0.0751
Jun-13	NB	15	3.6	220	0.26	0.18	0.02	0.12	0.09	0.0262	0.0106	0.0639
Jun-13	CS	1	8.9	51	0.65	0.37	0.06	0.16	0.15	0.120	0.0725	0.0686
Jun-13	CS	2	8.1	11	0.52	0.24	0.05	0.14	0.2	0.127	0.0697	0.107

Sample Period	Site	Depth (cm)	Dissolved Fe (µM)	Dissolved H_2S (µM)	Total C (wt%)	C_{org} (wt%)	N (wt%)	Total S (wt%)	S_{red} (wt%)	$Fe(II)_{HCl}$ (wt%)	$Fe(III)_{HCl}$ (wt%)	Fe_{py} (wt%)
Jun-13	CS	3	17	0.0	0.5	0.27	0.05	0.15	0.13	0.0897	0.0434	0.0711
Jun-13	CS	4	17	0.0	0.48	0.27	0.05	0.14	0.15	0.0847	0.0566	0.0858
Jun-13	CS	5	12	0.0	0.52	0.29	0.05	0.16	0.19	0.0966	0.0669	0.118
Jun-13	CS	7	8.1	0.0	0.29	0.11	0.03	0.11	0.3	0.1450	0.0515	0.190
Jun-13	CS	9	24	16	0.31	NA	0.03	0.12	0.09	0.0327	0.0489	0.0608
Jun-13	CS	11	16	50	0.42	0.2	0.04	0.19	0.22	0.1130	0.0228	0.133
Jun-13	CS	13	16	130	0.46	0.28	0.04	0.2	0.29	0.173	0.0150	0.170
Jun-13	CS	15	10	300	0.57	0.35	0.05	0.26	0.25	0.0875	0.0309	0.173
Jun-13	CB	1	8.9	0.0	0.15	0.11	0.01	0.05	0.01	0.0146	0.0336	0.00250
Jun-13	CB	2	9.6	3.0	0.13	0.08	0.01	0.04	0.01	0.0196	0.0250	0.000
Jun-13	CB	3	6.0	0.0	0.13	0.09	0.01	0.04	0.04	0.0594	0.000	0.00481
Jun-13	CB	4	7.4	0.0	0.17	0.09	0.01	0.04	0	0.000	0.0538	0.000
Jun-13	CB	5	8.1	3.0	0.14	0.04	0.01	0.03	0.01	0.0145	0.0181	0.000
Jun-13	CB	7	9.6	6.3	0.11	0.05	0.01	0.04	0.01	0.0105	0.0194	0.000
Jun-13	CB	9	6.7	88	0.14	0.07	0.01	0.03	0.01	0.0171	0.0184	0.000
Jun-13	CB	11	9.6	200	0.17	0.08	0.01	0.05	0.11	0.0556	0.0359	0.0644
Jun-13	CB	13	7.4	380	0.15	0.05	0.01	0.04	0.05	0.0451	0.0222	0.0178
Jun-13	CB	15	7.4	1000	0.2	0.08	0.01	0.06	0.06	0.0443	0.0490	0.0321
Jun-13	SS	1	90	0.0	0.47	0.1	0.04	0.18	0.29	0.188	0.0666	0.160
Jun-13	SS	2	45	0.0	0.26	0	0.02	0.12	0.15	0.0953	0.0192	0.0794
Jun-13	SS	3	40	0.0	0.44	0.04	0.03	0.15	0.16	0.105	0.0387	0.0908
Jun-13	SS	4	22	0.0	0.33	0	0.02	0.14	0.22	0.127	0.0506	0.126
Jun-13	SS	5	4.2	0.0	0.6	0.25	0.05	0.2	0.16	0.107	0.0376	0.0907
Jun-13	SS	7	8.3	0.0	0.33	0	0.02	0.14	0.17	0.0659	0.0429	0.112
Jun-13	SS	9	16	1.3	0.29	0	0.02	0.14	0.17	0.0881	0.0288	0.105

Sample Period	Site	Depth (cm)	Dissolved Fe (µM)	Dissolved H_2S (µM)	Total C (wt%)	C_{org} (wt%)	N (wt%)	Total S (wt%)	S_{red} (wt%)	$Fe(II)_{HCl}$ (wt%)	$Fe(III)_{HCl}$ (wt%)	Fe_{py} (wt%)
Jun-13	SS	11	33	0.0	0.29	0	0.02	0.11	0.11	0.0579	0.0304	0.0647
Jun-13	SS	13	48	0.0	0.78	0.39	0.05	0.28	0.3	0.137	0.0387	0.195
Jun-13	SS	15	22	0.0	0.72	0.41	0.05	0.28	0.42	0.175	0.0285	0.275
Jun-13	SB	1	27	0.0	0.5	0.14	0.04	0.19	0.19	0.0933	0.0825	0.115
Jun-13	SB	2	41	0.0	0.5	0.14	0.04	0.17	0.12	0.0604	0.0363	0.0745
Jun-13	SB	3	43	0.0	0.26	0	0.02	0.09	0.14	0.0544	0.0102	0.0982
Jun-13	SB	4	16	0.0	0.46	0.13	0.04	0.17	0.13	0.0274	0.0402	0.0954
Jun-13	SB	5	26	0.0	0.38	0.07	0.03	0.13	0.14	0.0786	0.0182	0.0803
Jun-13	SB	7	12	6.3	0.48	0.14	0.04	0.18	0.2	0.140	0.0525	0.101
Jun-13	SB	9	8.3	0.0	0.37	0.03	0.03	0.19	0.33	0.118	0.0208	0.228
Jun-13	SB	11	1.7	63	0.32	0.02	0.02	0.15	0.15	0.0460	0.0425	0.107
Jun-13	SB	13	2.5	88	0.48	0.13	0.03	0.2	0.38	0.0346	0.0157	0.313
Jun-13	SB	15	0.83	210	0.31	0	0.02	0.19	0.22	0.0451	0.0355	0.166
Aug-13	NS	1	4.0	17	NA	NA	NA	NA	NA	NA	NA	NA
Aug-13	NS	2	5.7	59	NA	NA	NA	NA	NA	NA	NA	NA
Aug-13	NS	3	4.0	47	NA	NA	NA	NA	NA	NA	NA	NA
Aug-13	NS	4	4.0	14	NA	NA	NA	NA	NA	NA	NA	NA
Aug-13	NS	5	7.3	49	NA	NA	NA	NA	NA	NA	NA	NA
Aug-13	NS	7	7.3	120	NA	NA	NA	NA	NA	NA	NA	NA
Aug-13	NS	9	7.3	170	NA	NA	NA	NA	NA	NA	NA	NA
Aug-13	NS	11	9.0	160	NA	NA	NA	NA	NA	NA	NA	NA
Aug-13	NS	13	7.3	160	NA	NA	NA	NA	NA	NA	NA	NA
Aug-13	NS	15	7.3	130	NA	NA	NA	NA	NA	NA	NA	NA
Aug-13	NB	1	12	12	NA	NA	NA	NA	NA	NA	NA	NA
Aug-13	NB	2	14	2.0	NA	NA	NA	NA	NA	NA	NA	NA
Aug-13	NB	3	7.3	3.7	NA	NA	NA	NA	NA	NA	NA	NA

Sample Period	Site	Depth (cm)	Dissolved Fe (µM)	Dissolved H_2S (µM)	Total C (wt%)	C_{org} (wt%)	N (wt%)	Total S (wt%)	S_{red} (wt%)	$Fe(II)_{HCl}$ (wt%)	$Fe(III)_{HCl}$ (wt%)	Fe_{py} (wt%)
Aug-13	NB	4	5.7	0.33	NA	NA	NA	NA	NA	NA	NA	NA
Aug-13	NB	5	5.7	10	NA	NA	NA	NA	NA	NA	NA	NA
Aug-13	NB	7	5.7	35	NA	NA	NA	NA	NA	NA	NA	NA
Aug-13	NB	9	5.7	42	NA	NA	NA	NA	NA	NA	NA	NA
Aug-13	NB	11	5.7	60	NA	NA	NA	NA	NA	NA	NA	NA
Aug-13	NB	13	7.3	70	NA	NA	NA	NA	NA	NA	NA	NA
Aug-13	NB	15	5.7	42	NA	NA	NA	NA	NA	NA	NA	NA
Aug-13	CS	1	7.3	0.0	NA	NA	NA	NA	NA	NA	NA	NA
Aug-13	CS	2	9.0	0.0	NA	NA	NA	NA	NA	NA	NA	NA
Aug-13	CS	3	9.0	19	NA	NA	NA	NA	NA	NA	NA	NA
Aug-13	CS	4	7.3	19	NA	NA	NA	NA	NA	NA	NA	NA
Aug-13	CS	5	7.3	42	NA	NA	NA	NA	NA	NA	NA	NA
Aug-13	CS	7	4.0	92	NA	NA	NA	NA	NA	NA	NA	NA
Aug-13	CS	9	5.7	87	NA	NA	NA	NA	NA	NA	NA	NA
Aug-13	CS	11	4.0	87	NA	NA	NA	NA	NA	NA	NA	NA
Aug-13	CS	13	2.3	92	NA	NA	NA	NA	NA	NA	NA	NA
Aug-13	CS	15	2.3	99	NA	NA	NA	NA	NA	NA	NA	NA
Aug-13	CB	1	2.3	0.0	NA	NA	NA	NA	NA	NA	NA	NA
Aug-13	CB	2	9.0	0.0	NA	NA	NA	NA	NA	NA	NA	NA
Aug-13	CB	3	5.7	0.0	NA	NA	NA	NA	NA	NA	NA	NA
Aug-13	CB	4	7.3	0.0	NA	NA	NA	NA	NA	NA	NA	NA
Aug-13	CB	5	5.7	0.0	NA	NA	NA	NA	NA	NA	NA	NA
Aug-13	CB	7	9.0	0.0	NA	NA	NA	NA	NA	NA	NA	NA
Aug-13	CB	9	7.3	7.0	NA	NA	NA	NA	NA	NA	NA	NA
Aug-13	CB	11	5.7	42	NA	NA	NA	NA	NA	NA	NA	NA
Aug-13	CB	13	9.0	85	NA	NA	NA	NA	NA	NA	NA	NA

Sample Period	Site	Depth (cm)	Dissolved Fe (µM)	Dissolved H_2S (µM)	Total C (wt%)	C_{org} (wt%)	N (wt%)	Total S (wt%)	S_{red} (wt%)	$Fe(II)_{HCl}$ (wt%)	$Fe(III)_{HCl}$ (wt%)	Fe_{py} (wt%)
Aug-13	CB	15	7.3	110	NA	NA	NA	NA	NA	NA	NA	NA
Aug-13	SS	1	32	0.0	NA	NA	NA	NA	NA	NA	NA	NA
Aug-13	SS	2	16	0.0	NA	NA	NA	NA	NA	NA	NA	NA
Aug-13	SS	3	16	15	NA	NA	NA	NA	NA	NA	NA	NA
Aug-13	SS	4	12	0.0	NA	NA	NA	NA	NA	NA	NA	NA
Aug-13	SS	5	11	0.0	NA	NA	NA	NA	NA	NA	NA	NA
Aug-13	SS	7	9.0	22	NA	NA	NA	NA	NA	NA	NA	NA
Aug-13	SS	9	7.3	40	NA	NA	NA	NA	NA	NA	NA	NA
Aug-13	SS	11	5.7	57	NA	NA	NA	NA	NA	NA	NA	NA
Aug-13	SS	13	7.3	39	NA	NA	NA	NA	NA	NA	NA	NA
Aug-13	SS	15	5.7	39	NA	NA	NA	NA	NA	NA	NA	NA
Aug-13	SB	1	5.7	44	NA	NA	NA	NA	NA	NA	NA	NA
Aug-13	SB	2	10	100	NA	NA	NA	NA	NA	NA	NA	NA
Aug-13	SB	3	7.3	110	NA	NA	NA	NA	NA	NA	NA	NA
Aug-13	SB	4	5.7	210	NA	NA	NA	NA	NA	NA	NA	NA
Aug-13	SB	5	5.7	80	NA	NA	NA	NA	NA	NA	NA	NA
Aug-13	SB	7	4.0	130	NA	NA	NA	NA	NA	NA	NA	NA
Aug-13	SB	9	4.0	120	NA	NA	NA	NA	NA	NA	NA	NA
Aug-13	SB	11	9.0	140	NA	NA	NA	NA	NA	NA	NA	NA
Aug-13	SB	13	5.7	190	NA	NA	NA	NA	NA	NA	NA	NA
Aug-13	SB	15	4.0	230	NA	NA	NA	NA	NA	NA	NA	NA
Oct-13	NS	1	7.4	53	0.63	0.43	0.07	0.2	0.27	0.0928	0.0178	0.191
Oct-13	NS	2	6.1	77	0.33	0.18	0.03	0.12	0.22	0.0534	0.0335	0.163
Oct-13	NS	3	4.3	110	0.65	0.5	0.08	0.21	0.26	0.0449	0.0217	0.203
Oct-13	NS	4	3.0	150	1	0.83	0.13	0.32	0.5	0.0942	0.0376	0.385
Oct-13	NS	5	2.4	120	0.46	0.31	0.07	0.18	0.24	0.0363	0.0254	0.190

Sample Period	Site	Depth (cm)	Dissolved Fe (µM)	Dissolved H_2S (µM)	Total C (wt%)	C_{org} (wt%)	N (wt%)	Total S (wt%)	S_{red} (wt%)	$Fe(II)_{HCl}$ (wt%)	$Fe(III)_{HCl}$ (wt%)	Fe_{py} (wt%)
Oct-13	NS	7	2.4	120	0.32	0.18	0.08	0.14	0.15	0.0200	0.0232	0.124
Oct-13	NS	9	11	160	0.32	0.18	0.09	0.14	0.18	0.0324	0.0208	0.143
Oct-13	NS	11	3.0	220	0.65	0.5	0.17	0.27	0.36	0.0660	0.0267	0.278
Oct-13	NS	13	2.4	170	0.52	0.37	0.06	0.26	0.34	0.0399	0.0322	0.273
Oct-13	NS	15	5.5	260	0.3	0.17	0.04	0.15	0.16	0.0179	0.0271	0.130
Oct-13	NB	1	13	90	0.42	0.31	0.04	0.11	0.15	0.0356	0.0364	0.114
Oct-13	NB	2	6.1	100	0.51	0.34	0.05	0.18	0.2	0.0641	0.0260	0.143
Oct-13	NB	3	3.0	180	0.51	0.38	0.05	0.19	0.25	0.0346	0.0288	0.201
Oct-13	NB	4	3.0	45	0.68	0.51	0.06	0.24	0.26	0.0543	0.0253	0.203
Oct-13	NB	5	4.9	120	0.39	0.22	0.03	0.16	0.17	0.0123	0.0241	0.145
Oct-13	NB	7	3.0	130	0.53	0.4	0.04	0.19	0.21	0.0209	0.0276	0.171
Oct-13	NB	9	8.0	210	0.39	0.28	0.02	0.15	0.17	0.0196	0.0297	0.142
Oct-13	NB	11	3.0	260	0.37	0.23	0.03	0.14	0.23	0.0179	0.0311	0.192
Oct-13	NB	13	3.6	250	0.35	0.15	0.03	0.16	0.2	0.0202	0.0266	0.163
Oct-13	NB	15	2.4	280	0.48	0.37	0.04	0.21	0.23	0.0322	0.0233	0.184
Oct-13	CS	1	5.2	62	0.34	0.15	0.04	0.07	0.1	0.0549	0.0557	0.0590
Oct-13	CS	2	21	58	0.44	0.25	0.11	0.16	0.14	0.0834	0.0440	0.0842
Oct-13	CS	3	11	70	0.36	0.18	0.09	0.12	0.18	0.0976	0.0714	0.108
Oct-13	CS	4	13	68	0.28	0.14	0.09	0.1	0.12	0.0928	0.0505	0.0605
Oct-13	CS	5	4.7	75	0.49	0.29	0.11	0.17	0.19	0.117	0.0491	0.104
Oct-13	CS	7	13	70	0.38	0.21	0.1	0.13	0.14	0.0975	0.0341	0.0752
Oct-13	CS	9	16	73	0.62	0.35	0.11	0.17	0.23	0.149	0.0507	0.128
Oct-13	CS	11	6.0	110	0.47	0.29	0.07	0.17	0.21	0.0990	0.0465	0.136
Oct-13	CS	13	16	130	0.49	0.24	0.11	0.17	0.29	0.150	0.0550	0.176
Oct-13	CS	15	3.5	130	0.35	0.17	0.09	0.16	0.21	0.102	0.0577	0.136
Oct-13	CB	1	15	73	0.18	0	0.03	0.05	0.09	0.0519	0.0791	0.0497

Sample Period	Site	Depth (cm)	Dissolved Fe (µM)	Dissolved H_2S (µM)	Total C (wt%)	C_{org} (wt%)	N (wt%)	Total S (wt%)	S_{red} (wt%)	$Fe(II)_{HCl}$ (wt%)	$Fe(III)_{HCl}$ (wt%)	Fe_{py} (wt%)
Oct-13	CB	2	6.5	77	NA	NA	NA	NA	NA	NA	NA	NA
Oct-13	CB	3	2.9	110	0.2	0.08	0.03	0.07	0.07	0.0430	0.0474	0.0399
Oct-13	CB	4	3.5	100	0.45	0.32	0.03	0.06	0.15	0.0920	0.0389	0.0867
Oct-13	CB	5	6.5	73	0.2	0.05	0.02	0.06	0.07	0.0457	0.0444	0.0399
Oct-13	CB	7	4.7	150	0.38	0.11	0.04	0.1	0.1	0.0697	0.0471	0.0515
Oct-13	CB	9	4.8	160	0.42	0.17	0.04	0.12	0.18	0.128	0.0456	0.0924
Oct-13	CB	11	4.7	170	0.52	0.26	0.06	0.14	0.25	0.136	0.0352	0.150
Oct-13	CB	13	4.7	180	0.68	0.42	0.07	0.24	0.4	0.165	0.0710	0.266
Oct-13	CB	15	3.3	150	0.68	0.42	0.07	0.23	0.38	0.148	0.0565	0.254
Oct-13	SS	1	21	100	1.01	0.66	0.05	0.82	0.27	0.113	0.0762	0.175
Oct-13	SS	2	18	98	0.38	0	0.03	0.15	0.23	0.105	0.0584	0.147
Oct-13	SS	3	30	100	0.26	0	0.02	0.12	0.18	0.0804	0.0551	0.115
Oct-13	SS	4	28	110	0.37	0	0.03	0.13	0.2	0.112	0.0338	0.123
Oct-13	SS	5	28	90	0.46	0.1	0.04	0.17	0.2	0.0751	0.0679	0.140
Oct-13	SS	7	38	100	0.33	0	0.03	0.16	0.19	0.0641	0.0561	0.131
Oct-13	SS	9	20	100	0.75	0.43	0.05	0.28	0.39	0.110	0.0370	0.289
Oct-13	SS	11	15	98	0.37	0	0.03	0.18	0.35	0.123	0.0353	0.241
Oct-13	SS	13	12	120	0.47	0.15	0.04	0.28	0.35	0.0950	0.0328	0.259
Oct-13	SS	15	8.3	130	0.56	0.23	0.04	0.26	0.33	0.109	0.0516	0.233
Oct-13	SB	1	18	90	0.46	0.11	0.06	0.2	0.22	0.0878	0.0807	0.148
Oct-13	SB	2	2.6	160	0.44	0.1	0.06	0.18	0.19	0.0923	0.0688	0.118
Oct-13	SB	3	5.4	120	0.53	0.2	0.06	0.21	0.26	0.129	0.0667	0.161
Oct-13	SB	4	4.0	180	0.68	0.36	0.06	0.22	0.3	0.127	0.0945	0.196
Oct-13	SB	5	7.6	140	0.51	0.18	0.04	0.22	0.33	0.157	0.0539	0.208
Oct-13	SB	7	6.1	190	0.71	0.3	0.06	0.37	0.35	0.150	0.0772	0.236
Oct-13	SB	9	5.4	210	0.93	0.58	0.08	0.44	0.47	0.142	0.0639	0.336

Sample Period	Site	Depth (cm)	Dissolved Fe (µM)	Dissolved H_2S (µM)	Total C (wt%)	C_{org} (wt%)	N (wt%)	Total S (wt%)	S_{red} (wt%)	$Fe(II)_{HCl}$ (wt%)	$Fe(III)_{HCl}$ (wt%)	Fe_{py} (wt%)
Oct-13	SB	11	6.1	120	0.66	0.33	0.05	0.29	0.35	0.0915	0.0492	0.261
Oct-13	SB	13	6.9	260	1.5	1.09	0.11	0.68	0.9	0.208	0.0689	0.678
Oct-13	SB	15	2.6	460	4.5	4.13	0.35	0.93	1.16	0.322	0.0728	0.852

Table A2. Pore water and sediment data collected in BBLEH. Sample locations are abbreviated with the segment letter N (North), C (Central), S (South) followed by either 'S' for seagrass or 'B' for barren sediments. 'NA' denotes "not available" due to no data for that point. Solid phase analysis was not completed in August 2012, March 2013, or August 2013.

Sample Period	Site	Depth (cm)	Ca (wt%)	Al (wt%)	Ti (wt%)	Fe_{total} (wt%)	Mn (ppm)	Co (ppm)	Ni (ppm)	Cu (ppm)	Mo (ppm)	U (ppm)
Oct-12	NS	1	0.46	2.40	0.52	1.53	234	4.6	9.0	17.8	4.4	1.5
Oct-12	NS	2	0.32	1.68	0.78	1.07	268	2.7	3.8	4.1	1.2	2.1
Oct-12	NS	3	0.40	1.83	0.92	1.19	378	3.0	6.2	7.0	1.2	3.3
Oct-12	NS	4	0.32	1.63	0.78	1.05	278	2.7	3.6	10.9	0.5	1.3
Oct-12	NS	5	0.29	1.43	0.77	1.01	275	2.5	3.5	1.6	0.6	1.6
Oct-12	NS	7	0.25	1.32	0.62	0.84	232	2.1	4.3	4.1	0.3	1.3
Oct-12	NS	9	0.30	1.43	0.66	0.83	208	2.2	3.1	3.8	1.2	1.6
Oct-12	NS	11	0.51	2.20	0.46	1.62	445	4.3	5.5	5.9	0.6	3.1
Oct-12	NS	13	0.24	1.20	0.81	1.01	274	2.2	3.0	3.0	0.7	2.8
Oct-12	NS	15	NA	NA	NA	NA	NA	NA	NA	NA	NA	NA
Oct-12	NB	1	0.31	1.62	0.63	0.90	219	2.4	3.8	4.4	0.5	1.3
Oct-12	NB	2	0.31	1.56	0.30	0.75	222	2.0	3.0	4.0	0.6	1.2
Oct-12	NB	3	0.35	1.53	0.82	0.98	285	2.2	3.0	3.9	0.9	1.3
Oct-12	NB	4	0.40	1.83	0.87	1.02	290	2.4	4.3	5.1	1.0	1.8
Oct-12	NB	5	0.32	1.55	0.62	0.74	196	1.9	2.9	1.5	1.0	1.1
Oct-12	NB	7	0.39	1.74	0.80	0.98	278	2.3	3.5	3.7	0.8	2.6
Oct-12	NB	9	NA	NA	NA	NA	NA	NA	NA	NA	NA	NA

Sample Period	Site	Depth (cm)	Ca (wt%)	Al (wt%)	Ti (wt%)	Fe_{total} (wt%)	Mn (ppm)	Co (ppm)	Ni (ppm)	Cu (ppm)	Mo (ppm)	U (ppm)
Oct-12	NB	11	0.29	1.46	0.49	0.68	172	1.9	3.3	1.6	0.3	1.1
Oct-12	NB	13	0.37	1.66	0.77	0.96	247	2.3	5.1	3.0	0.5	1.8
Oct-12	NB	15	0.28	1.39	0.76	0.80	254	2.0	3.1	0.9	0.9	1.1
Oct-12	CS	1	0.90	3.19	0.50	1.44	294	4.0	9.5	6.9	1.3	1.6
Oct-12	CS	2	1.08	3.74	0.60	1.79	341	5.3	12.3	10.3	5.0	2.8
Oct-12	CS	3	0.74	3.07	0.54	1.22	258	3.4	7.1	5.0	3.1	2.1
Oct-12	CS	4	0.82	3.22	0.62	1.45	311	3.9	8.8	7.4	2.0	2.1
Oct-12	CS	5	0.81	3.23	0.61	1.30	272	3.5	7.0	4.2	3.7	2.8
Oct-12	CS	7	0.90	3.08	0.74	1.45	337	4.0	8.2	5.4	3.5	3.5
Oct-12	CS	9	0.70	2.88	0.64	1.39	312	3.7	8.8	9.3	3.7	3.4
Oct-12	CS	11	0.63	2.62	0.30	1.03	199	3.3	6.7	6.3	1.1	2.9
Oct-12	CS	13	0.61	2.67	0.58	1.19	270	3.3	7.2	4.5	2.6	2.7
Oct-12	CS	15	0.86	3.46	0.79	1.53	341	4.1	9.2	8.0	4.7	3.1
Oct-12	CB	1	0.18	0.83	0.12	0.27	50	0.7	1.7	0.8	0.2	0.2
Oct-12	CB	2	0.24	1.10	0.23	0.43	88	1.1	2.3	0.5	0.3	0.6
Oct-12	CB	3	0.24	1.03	0.21	0.38	64	1.0	1.9	1.3	0.3	0.5
Oct-12	CB	4	0.21	0.92	0.24	0.39	89	1.0	1.5	0.0	0.2	0.5
Oct-12	CB	5	0.19	0.79	0.10	0.24	39	0.7	1.6	0.7	0.3	0.4
Oct-12	CB	7	0.26	0.78	0.16	0.32	63	0.9	1.9	1.7	0.3	0.6
Oct-12	CB	9	0.33	1.39	0.21	0.47	107	1.4	2.8	2.2	0.9	0.8
Oct-12	CB	11	0.49	2.14	0.41	0.90	164	2.3	4.7	4.9	1.2	1.7
Oct-12	CB	13	0.85	2.38	0.39	1.04	205	2.7	5.8	2.8	1.8	1.6
Oct-12	CB	15	NA	NA	NA	NA	NA	NA	NA	NA	NA	NA
Oct-12	SS	1	1.25	4.77	0.60	1.80	426	5.1	11.9	6.5	1.0	1.9
Oct-12	SS	2	1.18	4.25	0.53	1.67	392	4.9	12.3	6.3	1.3	1.7
Oct-12	SS	3	1.03	3.89	0.59	1.51	344	4.3	9.4	5.3	1.6	2.3

Sample Period	Site	Depth (cm)	Ca (wt%)	Al (wt%)	Ti (wt%)	Fe_{total} (wt%)	Mn (ppm)	Co (ppm)	Ni (ppm)	Cu (ppm)	Mo (ppm)	U (ppm)
Oct-12	SS	4	1.20	4.16	0.62	1.55	383	4.6	9.2	4.9	13.5	2.3
Oct-12	SS	5	0.90	3.71	0.48	1.20	258	3.4	7.8	5.8	1.8	1.3
Oct-12	SS	7	0.92	3.42	0.44	1.17	249	3.4	12.1	8.4	1.6	1.3
Oct-12	SS	9	0.67	2.68	0.33	0.82	176	2.4	6.2	0.1	1.1	1.7
Oct-12	SS	11	0.78	3.12	0.47	1.03	251	2.9	5.7	1.5	1.0	2.0
Oct-12	SS	13	0.69	2.93	0.46	0.95	232	2.7	6.6	1.5	1.0	1.6
Oct-12	SS	15	1.16	4.10	0.72	1.53	396	4.2	8.0	2.2	1.5	2.1
Oct-12	SB	1	1.17	4.69	0.36	1.44	304	4.3	11.0	5.7	0.6	1.1
Oct-12	SB	2	1.07	4.25	0.34	1.35	246	4.2	9.7	3.9	0.9	1.2
Oct-12	SB	3	1.12	4.68	0.36	1.47	263	4.6	11.0	4.1	1.3	1.4
Oct-12	SB	4	0.94	3.63	0.32	1.23	240	3.8	9.1	4.9	1.2	1.3
Oct-12	SB	5	1.05	4.23	0.36	1.28	266	3.9	8.6	5.6	1.1	1.5
Oct-12	SB	7	1.05	4.23	0.36	1.23	247	3.9	10.6	5.5	1.1	1.2
Oct-12	SB	9	0.99	3.92	0.33	1.05	229	3.4	9.3	3.5	1.5	1.4
Oct-12	SB	11	1.14	4.04	0.53	1.48	358	4.3	9.4	4.2	1.6	2.2
Oct-12	SB	13	0.96	4.25	0.37	1.34	256	4.1	9.6	4.9	2.7	3.1
Oct-12	SB	15	1.19	4.69	0.43	1.36	284	4.3	10.2	6.5	2.7	2.9
Jun-13	NS	1	0.43	2.04	0.72	1.15	255	2.8	4.8	2.8	0.7	1.3
Jun-13	NS	2	0.45	1.97	0.85	1.17	309	2.8	5.1	1.8	0.6	2.4
Jun-13	NS	3	NA	NA	NA	NA	NA	NA	NA	NA	NA	NA
Jun-13	NS	4	0.33	1.52	0.76	1.07	326	2.5	3.6	1.6	0.7	1.5
Jun-13	NS	5	0.39	1.87	0.61	1.13	294	3.0	4.6	5.4	0.9	2.4
Jun-13	NS	7	0.29	1.36	0.55	0.85	243	2.1	3.1	1.7	0.6	1.6
Jun-13	NS	9	0.28	1.44	0.65	0.91	290	2.2	2.7	0.4	0.3	2.1
Jun-13	NS	11	0.28	1.39	0.52	0.73	195	1.9	2.6	1.1	0.6	1.5
Jun-13	NS	13	0.31	1.66	0.50	0.85	202	2.4	3.2	2.4	0.4	1.3

Sample Period	Site	Depth (cm)	Ca (wt%)	Al (wt%)	Ti (wt%)	Fe_{total} (wt%)	Mn (ppm)	Co (ppm)	Ni (ppm)	Cu (ppm)	Mo (ppm)	U (ppm)
Jun-13	NS	15	0.39	1.80	0.82	1.14	297	2.8	4.1	3.4	0.8	1.8
Jun-13	NB	1	0.32	1.45	0.93	1.05	284	2.3	4.6	2.0	0.6	1.2
Jun-13	NB	2	0.32	1.54	0.87	1.04	254	2.3	3.3	8.8	0.4	1.6
Jun-13	NB	3	0.32	1.54	1.00	1.14	383	2.5	2.8	1.2	0.3	1.5
Jun-13	NB	4	0.30	1.47	0.82	0.86	260	2.0	2.7	0.0	0.5	1.3
Jun-13	NB	5	0.41	1.71	1.42	1.51	440	3.1	3.5	1.3	0.7	2.9
Jun-13	NB	7	0.41	1.81	0.90	1.11	299	2.5	3.4	1.9	1.1	2.1
Jun-13	NB	9	0.44	1.94	1.21	1.40	403	3.2	4.3	11.6	1.2	2.3
Jun-13	NB	11	0.42	1.95	1.08	1.35	366	3.0	4.9	4.3	1.6	2.3
Jun-13	NB	13	0.34	1.54	1.17	1.18	361	2.4	3.3	0.2	1.1	2.8
Jun-13	NB	15	0.26	1.30	0.56	0.69	191	1.6	2.5	0.1	0.9	1.2
Jun-13	CS	1	0.90	3.03	0.70	1.50	335	3.9	8.1	6.2	1.1	1.6
Jun-13	CS	2	0.93	3.38	0.80	1.69	390	4.5	9.0	6.6	1.8	2.7
Jun-13	CS	3	0.78	3.08	0.62	1.34	312	3.8	7.6	39.8	2.4	2.3
Jun-13	CS	4	0.69	2.80	0.62	1.25	299	3.2	6.3	6.1	1.5	2.0
Jun-13	CS	5	0.75	3.01	0.57	1.34	286	3.7	8.0	6.1	1.6	3.2
Jun-13	CS	7	0.62	2.53	0.43	1.01	222	2.8	5.5	0.9	1.0	1.9
Jun-13	CS	9	NA	NA	NA	NA	NA	NA	NA	NA	NA	NA
Jun-13	CS	11	0.70	2.82	0.56	1.20	244	3.4	9.4	6.3	2.1	2.5
Jun-13	CS	13	0.58	2.67	0.48	1.12	212	3.2	6.9	3.4	1.8	2.0
Jun-13	CS	15	0.72	3.20	0.66	1.46	267	4.0	8.7	8.1	3.1	2.3
Jun-13	CB	1	0.14	0.75	0.10	0.20	31	0.6	1.2	0.0	0.2	0.2
Jun-13	CB	2	0.16	0.82	0.11	0.19	38	1.0	1.1	0.0	0.1	0.2
Jun-13	CB	3	0.15	0.76	0.13	0.22	53	0.7	1.2	0.0	0.1	0.2
Jun-13	CB	4	0.25	0.80	0.22	0.30	66	0.7	1.2	0.0	0.2	0.5
Jun-13	CB	5	0.35	1.07	0.29	0.36	119	0.9	1.3	0.0	0.3	0.4

Sample Period	Site	Depth (cm)	Ca (wt%)	Al (wt%)	Ti (wt%)	Fe_{total} (wt%)	Mn (ppm)	Co (ppm)	Ni (ppm)	Cu (ppm)	Mo (ppm)	U (ppm)
Jun-13	CB	7	0.21	0.88	0.34	0.36	83	0.9	1.2	0.8	0.3	0.3
Jun-13	CB	9	0.22	0.80	0.13	0.18	29	0.5	3.7	0.0	0.2	0.3
Jun-13	CB	11	0.28	1.07	0.15	0.33	55	0.9	1.6	0.6	0.6	0.7
Jun-13	CB	13	0.34	1.24	0.34	0.58	123	1.4	2.6	2.8	0.4	0.6
Jun-13	CB	15	0.41	1.47	0.31	0.63	114	1.6	3.2	3.7	1.0	1.1
Jun-13	SS	1	1.19	4.36	0.62	1.66	403	4.6	9.4	2.0	0.5	1.5
Jun-13	SS	2	1.20	4.22	0.55	1.46	359	4.3	9.1	0.7	0.7	1.4
Jun-13	SS	3	1.31	4.53	0.50	1.49	337	4.5	9.7	2.0	1.3	1.8
Jun-13	SS	4	1.14	4.31	0.44	1.38	302	4.3	9.2	2.0	0.9	1.4
Jun-13	SS	5	1.16	4.35	0.45	1.43	291	4.3	9.1	3.1	2.0	1.8
Jun-13	SS	7	1.10	4.27	0.45	1.31	299	3.9	8.6	1.1	2.4	1.8
Jun-13	SS	9	1.13	3.33	0.64	1.58	393	4.5	8.6	1.2	1.8	3.8
Jun-13	SS	11	1.06	3.97	0.56	1.41	351	4.1	8.1	1.9	1.6	2.1
Jun-13	SS	13	1.27	4.89	0.62	2.04	416	6.2	14.6	6.6	2.9	3.6
Jun-13	SS	15	1.01	4.17	0.44	1.48	273	4.3	10.2	5.3	1.8	1.9
Jun-13	SB	1	1.17	4.37	0.44	1.54	304	4.6	10.1	3.6	0.6	1.1
Jun-13	SB	2	1.18	4.48	0.52	1.55	334	4.6	10.3	3.2	1.9	1.8
Jun-13	SB	3	1.10	4.13	0.44	1.26	300	3.8	8.0	1.9	0.6	1.2
Jun-13	SB	4	1.08	4.30	0.40	1.32	269	4.0	8.9	6.3	1.0	1.2
Jun-13	SB	5	1.04	3.75	0.37	1.13	239	3.5	7.7	3.7	3.2	1.2
Jun-13	SB	7	1.11	4.30	0.45	1.37	285	4.2	9.1	4.2	1.0	1.6
Jun-13	SB	9	1.12	4.26	0.48	1.43	322	4.3	8.9	4.8	1.6	1.7
Jun-13	SB	11	0.98	4.01	0.37	1.08	227	3.4	7.5	4.5	1.4	1.3
Jun-13	SB	13	1.15	4.29	0.54	1.54	348	4.5	8.9	2.5	1.7	2.3
Jun-13	SB	15	1.04	4.13	0.45	1.25	286	3.7	7.6	1.4	1.7	2.2
Oct-13	NS	1	0.66	2.98	0.50	1.18	227	3.3	6.7	8.7	0.9	1.1

Sample Period	Site	Depth (cm)	Ca (wt%)	Al (wt%)	Ti (wt%)	Fe_{total} (wt%)	Mn (ppm)	Co (ppm)	Ni (ppm)	Cu (ppm)	Mo (ppm)	U (ppm)
Oct-13	NS	2	0.48	2.23	0.44	0.84	175	2.3	4.7	5.5	1.0	1.0
Oct-13	NS	3	0.47	2.21	0.39	0.89	183	2.6	5.0	7.6	1.4	1.3
Oct-13	NS	4	0.53	2.57	0.49	1.14	227	3.4	6.8	12.2	2.1	1.6
Oct-13	NS	5	0.50	2.42	0.44	0.91	226	2.7	4.9	6.4	1.6	1.1
Oct-13	NS	7	0.48	2.18	0.59	0.97	239	2.7	27.3	4.8	0.9	1.7
Oct-13	NS	9	0.47	1.98	0.35	0.75	149	2.0	5.1	1.8	2.2	1.1
Oct-13	NS	11	0.48	2.39	0.41	0.97	199	3.0	5.7	4.1	1.2	1.9
Oct-13	NS	13	0.48	1.88	0.38	0.78	166	1.9	3.7	0.6	0.3	1.1
Oct-13	NS	15	0.43	1.94	0.43	0.83	188	2.3	4.8	2.5	1.5	1.6
Oct-13	NB	1	0.38	1.84	0.33	0.68	139	1.9	3.4	1.9	0.2	0.7
Oct-13	NB	2	0.55	2.69	0.46	1.00	202	2.8	5.7	7.8	0.9	1.2
Oct-13	NB	3	0.42	2.03	0.38	0.76	156	2.2	4.1	5.3	1.0	1.0
Oct-13	NB	4	0.54	2.58	0.44	1.00	205	3.0	5.9	8.7	2.0	1.3
Oct-13	NB	5	0.56	2.57	0.51	0.99	210	3.0	5.3	6.4	1.7	1.6
Oct-13	NB	7	0.43	2.11	0.48	0.91	190	2.8	4.9	5.8	1.5	1.4
Oct-13	NB	9	0.39	1.91	0.42	0.76	177	2.2	3.9	5.6	0.9	0.9
Oct-13	NB	11	0.46	1.95	0.42	0.76	174	2.1	4.1	4.7	0.8	1.0
Oct-13	NB	13	0.67	2.89	0.64	1.23	290	3.2	21.7	5.1	1.5	1.9
Oct-13	NB	15	0.38	1.88	0.35	0.76	152	2.3	4.8	3.8	1.9	1.1
Oct-13	CS	1	0.64	2.23	0.53	1.00	210	2.3	4.8	1.3	0.7	1.0
Oct-13	CS	2	0.61	2.26	0.41	0.97	190	2.5	7.3	2.4	0.6	0.8
Oct-13	CS	3	0.58	2.16	0.48	1.01	208	2.6	4.9	4.4	0.9	1.3
Oct-13	CS	4	0.48	1.97	0.32	0.72	133	1.9	4.2	1.3	0.7	0.8
Oct-13	CS	5	0.65	2.37	0.35	0.96	159	2.6	5.8	2.2	1.2	1.2
Oct-13	CS	7	0.57	2.22	0.50	1.02	208	2.5	4.7	1.8	1.2	1.4
Oct-13	CS	9	0.87	2.44	0.44	1.14	207	3.1	8.4	2.7	1.8	1.4

Sample Period	Site	Depth (cm)	Ca (wt%)	Al (wt%)	Ti (wt%)	Fe_{total} (wt%)	Mn (ppm)	Co (ppm)	Ni (ppm)	Cu (ppm)	Mo (ppm)	U (ppm)
Oct-13	CS	11	0.59	2.24	0.36	1.00	166	2.6	5.7	3.0	1.0	1.1
Oct-13	CS	13	0.82	2.34	0.48	1.07	227	2.6	5.8	2.4	2.2	1.9
Oct-13	CS	15	0.62	2.21	0.35	0.98	190	2.5	5.4	2.0	1.7	1.5
Oct-13	CB	1	0.86	2.40	0.62	1.13	257	2.7	5.1	0.6	0.7	1.4
Oct-13	CB	2	NA	NA	NA	NA	NA	NA	NA	NA	NA	NA
Oct-13	CB	3	0.40	1.89	0.39	0.78	190	2.2	3.7	4.6	1.3	1.1
Oct-13	CB	4	0.41	2.03	0.39	0.90	183	2.6	5.6	2.9	1.7	1.2
Oct-13	CB	5	0.51	2.04	0.51	0.83	176	2.0	4.2	0.1	0.6	0.9
Oct-13	CB	7	0.90	2.90	0.57	1.30	254	3.3	6.3	3.4	1.0	2.0
Oct-13	CB	9	0.84	2.66	0.46	1.13	201	2.9	6.0	4.0	1.1	1.4
Oct-13	CB	11	0.85	2.73	0.52	1.26	240	3.3	7.7	4.0	1.3	1.8
Oct-13	CB	13	0.84	3.02	0.40	1.40	230	3.7	9.4	6.4	2.1	1.8
Oct-13	CB	15	0.84	3.08	0.45	1.44	228	4.0	9.2	6.6	4.9	2.1
Oct-13	SS	1	1.16	4.14	0.53	1.62	364	4.7	10.5	3.1	0.5	1.8
Oct-13	SS	2	1.25	4.18	0.64	1.71	410	4.8	9.5	1.7	0.6	2.3
Oct-13	SS	3	1.13	4.30	0.48	1.35	296	4.1	8.5	0.9	0.7	1.6
Oct-13	SS	4	1.25	4.21	0.59	1.62	387	4.8	9.4	1.0	1.0	2.2
Oct-13	SS	5	1.17	4.44	0.48	1.43	306	4.2	9.0	1.8	1.3	1.9
Oct-13	SS	7	1.09	4.15	0.44	1.35	288	4.0	8.2	0.8	1.4	1.8
Oct-13	SS	9	1.01	4.08	0.40	1.31	269	3.9	8.4	2.1	3.4	1.9
Oct-13	SS	11	1.24	4.27	0.60	1.57	371	4.4	9.8	1.9	2.1	2.6
Oct-13	SS	13	1.05	4.39	0.36	1.38	255	4.2	9.6	3.7	2.6	2.7
Oct-13	SS	15	1.09	4.48	0.40	1.39	270	4.3	9.6	4.3	2.1	2.1
Oct-13	SB	1	1.15	4.11	0.47	1.48	334	4.3	9.1	2.1	0.7	1.3
Oct-13	SB	2	1.11	4.27	0.46	1.44	333	4.2	9.2	1.8	1.3	1.7
Oct-13	SB	3	1.09	4.45	0.37	1.38	284	4.2	10.4	1.5	1.4	1.3

Sample Period	Site	Depth (cm)	Ca (wt%)	Al (wt%)	Ti (wt%)	Fe_{total} (wt%)	Mn (ppm)	Co (ppm)	Ni (ppm)	Cu (ppm)	Mo (ppm)	U (ppm)
Oct-13	SB	4	1.06	4.12	0.36	1.41	273	4.6	11.1	8.0	3.2	1.6
Oct-13	SB	5	1.08	4.45	0.33	1.35	268	4.1	9.4	2.4	1.7	1.4
Oct-13	SB	7	1.31	4.72	0.44	1.94	341	5.9	14.6	6.9	3.1	2.2
Oct-13	SB	9	1.12	4.53	0.44	1.92	338	5.8	13.8	7.4	3.8	2.5
Oct-13	SB	11	1.10	4.33	0.42	1.55	310	4.5	10.6	4.0	3.2	2.5
Oct-13	SB	13	1.31	5.47	0.45	2.38	359	7.1	19.6	14.4	5.9	2.8
Oct-13	SB	15	1.05	4.08	0.37	3.35	357	10.7	29.4	30.6	4.7	2.8

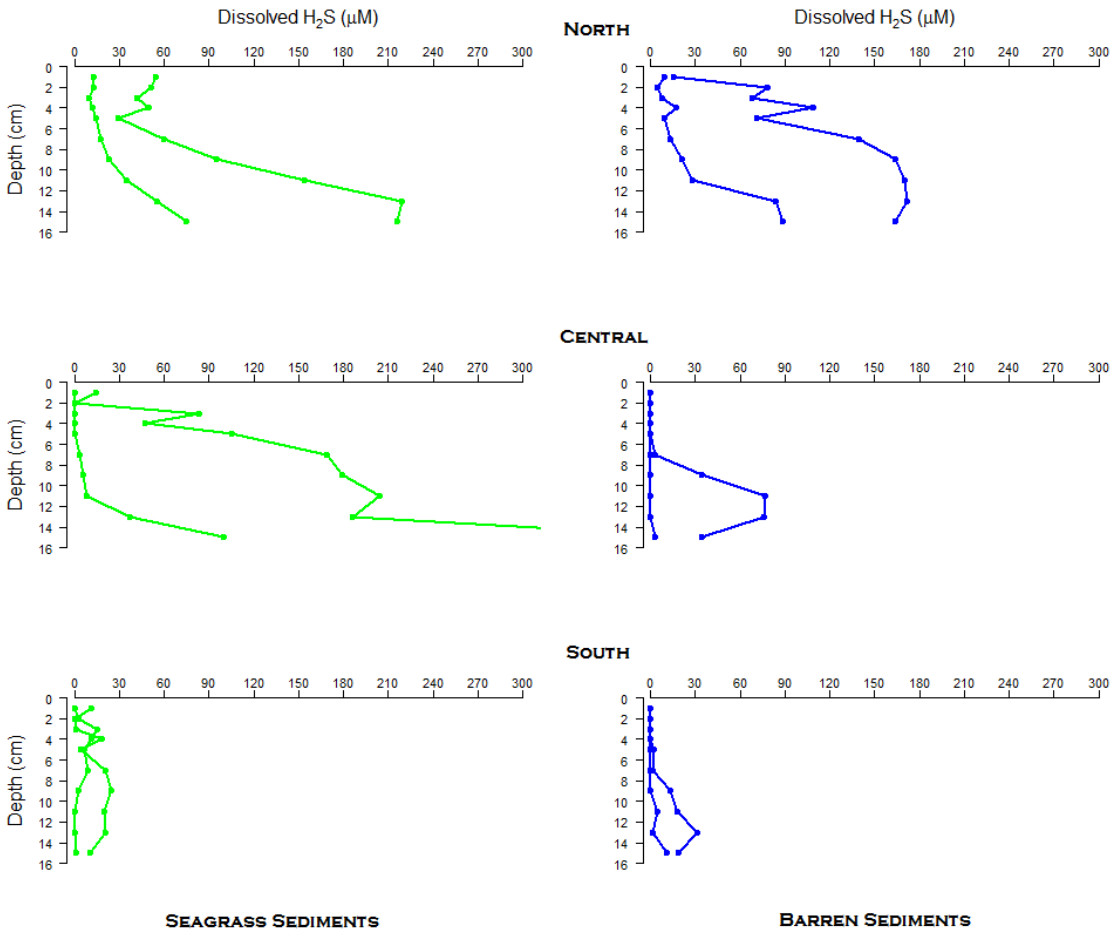

Figure A1. Dissolved H_2S at individual sites in BBLEH in October 2012.

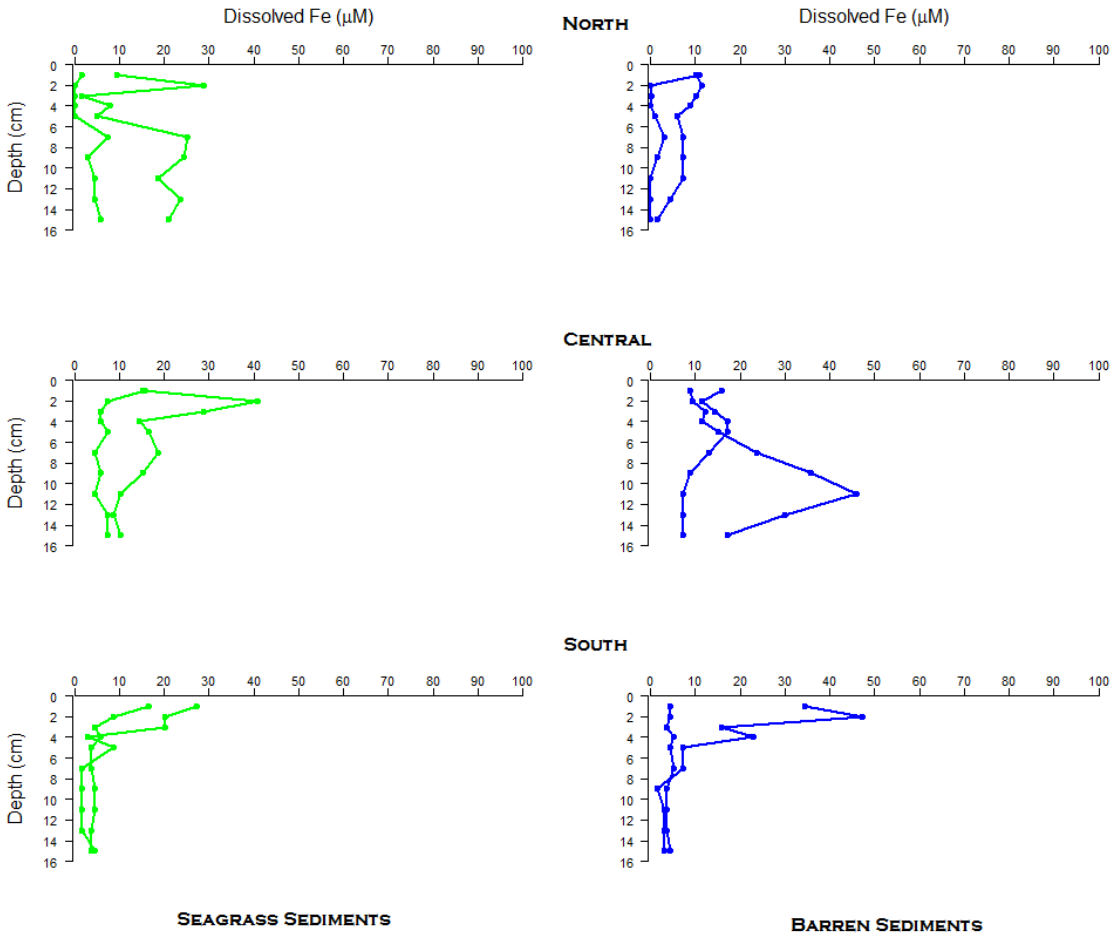

Figure A2. Dissolved Fe at individual sites in BBLEH in October 2012.

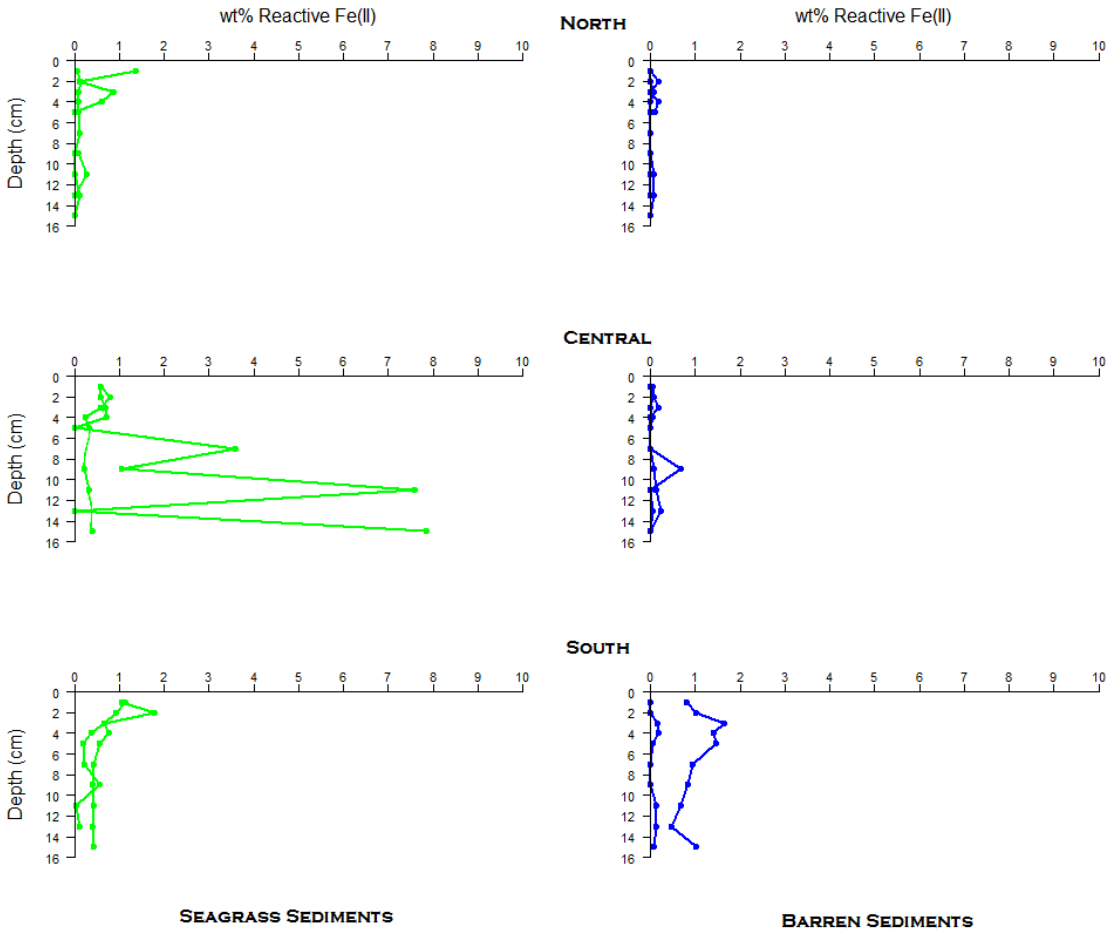

Figure A3. Reactive Fe(II) at individual sites in BBLEH in October 2012.

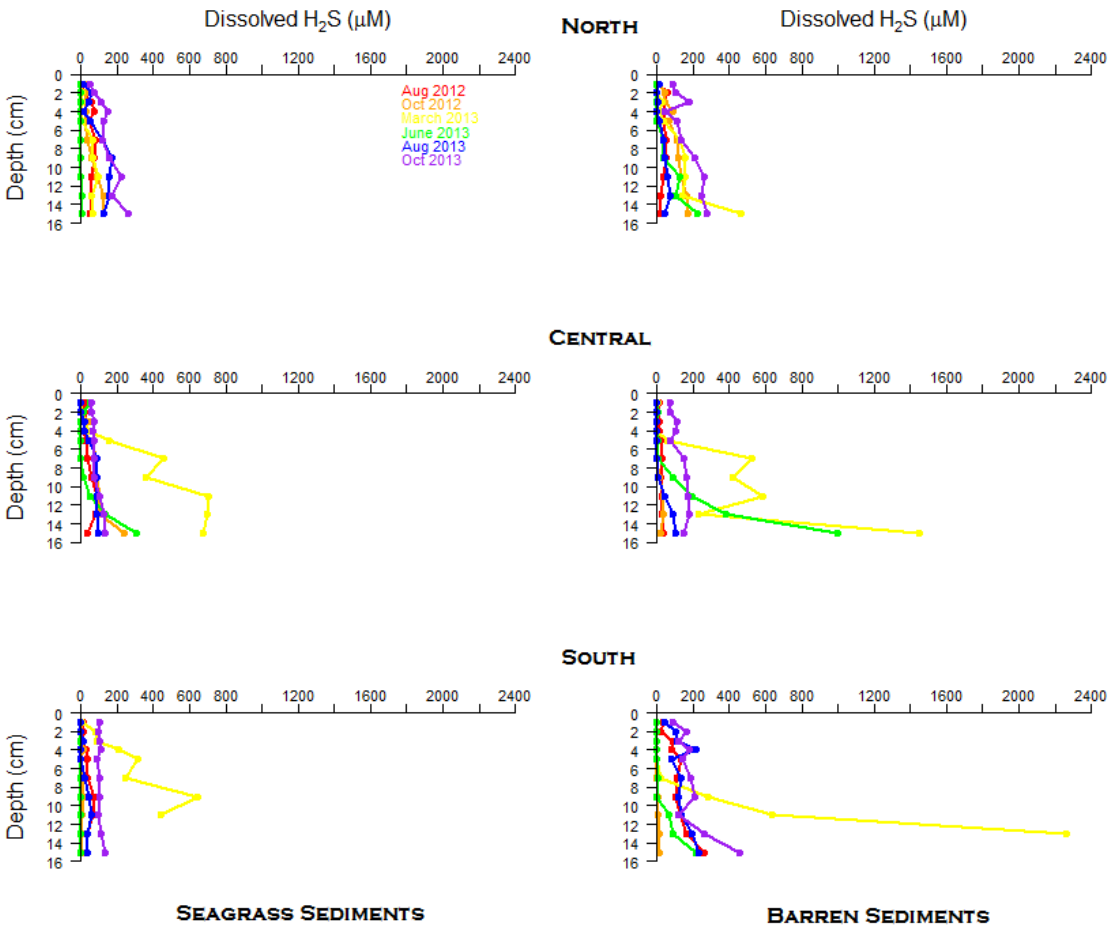

Figure A4. Dissolved H_2S in BBLEH sediments for individual sampling periods. Aug 2012, Oct 2012, March 2013, June 2013, Aug 2013, Oct 2013 are in red, orange, yellow, green, blue, and purple, respectively.

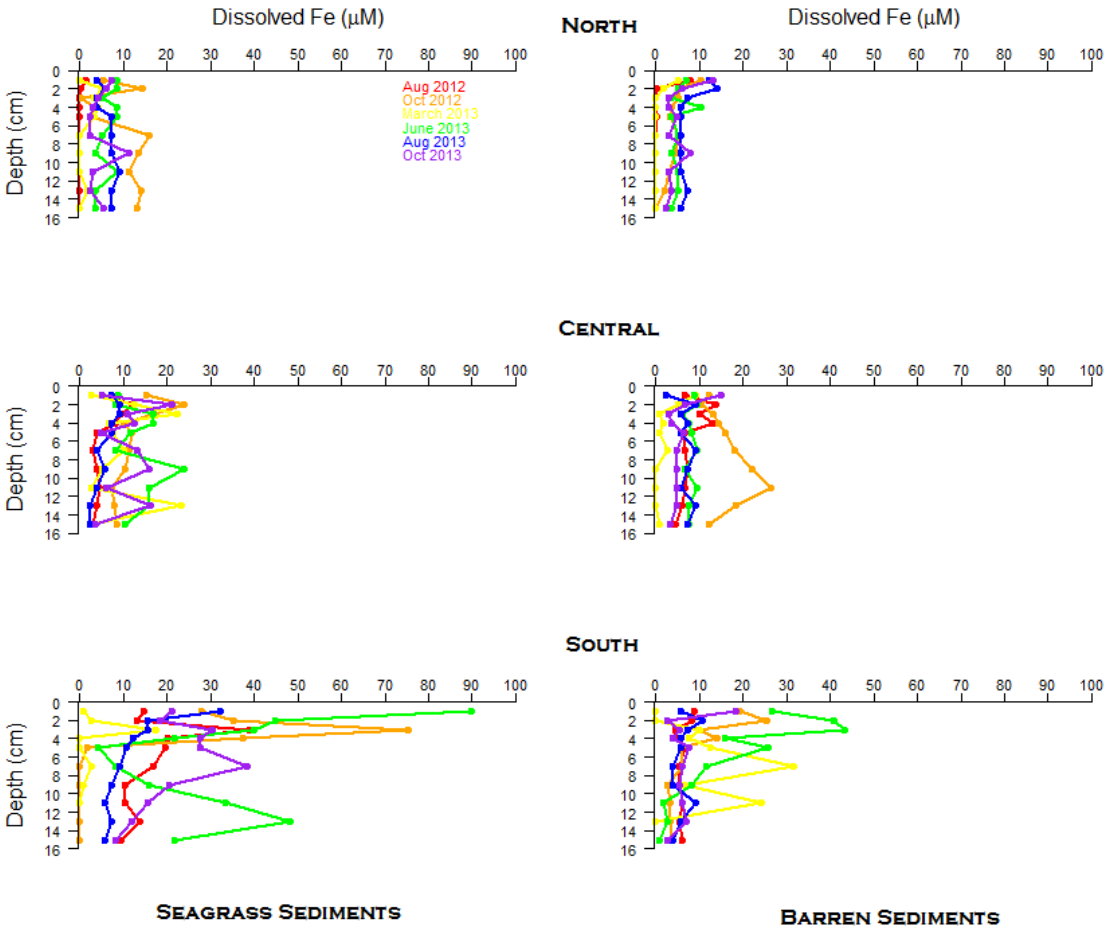

Figure A5. Dissolved Fe in BBLEH sediments for individual sampling periods. Aug 2012, Oct 2012, March 2013, June 2013, Aug 2013, Oct 2013 are in red, orange, yellow, green, blue, and purple, respectively.

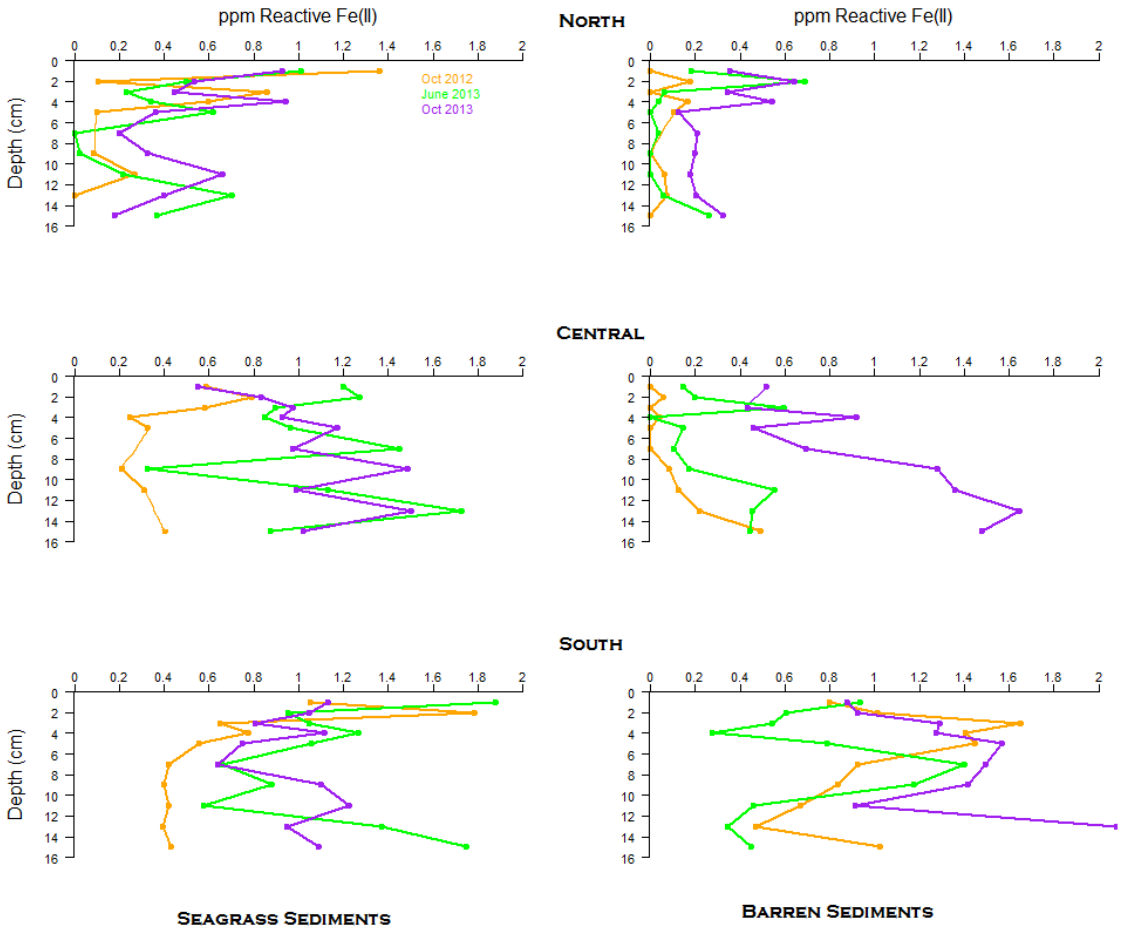

Figure A6. Reactive Fe(II) in BBLEH sediments for individual sampling periods. Oct 2012, June 2013, Oct 2013 are in orange, green, and purple, respectively.

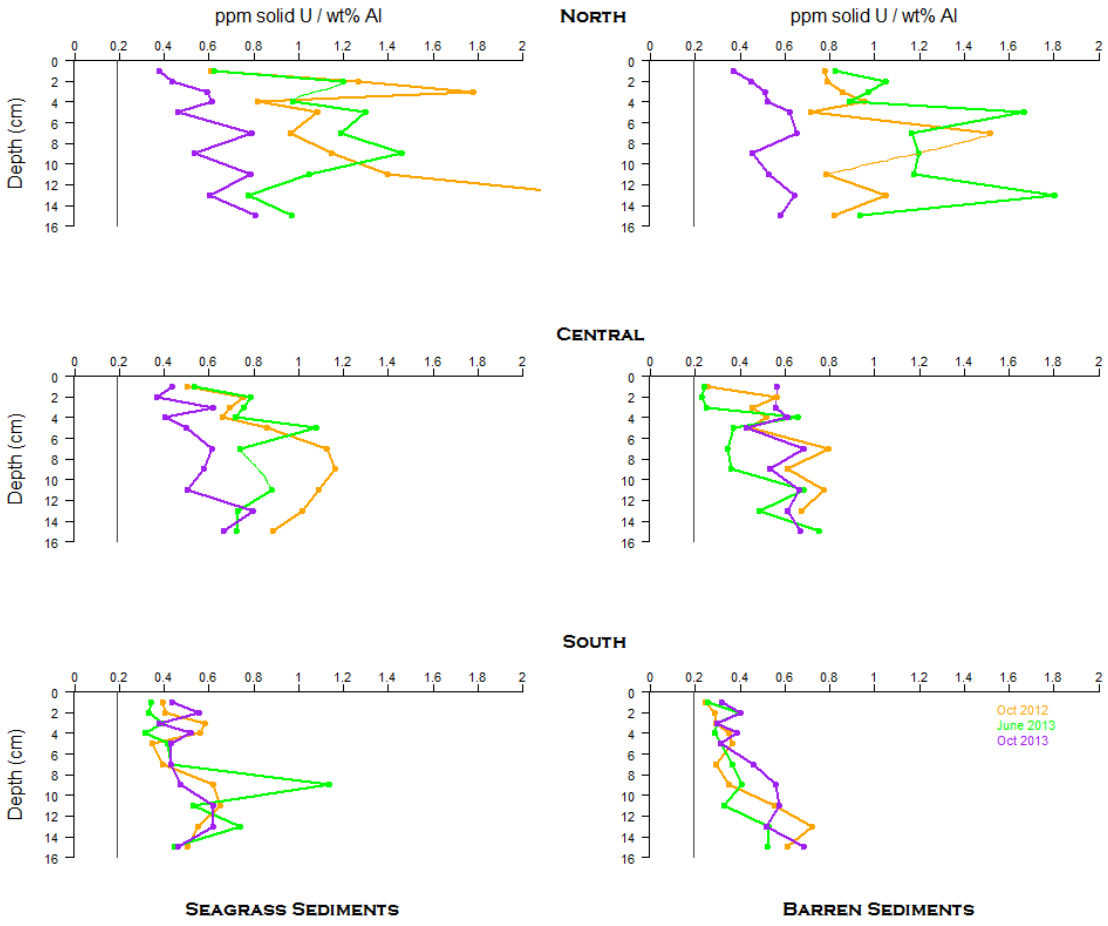

Figure A7. U(s)/Al(s) in BBLEH sediments for individual sampling periods. Oct 2012, June 2013, Oct 2013 are in orange, green, and purple, respectively.

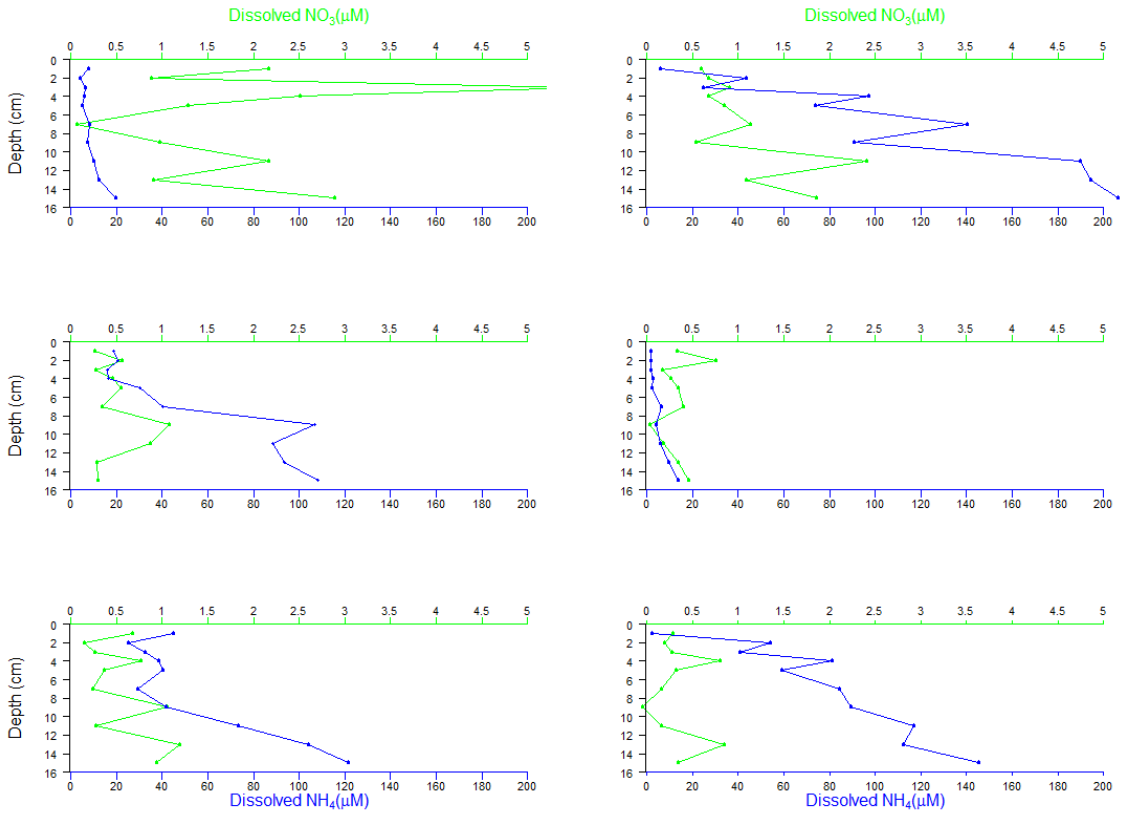

Figure A8. Dissolved NO_3 (green) and NH_4 (blue) in BBLEH sediments in June 2013.